In search of breast cancer cell secretions with therapeutic and diagnostic value.

In search of breast cancer cell secretions with therapeutic and diagnostic value.

A dissertation presented

by

Nefeli Eleonora Georgoulia

to

The School of Engineering and Applied Sciences

in partial fulfillment of the requirements

for the degree of

Doctor of Philosophy

in the subject of

Applied Physics

Harvard University

Cambridge, Massachusetts

April 2014

Dissertation advisor
Timothy J. Mitchison

Author
Nefeli Eleonora Georgoulia

In search of breast cancer cell secretions with therapeutic and diagnostic value.

Abstract

The first end point of this study was to identify specific pro-apoptotic or anti-proliferative factors in the breast cancer cell secretome. To this end, we designed an *in vitro* screen that effectively cross-cultured 20 breast cancer cell lines in each other's conditioned media. We selected the strongest pro-apoptotic hits and performed further proteomic and biochemical characterization in order to analyze their composition. We determined that the pro-apoptotic activity resided in the soluble, exosome-free secreted fraction of triple negative breast cancer cell conditioned medium and used proteomic insights in order to narrow down the list of possible candidate molecules responsible for the apoptotic effect. The second endpoint of this study was to evaluate the particulate fraction found in breast cancer cell conditioned media for diagnostically significant molecules. We isolated cancer exosomes, employing a serial ultracentrifugation protocol, and were able to establish that the exosome cell surface receptors identically reflect the molecular identity of their cell lines of origin. However, downstream protein kinases within exosomes display patterns of depletion or enrichment in comparison to the corresponding cell lines. Overall, we found that the exosome protein composition in breast cancer is informative enough to guide the choice of specific inhibitor treatment in a clinical setting.

Table of Contents

Acknowledgements

This research would not have been possible without the support and encouragement from a multitude of people. First and foremost I want to thank my thesis advisor Professor Timothy Mitchison, for welcoming me in his laboratory and presenting me with the opportunity of a very exciting research project in the area of breast cancer. I learned a great deal of biology while in Tim's lab, either directly from him or from the range of talented scientists that Tim carefully selects to work for him. In addition, I am very grateful to Tim for initiating me to the world of molecular mechanism and converting me to that frame of mind. Ultimately, the fruits of that labor were extremely gratifying for me on a personal level.

I also want to express my gratitude to my academic committee members Professors Neel Joshi and Michael Brenner. They both shepherded me through my PhD by participating in regular committee meetings, encouraging me and supporting me through difficult moments. I am particularly grateful to Dr. Mario Niepel for his guidance and scientific insights during our investigation of cancer exosomes. Mario was an invaluable source of expertise and information that discretely yet firmly guided me through this research project. Along with Mario, I also want to offer special thanks to Professor Peter Sorger that met with me and participated in committee meetings whenever called upon. Professor Sorger's opinions and insights in cancer biology were much appreciated and helped guide our choice of research direction.

It would be extremely challenging to execute experiments without Kathleen Buhl, our laboratory manager whose efficiency kept the lab running seamlessly throughout the years. I would also like to extend my thanks to Margaret Coughlin who spent her time so generously, teaching me about electron microscopy during the beginning stages of investigating cancer exosomes. I want to acknowledge the help provided by Ruomu Jiang on data analysis and data representation. I wish to thank various people in the Mitchison lab for their occasional contributions to my research and for fruitful scientific discussions: Edwin Tan, Zoltan Maliga, Sujeong Kim, Hallie Kuhn, Kristin Krukenberg, Paul Choi, Lingyin Li, Peter Koch and Stefan Florian. I am grateful to all of the Mitchison lab and the department of Systems Biology at Harvard Medical School for their camaraderie and congeniality throughout the years.

I am particularly grateful for the assistance of Professor Dimitris Iliopoulos and the postdoctoral researcher in his laboratory Dr. Giorgos Koukos, with whom I worked closely on isolating microRNAs from breast cancer exosomes. I value this skill set I developed and I would not have been able to acquire it without their assistance. I also want to direct a special thank to my friend and colleague Dr. Dariela Almeda who shared protocols with me on phospholipid quantitation and membrane fusion assays. Dariela's vision and enthusiasm about my research project carried me through difficult times of self-doubt and discouragement.

I want to express my deepest gratitude to my father, Professor Vassilis Georgoulias who proof-read and evaluated my work throughout the years, offering his much valued clinical perspective on my research project. I am also grateful to him for introducing me to a very talented community of oncology researchers that embraced me and offered much needed companionship at medical conferences and scientific meetings.

Lastly, I am very appreciative of the support I have been given by my family - my parents, sister and fiancé Mehron - during my years of graduate work. Their love, encouragement and light-hearted humor were the perfect antidote for the multitude of pressures and disappointments inherent to the journey of research. Along with my friends, they have always been by my side to puzzle over roadblocks and celebrate small and large victories. Thank you so much.

Dedicated in loving memory of friends and family who were handed an unfavorable diagnosis and fought a losing battle to cancer. They were constantly on my mind as I strived to make my small yet -I hope- meaningful contribution to this research field.

Chapter 1

Introduction

Abstract

In this chapter we provide the context within which the present study and its' scientific aims were set. We begin with a description of how our understanding of cancer has changed in the last two decades, and in particular the role of tumor heterogeneity. Once considered a disease of sequentially acquired genetic mutations leading to clonally identical tumor cells, we now know that cues from the tumor microenvironment strongly contribute to disease onset and progression. In addition, it is now recognized that a significant amount of epigenetic plasticity drives disease progression. It is also recognized that a significant amount of phenotypic plasticity allows cancer cells to adapt to different environments during the metastatic process. As a result of all these processes – mutation, environment and epigenetics – acting differentially on cells within a tumor, strong heterogeneity is observed within primary tumors as well as between primary tumors and their metastatic sites.

After discussing recent advances in cancer understanding we turn our attention to novel therapeutics. As our understanding of the molecular pathways governing cancer deepens, the list of tyrosine-kinase inhibitors rationally designed as cancer treatments expands. We discuss the most important of these inhibitors as well as

their performance in the clinic. Due to the development of this highly specialized artillery against cancer, the need for diagnostic tools that will connect the molecular makeup of specific tumors to the adequate therapeutic compound is now more pressing than ever. We relate a selection of studies that use cancer cell line collections in order to extract 'biomarker signatures' that will predict clinical sensitivity to inhibitors. 'Biomarker', in this context, means a measurement made of a human tumor, or a measurement made in cell culture that could potentially be extended to a human tumor. Beyond that, we also discuss 'liquid biopsy' diagnostic technologies that are currently under development. These technologies aim to establish molecular typing of cancer from patient blood samples and obviate the risks and limitations inherent to tumor biopsies. We close this chapter by presenting our list of specific aims and the order in which these will be addressed in the chapters that follow.

1.1 Phenotypic plasticity and clonal evolution of cancer cells

In the first part of my PhD I analyzed interactions between many breast cancer cell lines chosen for their genetic diversity. The goal of this undertaking was to understand the functional consequences of cancer heterogeneity in terms of how factors secreted by one cancer clone might affect another. To set up this part of my work I will introduce the concept of heterogeneity in tumors – how it arises and what its functional consequences might be.

Cancer is known to arise in accordance with the modern dogma of cancer genesis, which stipulates that a tumor evolves from a single cell that undergoes gradual malignant transformation[1]. In their seminal review publication, Hanahan and Weinberg describe the six hallmarks of cancer, a set of genetic mutations gradually acquired by cancer cells and driving disease progression and metastasis. In the ensuing decade however, it became exceedingly clear that a tumor is much more than a collection of identical genetically mutated cells. Beyond genetic mutation, the tumor microenvironment plays a paramount role in cancer development and progression[2]. In the last decade cancer research has brought forth deeper insights regarding the varied cellular composition of solid tumors, the transient epigenetic plasticity of cancer cells, as well as the role of ambient mechanical and biochemical signals, all major contributors to malignant progression.

Non-soluble cues in the tumor microenvironment

Cell fate within a tumor is regulated by a variety of signals the cell receives from its environment. These cues can be of a chemical or mechanical nature, but what they have in common is that they both initiate molecular programs within the cell that lead to proliferation, differentiation, senescence, apoptosis and migration[3]. In recent years cell substrate stiffness has been increasingly recognized as a regulator of cell fate and a significant contributor in cancer progression. Ulrich et al. confirm this by culturing glioblastoma cells on fibronectin substrates of defined mechanical rigidity and show that both proliferation and the development of a migratory phenotype in this highly malignant cell type is dependent on substrate stiffness[4]. In the same vein,

the actual tissue architecture in which a cancer cell is embedded is of paramount importance in determining whether a tumor will develop. Weaver et al. show that mammary epithelial cells incorporated in polarized 3D structures, biomimetic of physiological mammary gland architecture, are resistant to death cues such as chemotherapeutic agents, tumor necrosis factor (TNF) and TNF-related apoptosis-inducing ligand (TRAIL). The same cells, when grown in 2D monolayers are supremely sensitive to cell death induced by these stimuli[5].

Another informative experiment regarding the interplay between environmental cues and genetic mutations on breast tumorigenesis was performed by Debnath et al. who developed a protocol for culturing MCF-10A, a non-transformed mammary epithelial cell line, in Matrigel basement membrane matrix. This method allowed them to reconstitute *in vitro* acinar luminal structures reminiscent of normal mammary ducts over a period of 15 days. They experimented with transformation of MCF-10A cells by a variety of oncogenes and found that certain oncogenes (such as Erbb2) were successful at generating solid filled structures resembling *carcinoma in situ* histopathology, while others (such as CyclinD1 and HPV16) were not sufficient to disturb luminal architecture of the spheroids[6].

Reversal of the cancerous phenotype in response to environmental cues

Perhaps the most telling experiments of phenotypic plasticity of cancer cells and by consequence the importance of environmental cues to tumor formation are the ones reprogramming cancer cells by injecting them in embryonic milieus. In one such

experiment Lee et al. implanted the metastatic melanoma cell line C8161 in zebrafish embryos. They found that melanoma cells did not proliferate but instead remained dormant in adult fish for up to 3 months. However, when the same cells were transplanted into zebrafish eggs 2 days post fertilization, after the completion of morphogenesis and organogenesis, the cells not only divided but also developed into vascularized tumors[7]. In a similar experiment Kulesa et al. implanted metastatic melanoma cells in chick embryos adjacent to the embryo's premigratory neural crest cells. Surprisingly, the melanoma cells did not form tumors. Instead they populated host neuronal structures and co-expressed neuronal markers along with melanocyte-specific markers[8]. A similar study was performed in 1973 using murine mammary tumor cells by DeCosse et al.. The authors employed a precursor of what is known today as transwell culture to co-culture murine mammary tumor cells in the presence of soluble signals from embryonic mouse mammary. They observed that in response to embryonic cues the tumor cells proliferated less and formed tubules characteristic of normal mammary gland histology[9]. These findings suggest that the developmental signaling taking place in embryonic environments has an inhibitory effect on cancer cells. More broadly, these studies demonstrate the important role of environmental cues in cancer development.

Heterogeneity and clonal evolution in breast cancer

So far we discussed the phenotypic plasticity of cancer cells in response to micro-environmental cues, both of mechanical and soluble nature. We now turn our attention to the heterogeneity of solid tumors and the local competition arising

between cancer cells in an environment of limited oxygen and nutrient supply. Multiple studies have documented that breast tumors are heterogeneous, composed of a variety of cell types that differ in features such as size, proliferation rate, metastatic potential, drug response and phenotype[10–12]. In one of these studies, H Fuji et al.[13] performed PCR analysis on microsatellite markers of 23 breast tumors, and recorded patterns of allelic loss. It emerged that individual tumor foci exhibited genetically divergent populations with respect to some allelic changes, a divergence that was more common in the *in situ* tumors with synchronous invasive cancers, rather than in tumors of *in situ* cancer only. They concluded that this genetic divergence is a form of clonal evolution within the tumor site, driven by the progression of *in situ* to invasive carcinoma.

Most research converges in observing that indeed metastases and primary tumor are clonaly related[14,15]. Yet, there are conflicting reports within the literature regarding the dominance of the metastatic clone within the primary tumor site. What invariably complicates tracing a clonal relationship between primary tumor and metastatic lesions is the fact that genetic instability and clonal evolution is ongoing at metastatic sites. Kukarsjavi et al.[14] performed CGH cytogenetic analysis as well as X-chromosome inactivation tests on 29 primary breast carcinomas and their various metastases. They found that synchronous lymph node metastases are much more closely related to the primary tumor than asynchronous soft-tissue metastases, the latter having more time to genetically drift further from the original clone. A study by Symmans et al.[15] looked at DNA ploidy by image analysis of 17

invasive breast cancers and their 82 corresponding metastases. It emerged that in 90% of metastatic samples, the corresponding clone was identified in the primary tumor sample representing a quarter or more of the tumor cell population (hence deemed a dominant clone). They were able to identify a majority DNA clone in 60% of primary tumors and in 70% of metastatic tumors. However, there clearly were tumors where the identification of a major, dominant clone was not possible. Furthermore, in approximately half of the metastatic samples an 'unexpected majority' clone was identified -that is, a clone that was deemed a minority in the primary tumor site and by consequence was not expected to metastasize.

1.2 Advances in Cancer Treatment

In my PhD, I investigated potential biomarkers that could in theory predict, on the basis of blood measurements alone, response of tumors to certain types of drugs. The drugs that interested me were not the classic cytotoxic treatments that so many patients have to endure, but rather the more modern 'targeted therapies'. These are drugs designed to block the pathways that drive the cancer, and the hope is for much more selective treatment, and much less toxicity. To set up this part of my work I will briefly review this type of treatment as it is starting to emerge in breast cancer.

Clinical snapshot: emerging targeted therapies for breast cancer

Breast cancer treatment primarily involves surgical resection of the diseased tissue followed by adjuvant drug treatment, which is dependent on the histology of the

resected lesion and its ensuing molecular subtype[16]. In terms of molecular identity, breast tumors are binned in three categories according to the presence of three receptors. The overexpression of the estrogen (ER) and/or progesterone receptors (PR) defines a hormone receptor positive tumor (HR+) and patients with this disease are treated with HR antagonists such as tamoxifen[17,18]. The amplification of the receptor tyrosine kinase ErbB2, also known as HER2, defines HER2 positive lesions, which are treated with targeted antibody-therapy such as Trastuzumab or Pertuzumab[19–21]. All other breast tumors are categorized as triple negative breast cancer (TNBC) since they lack the presence of all three receptors mentioned above. Due to the lack of specific molecular therapy, TNBC is often treated with a combination of aggressive chemotherapy and radiation. TNBC tumors show a more aggressive phenotype than other breast tumors[22] and patients with this diagnosis have poor prognosis[23]. Both the absence of molecular therapeutics for TNBC tumors as well as the development of Trastuzumab resistance[24] in HER2-amplified breast tumors, underscores the need for better biomarkers and diagnostic specificity in breast cancer classification and treatment.

Tyrosine kinase receptors localize on the plasma membrane. Before binding of the signaling molecule, the receptors act as monomers. Each of these individual monomer units have an extracellular ligand-binding site, an alpha-helix in the membrane, a ligand binding site, and an intracellular tail featuring tyrosine amino acids. Upon ligand binding the two monomers dimerize. The process of dimerization activates the tyrosine kinase region of each individual monomer. Both of these

tyrosine kinases add a phosphate from an ATP molecule to a tyrosine on the tail of the other monomer. Once the receptor gets activated, it becomes recognized by specific relay proteins located within the cell. Each protein binds to a specific phosphorylated tyrosine, leading to a structural alteration which activates the bound protein. Each of these activated proteins trigger a transduction pathway, culminating to a change in gene expression and resulting in cellular response. The main two pathways downstream of receptor tyrosine kinases are the PI3K/AKT/mTOR pathway and the Ras/Raf/MEK/Erk pathway, as shown in figure 1.1.

In recognition of the differences in pathway activity, disease progression and response to therapy in cancer, over 800 small molecule and biological inhibitors are now under development for the treatment of human malignancies. These inhibitors vary in strength and specificity. Some, like rapamycin, are pharmaceutical agents whose molecular target was identified years after they were introduced in the clinic. Most often however, these inhibitors are the product of rational design exhibiting high target specificity. Below we summarize the main molecular pathways implicated in cancer and the multiple opportunities they present for pharmacological inhibition.

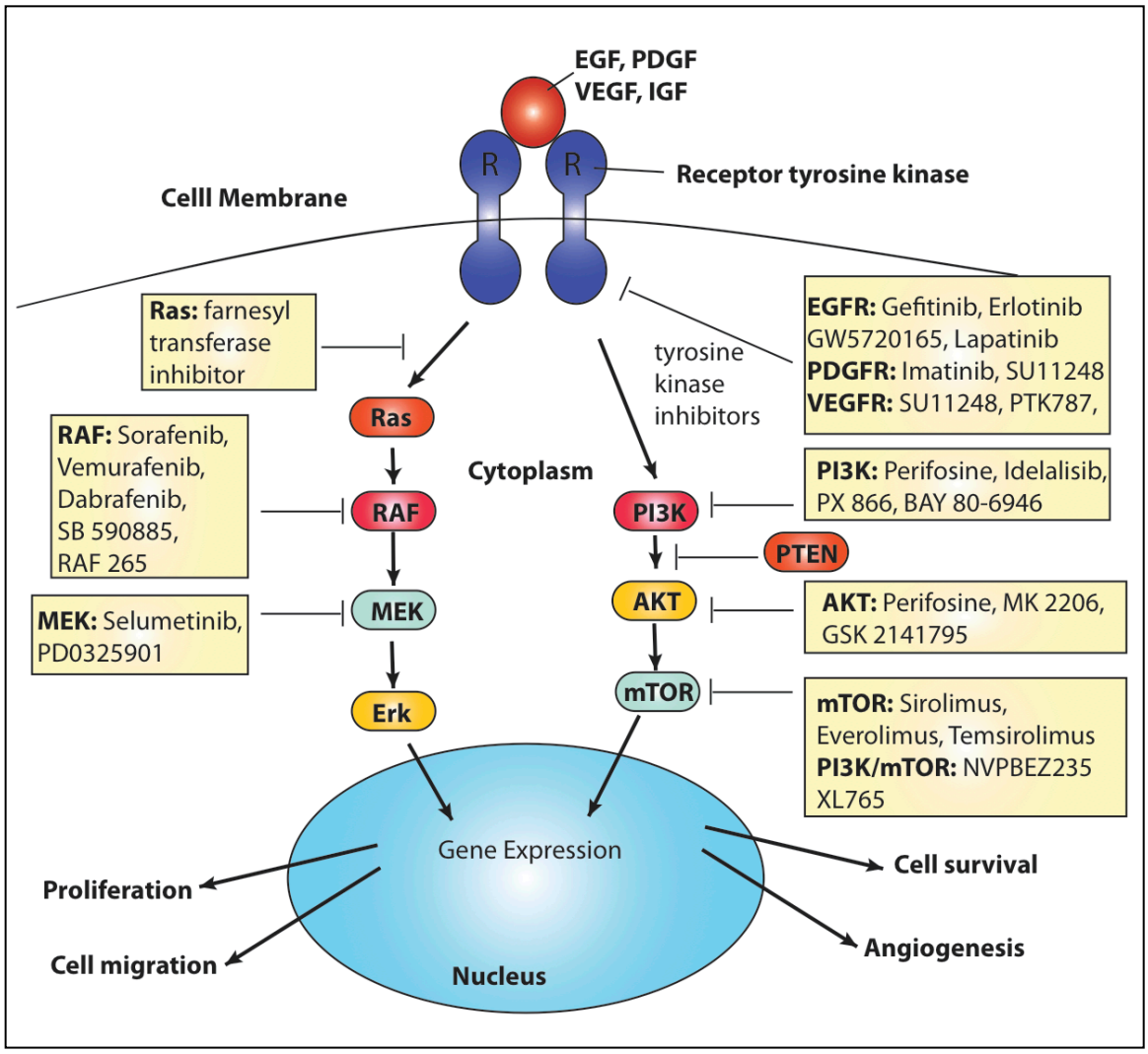

Figure 1.1: Targeted pharmacological inhibition of protein tyrosine kinase receptor pathways in cancer. Image adapted from Faivre et al.[55]

Pharmacological inhibition of the PI3K/AKT/mTOR pathway

Rapamycin (Sirolimus), originally an antifungal agent, was identified as an mTOR C1 allosteric inhibitor in 1991. Rapamycin's commercial semi-synthetic successors, the rapalogues Everolimus[25] and Temsirolimus[26], conserved the selectivity of the parent molecule while boasting an improved pharmacokinetic profile. However, instead of the expected wide-spectrum anti-cancer sensitivity, favorable results with

rapalogues have been seen in only a small handful of cancers. Specifically, rapalogue treatment prolonged progression-free survival in patients with renal cell carcinoma[27]. Similarly, temsirolimus was efficacious in the treatment of refractory mantle cell lymphoma[28] and everolimus was successful in treating pancreatic neuroendocrine tumors[29]. Beyond this limited list of applications rapamycin, and the ensuing rapalogues, have fallen short of expectations as cancer treatment. A study of breast cancer tissue samples, after four weeks of everolimus treatment showed increased levels of activated AKT when compared to untreated tissue[30]. This suggests that mTORC1 inhibition by rapalogues stimulates the PI3K-AKT pathway and may actually increase the survival and proliferation of cancer cells. Another explanation of rapamycin failure is that cancer cells that have acquired sufficiently high levels of constitutive mTORC1 activation are able to evade pharmacological inhibition of proliferation[31]. To remedy these inefficiencies, dual inhibitors of mTOR with either downstream or upstream regulators are currently in clinical trials. Notably, Novartis has generated the dual PI3K/mTOR inhibitor NVPBEZ235 that was effective in preclinical testing[32,33] and is currently in Phase II trials of advanced solid tumors in metastatic breast cancer[34]. A similar PI3K/mTOR dual inhibitor introduced by Sanofi-Aventis, was tested in Phase I trials. Results showed downregulation of PI3K-mTORC2 dependent AKT phosphorylation and reduced tumor growth[35]. Moreover, combining IGF1R antagonists with rapalogues has been shown to yield anti-proliferative effects in breast and prostate cancer[36]. This approach has also been extended to the EGFR receptor[37].

Pharmacological inhibition of the Ras/Raf/MEK/Erk pathway

The mitogen-activated protein kinase (MAPK) cascade is a key intracellular signaling pathway that regulates diverse cellular functions. The cascade is initiated by receptor tyrosine kinases at the cell surface. The pivotal role of the Ras/Raf/MEK/Erk pathway in a multitude of cellular functions underlies the importance of the cascade in oncogenesis and growth of transformed cells. Therefore, therapeutic targeting of these kinases cascade has been extensively investigated in cancer.

RAS activation is the first step in activation of the MAPK signaling cascade. Human tumors frequently feature point mutations in the RAS gene, a notable example being KRAS mutation in colorectal carcinoma, the detection of which is established as an independent prognostic marker in response to EGFR inhibitor treatment (cetuximab) in these tumors[38,39]. The covalent attachment of the farnesyl isoprenoid group to the HRAS, KRAS and NRAS proteins is the post-translational modification responsible for the stable localization of RAS to the plasma membrane and subsequent RAS activation. Therefore this was an obvious early target for the design of rational therapies in this pathway. Indeed, farnesyltransferase inhibitors showed promise in early murine models of mammary carcinomas, where tumors regressed impressively in response to treatment[40]. In addition, the drug was well tolerated by the animals. Unfortunately similar results have not been achieved in clinical trials with human patients, where farnesyltransferase inhibitors have been surprisingly ineffective.

The next step in the MAPK signaling cascade is RAF activation. Mutations of the RAF gene are not as ubiquitous as RAS mutations. However, they are prevalent in a few specific malignancies. B-RAF mutations can be found in approximately 63%[41] of melanomas, 45% of papillary thyroid cancers[42] and 36% of ovarian cancers[43]. Mutations on the BRAF gene occur almost invariably at the V600E position and result in a 'gain of function' constitutively active BRAF. The first RAF inhibitor to be investigated in clinical trials of melanoma was sorafenib, designed to block the downstream CRAF, rather than BRAF, which demonstrated modest response rates as an adjuvant treatment in patients receiving chemotherapy[44]. Sorafenib may therefore be valuable in combination therapy with V600E BRAF inhibitors. Vemurafenib was a newer and selective inhibitor of active V600E BRAF approved in 2011 by the FDA for the treatment of late-stage melanoma. Vemurafenib displayed marked selectivity in both cell-based assays and animal models. Potent cytotoxic effects were limited to BRAF-mutated cells and led to tumor regression without significant generalized toxicity[45]. Vemurafenib has fared well in the clinic. Most patients respond to the drug leading to longer progression-free survival rates[46]. Here too however resistance inevitably sets in which indicates the need for combination therapy with upstream/downstream inhibitors.

Further down the MAPK cascade are the MEK and Erk protein kinases. Blocking MAPK via small-molecule MEK inhibitors has come to the forefront as an exciting approach in cancer therapeutics. Initial MEK inhibitors were effective in preclinical

studies but lacked the desirable pharmacokinetic profile for human testing. Optimization led to the design of the second-generation MEK inhibitor Selumetinib (AZD6244) that proceeded to clinical trials. Pre-treatment and post-treatment tumor biopsies obtained from 17 patients showed a mean 83% reduction in nuclear Erk phosphorylation, an indication that Selumetinib achieved target modulation[47]. However, in terms of efficacy endpoints no objective response to treatment was identified in these patients other than stable disease lasting over 5 months. PD0325901, another MEK inhibitor that was evaluated in the clinic, demonstrated a similar result of 84% suppression in Erk phosphorylation as compared to baseline expression[48]. Development of this compound however was stopped due to high toxicity associated with treatment.

Molecular Signatures Predict Drug Response in Breast Cancer Cell Lines

As the list of experimental tyrosine kinase inhibitors grows, the need for tools that will successfully predict patient response on the basis of the molecular make-up of the particular tumor becomes ever more pressing. Specifically in breast cancer, an initiative across academic institutions was spurred in order to study the varied genomic profiles across a large collection of breast cancer cell lines and extract signatures that will predict breast tumor response to particular inhibitors. In a pioneering research paper Neve et al.[49] confirm that cell lines display the same heterogeneity in copy number and expression abnormalities as primary breast tumors. The 51 cell lines employed in this study carried almost all of the recurrent genomic abnormalities associated with clinical outcome in primary tumors. In

addition the breast cancer cell lines clustered into basal-like and luminal expression subsets, much like primary tumors do. In regards to molecular signatures indicative of response to Trastuzumab, they found that increased protein levels of MEK, ESR1, TYK2, FASN, GRB7 and MAPK1/3 most strongly correlated with response to treatment. Conversely protein levels associated with Trastuzumab resistance included high levels of SFN, CAV2, GRB2, RB1 and FLNA. Gene ontology analysis suggests that the upregulation of genes involved in insulin/MAPK signaling predicts response to Herceptin, whereas the mTOR pathway, Toll-like receptor pathway, N-glycan biosynthesis and inositol-phosphate signaling are associated with resistance[49].

In a subsequent study this approach was expanded to a screen of 49 breast cancer cell lines for response to 77 therapeutic compounds, including hormonal inhibitors, kinase inhibitors and conventional chemotherapeutic agents (taxanes, platinum compounds and anthracyclins)[50] . The authors found that overall responses to drugs with similar mechanisms and targets were highly correlated across the cell lines. Namely HER2-amplified cell lines were preferentially sensitive to compounds targeting EGFR and/or HER2, like AG1478, BIBW2992 and Gefitinib. The chemotherapeutics Etoposide, Docetaxel and cisplatin showed preferential activity in basal or claudin-low cell lines, which was in accordance with clinical observations[51,52]. Moreover, some compounds targeting the mitotic apparatus, Ispinisib and GSK913195, showed no significant subtype specificity. The authors concluded by noting that additional work remains before the signatures reported in

their study could be used to select patients for clinical trials. Robust and reliable molecular assays to evaluate clinical samples are currently lacking.

Another study further expanded this approach by screening a total of 479 cancer cell lines with 24 anti-cancer drugs[53]. Their findings echoed those of Heiser et al. regarding EGFR mutations and HER2 amplifications being predictors of Erlotinib and Lapatinib response respectively. Moreover, and not surprisingly, they found that BRAF and NRAS mutations were among the top four predictors of sensitivity to the MEK inhibitor PD-0325901. Additional predictive features for MEK inhibition included expression of PTEN, PTPN5 and SPRY2. Because this study was done across cancer cell lines derived from a variety of solid tumors as well as leukemias and lymphomas, predictions connecting the cell line lineage to drug response were made possible. Namely, the haematological lineage of the cancer was a predictor of HDAC inhibitor (Panobinoblast) sensitivity. Similarly, most myeloma cell lines were sensitive to IGF1 receptor inhibitor AEW541.

Finally, a study carried out by Niepel et al.[54] offered an insightful variation in this line of research. Here the authors profiled signaling pathway activity in a collection of 37 breast cancer cell lines before and after stimulation with physiologically relevant ligands. Based on their measurements they constructed models that significantly predicted sensitivity to 23 targeted therapeutics. They found that the response to the growth factor receptor ligand heregulin effectively predicted the sensitivity of cells to drugs targeting the PI3K and Akt pathway, whereas in contrast

the abundance of Akt or the mutational status of the enzymes in the pathway did not. They observed that unsupervised clustering divided the cell lines into clusters primarily on the basis of the abundance of ligand responsiveness of receptors such as c-MET, FGFR4 and IL-6R. TNBC cells were more responsive to EGF and the c-Met ligand HGF, whereas HR+ cells responded robustly to FGF-2 and HRG (heregulin). HER2-amplified cell lines responded weakly to most growth factors, but a subset of them responded to IL-6.

1.3 Novel diagnostic tools in breast cancer

The last part of my PhD involved analysis of exosomes, small vesicles derived from breast cancer cells, in the hope of identifying biomarkers that predict drug responsiveness. To set up this part of my work I will review novel approaches aimed to develop predictive biomarkers, with a focus on methods that do not require inserting a needle or biopsy gun into the primary tumor.

As discussed previously, molecular profiling of cancer is a preferred method of classifying tumors and matching patients with targeted therapeutics. Still, the clinical tools that will facilitate this matching process are not yet in place. Currently, physicians rely on serial surgical biopsies in order to characterize the molecular subtype of a cancerous lesion. However, biopsies are invasive procedures that carry morbidity risk due to seeding, the spread of cancer cells along the path of the needle track at the biopsy site[56]. Another clinical practice is the immuno-histological staining of archival resected tissue in order to drive clinical decisions at later stages

of the disease. This method discounts the previously discussed clonal and molecular drift that a cancer undergoes during the metastatic process. Treatment decisions are often made according to the molecular subtype of the primary tumor, but it is the metastatic disease that invariably proves fatal to patients. Another shortcoming of current diagnostic practices is that once a primary lesion has been resected there is no clinical method to diagnose micrometastatic disease before it becomes radiographically detectable and/or symptomatic. Moreover, despite some impressive clinical successes with kinase-targeting therapies, treatment-responsive patients ultimately relapse as a result of acquired resistance. This too underlines the dire need for biodynamic diagnostic tools that closely monitor treatment efficacy. Below we will discuss some recent advances in the development of liquid biopsies, a novel term describing the variety of new technologies aiming to identify cancer biomarkers present in the bloodstream of patients.

Cell free nucleic acids

Cell-free nucleic acids (cfNAs) came to the forefront as a possible diagnostic tool in 1994 when two independent studies published the detection of mutated RAS fragments in the blood of cancer patients[57,58]. cfNAs is a broad category encompassing cell free DNA as well as cell free RNA. Particularly cfDNA is thought to arise in the blood stream of patients via a variety of processes. It is primarily thought to be a result of apoptotic or necrotic cell death of cancer cells in the tumor microenvironment, while other studies show the active secretion of mitochondria, containing cfDNA[59]. Lastly cfDNA is thought to be released in the bloodstream upon

the death of circulating tumor cells (CTCs)[60,61]. In terms of stability, cfDNA is cleared from the blood by the liver and kidney and has an approximate half-life in circulation ranging from 15 minutes to several hours[62]. Cell free RNA (cfRNA) appears to be highly stable in the bloodstream, although its clearance rate has not been explicitly quantified yet. This implies that cfRNA may be protected from degradation by being packaged into exosomes, microparticles or microvesicles that are either actively secreted or shed from cellular surfaces into the bloodstream[63,64].

The hope regarding cfDNA is that it will carry specific gene mutations relevant in cancer therapy, such as KRAS, BRAF and EGFR. However, as this technology is still in a nascent stage issues of assay specificity and sensitivity need to be addressed. Assays targeting DNA mutations require that the mutation in the tumor occur frequently and at a specific genomic site. However, that is generally not the case for clinically relevant mutations. An illustrative example is the detection of KRAS mutation in tumor tissue derived from pancreas, colon and lung but the failure of detecting the mutation in cfDNA derived from the respective patient's blood samples[65–67]. Beyond cfDNA, circulating nucleosomes -which are histone octamer structures wrapped by a 200 base pair-long DNA strand- are also found in patient circulation. The presence of circulating nucleosomes in itself is not an indicator of malignant disease[68]. However, due to the fact that nucleosomes are typically products of cancer cell death, they have been used for monitoring the efficacy of cytotoxic cancer therapies. For example, platinum-based chemotherapy induced caspase-dependent apoptosis of tumor cells and an increase in circulating

nucleosomes in the blood of patients with ovarian cancer[69]. Overall the cfNA technologies are facing practical difficulties of standardizing procedures across clinical centers. Below we will specifically discuss alternate technologies that have gained FDA-approval and have translated in clinical practice.

Circulating tumor cells (CTCs)

Tumor-derived epithelial cells have been identified in peripheral blood of cancer patients and are thought to be the origin of intractable metastatic disease[70–72]. The advantage of CTCs as a diagnostic technology is that they are rarely found in healthy subjects, while they are prevalent and detectable in patients with solid tumors. Particularly studies performed in breast[70], colorectal[73] and prostate[74] cancer have established the number of CTCs before treatment as an independent predictor of progression-free survival. CellSearch, was the first diagnostic technology to receive FDA-approval for the isolation of CTCs from peripheral blood. The technology relies on immuno-magnetic separation of epithelial cells using anti-epithelial cell adhesion molecule (EpCAM) antibodies and subsequent staining for visualization[75]. There are a number of caveats associated with this approach. EpCAM-based detection has low sensitivity in EpCAM-negative cancers. Agressive tumor cells often downregulate EpCAM as a result of the epithelial-mesenchymal transition process during metastasis and can pass undetected through the CellSearch system[76]. In addition, the lengthy isolation and staining steps are accompanied by considerable cell loss[77,78]. Taking into consideration that CTCs are already extremely rare in the bloodstream, comprising as few as one cell for every 10^9 blood cells in the

circulation of patients with metastatic cancer[79,80], cell losses during the isolation process hold the potential of a false-negative diagnosis. To remedy these issues, novel technologies are under investigation that would improve the capturing rate of CTCs. These include but are not limited to nuclear magnetic resonance profiling[81] and microfluidic approaches[82].

Cancer exosomes and microvesicles

Exosomes are nanovesicles of 30 to 100nm diameter that form in the endosomal cytoplasmic compartment and are subsequently released in the extracellular space. Exosome production is not unique to epithelial cancer cells. On the contrary, a wide variety of cell types have demonstrated the capability of producing these vesicles, including reticulocytes, dendritic cells, B cells, T cells, mast cells and embryonic cells[83,84]. However, their accumulation in the peripheral circulation appears to be unique to cancer and pregnancy[85,86].

Clinical studies performed in melanoma and glioblastoma have shown that exosomes carry cancer-specific protein signatures characteristic of the primary tumor mass[87,88]. In vitro proteomic studies of the colon tumor cell line LIM1215 and the breast cancer cell line MDAMB231 reinforce these clinical findings and confirm the presence of multiple host cell-specific proteins in the corresponding exosomes[89,90]. In addition to the specificity of the exosome protein content, the exosomal protein concentration in itself has been recognized as a clinical marker of disease progression. Peinado et al. showed that in melanoma-derived exosomes,

protein concentration in patients with stage 4 disease was the highest compared to all other stages and normal controls[87]. Taylor et al. recorded an equivalent observation in exosomes derived from patients with varying stages of ovarian cancer[91]. Beyond their protein composition, exosomes carry yet another payload of diagnostic value: microRNAs. Studies in glioblastoma[92] and ovarian cancer[91] have identified miRNA signatures indicative of the specific malignancy in circulating exosomes. Nilsson et al.[93] reached a similar conclusion in a study that examined urine-derived exosomes from patients with prostate cancer for mRNA biomarkers.

In terms of their physiological role during disease progression, cancer exosomes are thought to be modulators of the tumor microenvironment and once in circulation, to participate in the priming of the metastatic niche. Exosomes are known to promote the horizontal transfer of molecules to recipient cells[94–96]. In particular, Skog et al. showed that glioblastoma exosomes carry angiogenic proteins that stimulate endothelial cells and furthermore promote the proliferation of glioma cells[92]. Peinado et al. published another illustrative example of exosome activity. The authors incubated bone marrow-derived cells with purified exosomes from highly metastatic melanoma carrying the tyrosine kinase MET receptor. They showed that a functional MET was successfully transferred on the surface of the bone marrow cells and were subsequently able to detect the phosphorylation of downstream mediators of MET upon treatment of the cells with hepatocyte growth factor[87]. Yet another study in breast cancer, linked HER2-overexpressing breast tumor derived exosomes with chemoresistance to targeted Trastuzumab and Lapatinib therapies.

The authors showed that exosomes carry a functional HER2 on their surface that successfully binds the targeted therapies. Their findings suggest that cancer exosomes can act as a drug sink in the patients' circulation, modulating targeted therapy sensitivity[97].

In contrast to the rareness of circulating tumor cells (CTCs), tumor exosomes are advantageous for diagnostic purposes due to their ubiquity in the circulation of patients with malignant and advanced disease. However, diagnostic technologies geared towards exosome isolation from plasma face some common challenges with the technologies developed for CTC detection. Protocols for exosome purification usually entail multiple rounds of ultracentrifugation in order to pellet the small vesicles. In addition to tumor exosomes, ultracentrifugation co-precipitates exosomes of blood and immune cell origin. These contaminating vesicles carry miRNAs, which can confound miRNA cancer specific signatures leading to clinical diagnoses[98]. In order to separate specifically the tumor-derived vesicles, immunoprecipitation with EpCAM antibodies is frequently employed[89,91]. Much like in CTC isolation, exosomes from aggressive tumor cells that downregulate EpCAM will remain undetected by this method. It is therefore not surprising that the first exosome diagnostic technology to make it to the clinic is a kit commercializing the purification of exosomes from urine samples –a significantly simpler biological fluid- for the detection of kidney and prostate cancer[99]. The absence of contaminating vesicles from non-tumor cell sources in urine obviates the need for an immunoprecipitation step. In addition to this approach, alternative technologies

for exosome capture –such as nuclear magnetic resonance profiling[88] and microfluidic approaches[100]- have been scaled to the exosome nanometer length-scale and are being tested for exosome capture efficacy.

1.4 Specific aims of the present study

Specific aim #1: This research aims to identify chemical cues secreted by breast cancer cells, and more specifically focuses on the unveiling of anti-proliferative and pro-apoptotic signals among the prolific secretions of breast cancer cell lines.

The epigenetic plasticity of cancer cells along with the heterogeneity and clonal evolution observed within solid tumors were the spring board for this research project. While heterogeneity in tumors has been well documented, the consequences of this heterogeneity on the growth of different cell clones has not been systematically investigated until now. Seeing that tumor clones physiologically compete for dominance given a re stricted nutrient environment, we anchor our research in the hypothesis that cancer cells are in competition to either halt the growth or downright initiate an apoptotic cascade on neighboring clones. We reason that cancer cell secreted factors that hamper the growth of neighboring cell lines make attractive low-toxicity drug candidates, since such molecules might specifically target malignancy while leaving healthy tissue intact.

In chapter 2, we launch this investigation by presenting a 20x20 conditioned medium (CM) breast cancer cell culture screen. This screen reveals two conditioned

media that have strong pro-apoptotic activity on the majority of cell lines tested. We embark in further biochemical characterization of the strongest apoptosis-inducing conditioned media. Next, we fractionate the CMs into a particulate and a soluble fraction by ultracentrifugation and test both fractions for apoptotic activity. In chapter 3 transcriptomic and proteomic approaches are employed to identify gene and protein candidates in the cancer cell secretions that have pro-apototic activity. We conclude the chapter with a comparison of the proteomic content of the particulate fractions to the full conditioned media. We identify a small number of proteins unique to the CMs and absent from the activity-free particulate fractions, which are mechanistic candidates for the apoptotic activity.

Specific aim #2: This research aims to evaluate the effectiveness and functionality of breast cancer exosomes as diagnostic material.

In addition to soluble extracellular signals, the literature indicates and our experiments confirm that cancer cell lines also secrete a particulate fraction: cancer exosomes. Several studies have highlighted the diagnostic potential of cancer exosomes. However no study has specifically and systematically addressed the protein composition of breast cancer exosomes. We hypothesize that breast cancer exosomes carry cell line receptors, and possibly also downstream cytoplasmic kinases, matching their cell lines of origin. The implications of this finding would carry diagnostic significance, seeing that the protein profiling of tumor exosomes could guide the choice of specific inhibitor treatment in a clinical setting.

In chapter 4 we therefore explore the diagnostic potential of exosomes, by screening six breast cancer cell lines and their corresponding exosomes for common diagnostic markers as well as downstream protein kinases. We follow this up by a proteomic analysis of two types of breast cancer exosomes, in order to formulate a broader understanding of overall content of these vesicles and the possible cellular functions conserved within these anuclear units.

References

1. Hanahan, D. & Weinberg, R. A. The Hallmarks of Cancer. *Cell* **100,** 57–70 (2000).

2. Hanahan, D. & Weinberg, R. a. Hallmarks of cancer: the next generation. *Cell* **144,** 646–74 (2011).

3. DuFort, C. C., Paszek, M. J. & Weaver, V. M. Balancing forces: architectural control of mechanotransduction. *Nat. Rev. Mol. Cell Biol.* **12,** 308–19 (2011).

4. Ulrich, T. a, de Juan Pardo, E. M. & Kumar, S. The mechanical rigidity of the extracellular matrix regulates the structure, motility, and proliferation of glioma cells. *Cancer Res.* **69,** 4167–74 (2009).

5. Weaver, V. M. *et al*. Beta4 Integrin-Dependent Formation of Polarized Three-Dimensional Architecture Confers Resistance To Apoptosis in Normal and Malignant Mammary Epithelium. *Cancer Cell* **2,** 205–16 (2002).

6. Debnath, J. *et al*. The Role of Apoptosis in Creating and Maintaining Luminal Space within Normal and Oncogene-Expressing Mammary Acini Brigham and Women ' s Hospital. *Cell* **111,** 648–649 (2002).

7. Lee, L. M. J., Seftor, E. a, Bonde, G., Cornell, R. a & Hendrix, M. J. C. The fate of human malignant melanoma cells transplanted into zebrafish embryos: assessment of migration and cell division in the absence of tumor formation. *Dev. Dyn.* **233,** 1560–70 (2005).

8. Kulesa, P. M. *et al*. Reprogramming metastatic melanoma cells to assume a neural crest cell-like phenotype in an embryonic microenvironment. *Proc. Natl. Acad. Sci. U. S. A.* **103,** 3752–7 (2006).

9. DeCosse, J. J., Gossens, C. L., Kuzma, J. F. & Unsworth, B. R. Breast Cancer: Induction of Differentiation by Embryonic Tissue. *Sci. New Ser.* **181,** 1057–1058 (1973).

10. Polyak, K. Breast cancer : origins and evolution. *J. Clin. Invest.* **117,** 3155–3163 (2007).

11. Heppner, G. H. Tumor Cell Societies. *J. Natl. Cancer Inst*. 648–649 (1989).

12. Heppner, G. H. Tumor heterogeneity. *Cancer Res*. **44,** 2259–65 (1984).

13. Fujii, H., Marsh, C., Cairns, P., Sidransky, D. & Gabrielson, E. Genetic Divergence in the Clonal Evolution of Breast Cancer. *Cancer Res*. **56,** 1493–1497 (1996).

14. Kuukasjärvi, T. *et al*. Genetic Heterogeneity and Clonal Evolution Underlying Development of Asynchronous Metastasis in Human Breast Cancer Genetic Heterogeneity and Clonal Evolution Underlying Development of Asynchronous Metastasis in Human Breast Cancer '. *Cancer Res*. **57,** 1597–1604 (1997).

15. Symmans, W. F., Liu, J., Knowles, D. M. & Inghirami, G. Breast cancer heterogeneity: evaluation of clonality in primary and metastatic lesions. *Hum. Pathol*. **26,** 210–6 (1995).

16. www.cancer.gov/cancertopics/pdq/treatment/breast/healthprofessional. *Natl. Cancer Inst*.

17. Breast, E., Trialists, C. & Group, C. Effects of chemotherapy and hormonal therapy for early breast cancer on recurrence and 15-year survival: an overview of the randomised trials. *Lancet* **365,** 1687–717 (2005).

18. Colleoni, M. *et al*. Tamoxifen after adjuvant chemotherapy for premenopausal women with lymph node-positive breast cancer: International Breast Cancer Study Group Trial 13-93. *J. Clin. Oncol*. **24,** 1332–41 (2006).

19. Vogel, B. C. L. *et al*. Efficacy and Safety of Trastuzumab as a Single Agent in First-Line Treatment of HER2-Overexpressing Metastatic Breast Cancer. **20,** 719–726 (2003).

20. Cobleigh, M. a *et al*. Multinational study of the efficacy and safety of humanized anti-HER2 monoclonal antibody in women who have HER2-overexpressing metastatic breast cancer that has progressed after chemotherapy for metastatic disease. *J. Clin. Oncol*. **17,** 2639–48 (1999).

21. Gianni, L. *et al*. Efficacy and safety of neoadjuvant pertuzumab and trastuzumab in women with locally advanced, inflammatory, or early HER2-positive breast cancer (NeoSphere): a randomised multicentre, open-label, phase 2 trial. *Lancet Oncol*. **13,** 25–32 (2012).

22. Dent, R. *et al*. Triple-negative breast cancer: clinical features and patterns of recurrence. *Clin. Cancer Res*. **13,** 4429–34 (2007).

23. Shastry, M. & Yardley, D. a. Updates in the treatment of basal/triple-negative breast cancer. *Curr. Opin. Obstet. Gynecol*. **25,** 40–8 (2013).

24. Valabrega, G., Montemurro, F. & Aglietta, M. Trastuzumab: mechanism of action, resistance and future perspectives in HER2-overexpressing breast cancer. *Ann. Oncol*. **18,** 977–84 (2007).

25. Rini, B. I. Temsirolimus, an inhibitor of mammalian target of rapamycin. *Clin. Cancer Res*. **14,** 1286–90 (2008).

26. Gabardi, S. & Baroletti, S. a. Everolimus: a proliferation signal inhibitor with clinical applications in organ transplantation, oncology, and cardiology. *Pharmacotherapy* **30,** 1044–56 (2010).

27. Hudes, G. *et al*. Temsirolimus, interferon alfa, or both for advanced renal-cell carcinoma. *N. Engl. J. Med*. **356,** 2271–81 (2007).

28. Hess, G. *et al*. Phase III study to evaluate temsirolimus compared with investigator's choice therapy for the treatment of relapsed or refractory mantle cell lymphoma. *J. Clin. Oncol*. **27,** 3822–9 (2009).

29. Yao, J. C. *et al*. Everolimus for advanced pancreatic neuroendocrine tumors. *N. Engl. J. Med*. **364,** 514–23 (2011).

30. O'Reilly, K. E. *et al*. mTOR inhibition induces upstream receptor tyrosine kinase signaling and activates Akt. *Cancer Res*. **66,** 1500–8 (2006).

31. Dowling, R. J. O. *et al*. mTORC1-mediated cell proliferation, but not cell growth, controlled by the 4E-BPs. *Science* **328,** 1172–6 (2010).

32. Baumann, P., Mandl-Weber, S., Oduncu, F. & Schmidmaier, R. The novel orally bioavailable inhibitor of phosphoinositol-3-kinase and mammalian target of rapamycin, NVP-BEZ235, inhibits growth and proliferation in multiple myeloma. *Exp. Cell Res*. **315,** 485–97 (2009).

33. Manara, M. C. *et al*. NVP-BEZ235 as a new therapeutic option for sarcomas. *Clin. Cancer Res*. **16,** 530–40 (2010).

34. clinicaltrials.gov/ct2/results?term=NVPBEZ235. *ClinicalTrials.gov*

35. Molckovsky, A. & Siu, L. L. First-in-class, first-in-human phase I results of targeted agents: highlights of the 2008 American society of clinical oncology meeting. *J. Hematol. Oncol*. **1,** 20 (2008).

36. Baumann, P., Hagemeier, H., Mandl-Weber, S., Franke, D. & Schmidmaier, R. Myeloma cell growth inhibition is augmented by synchronous inhibition of the insulin-like growth factor-1 receptor by NVP-AEW541 and inhibition of mammalian target of rapamycin by Rad001. *Anticancer. Drugs* **20,** 259–66 (2009).

37. Rao, R. D. *et al*. Disruption of Parallel and Converging Signaling Pathways Contributes to the Synergistic Antitumor Effects of Simultaneous mTOR and EGFR Inhibition in GBM Cells. *Neoplasia* **7,** 921–929 (2005).

38. Lièvre, A. *et al*. KRAS mutations as an independent prognostic factor in patients with advanced colorectal cancer treated with cetuximab. *J. Clin. Oncol*. **26,** 374–9 (2008).

39. Di Fiore, F. *et al*. Clinical relevance of KRAS mutation detection in metastatic colorectal cancer treated by Cetuximab plus chemotherapy. *Br. J. Cancer* **96,** 1166–9 (2007).

40. Kohl, N. E. *et al*. Inhibition of farnesyltransferase induces regression of mammary and salivary carcinomas in ras transgenic mice. *Nat. Med*. **1,** 792–797 (1995).

41. Brose, M. S. *et al*. BRAF and RAS Mutations in Human Lung Cancer and Melanoma BRAF and RAS Mutations in Human Lung Cancer and Melanoma 1. 6997–7000 (2002).

42. Xing, M. BRAF mutation in thyroid cancer. *Endocr. Relat. Cancer* **12,** 245–62 (2005).

43. Sieben, N. L. G. *et al*. In ovarian neoplasms, BRAF, but not KRAS, mutations are restricted to low-grade serous tumours. *J. Pathol*. **202,** 336–40 (2004).

44. Agarwala, S. S. *et al*. Randomized phase III study of paclitaxel plus carboplatin with or without sorafenib as second-line treatment in patients with advanced melanoma. *J. Clin. Oncol*. **25,** 8510 (2007).

45. Yang, H. *et al*. RG7204 (PLX4032), a selective BRAFV600E inhibitor, displays potent antitumor activity in preclinical melanoma models. *Cancer Res*. **70,** 5518–27 (2010).

46. Flaherty, K. T. *et al*. Inhibition of mutated, activated BRAF in metastatic melanoma. *N. Engl. J. Med*. **363,** 809–19 (2010).

47. Adjei, A. a *et al*. Phase I pharmacokinetic and pharmacodynamic study of the oral, small-molecule mitogen-activated protein kinase kinase 1/2 inhibitor AZD6244 (ARRY-142886) in patients with advanced cancers. *J. Clin. Oncol*. **26,** 2139–46 (2008).

48. Lorusso, P. *et al*. A phase 1-2 clinical study of a second generation oral MEK inhibitor, PD 0325901 in patients with advanced cancer. *J Clin Oncol (Meeting Abstr*. **23,** 3011– (2005).

49. Neve, R. M. *et al*. A collection of breast cancer cell lines for the study of functionally distinct cancer subtypes. *Cancer Cell* **10,** 515–27 (2006).

50. Heiser, L. M. *et al*. Subtype and pathway speci fi c responses to anticancer compounds in breast cancer. (2011). doi:10.1073/pnas.1018854108/-/DCSupplemental.www.pnas.org/cgi/doi/10.1073/pnas.1018854108

51. Carey, L. a *et al*. The triple negative paradox: primary tumor chemosensitivity of breast cancer subtypes. *Clin. Cancer Res*. **13,** 2329–34 (2007).

52. Silver, D. P. *et al*. Efficacy of neoadjuvant Cisplatin in triple-negative breast cancer. *J. Clin. Oncol*. **28,** 1145–53 (2010).

53. Barretina, J. *et al*. The Cancer Cell Line Encyclopedia enables predictive modelling of anticancer drug sensitivity. *Nature* **483,** 603–7 (2012).

54. Niepel, M. *et al*. Profiles of Basal and stimulated receptor signaling networks predict drug response in breast cancer lines. *Sci. Signal*. **6,** ra84 (2013).

55. Faivre, S., Kroemer, G. & Raymond, E. Current development of mTOR inhibitors as anticancer agents. *Nat. Rev. Drug Discov*. **5,** 671–88 (2006).

56. Robertson, E. G. & Baxter, G. Tumour seeding following percutaneous needle biopsy: the real story! *Clin. Radiol*. **66,** 1007–14 (2011).

57. Sorenson, G. D. *et al*. Soluble normal and mutated DNA sequences from single-copy genes in human blood. *Cancer Epidemiol. Biomarkers Prev*. **3,** 67–71 (1994).

58. Vasioukhin, V. *et al*. Point mutations of the N-ras gene in the blood plasma DNA of patients with myelodysplastic syndrome or acute myelogenous leukaemia. *Br. J. Haematol*. **86,** 774–9 (1994).

59. Stroun, M. *et al*. The origin and mechanism of circulating DNA. *Ann. N. Y. Acad. Sci*. **906,** 161–8 (2000).

60. Schwarzenbach, H. *et al*. Detection of tumor-specific DNA in blood and bone marrow plasma from patients with prostate cancer. *Int. J. Cancer* **120,** 1465–71 (2007).

61. Schwarzenbach, H. *et al*. Cell-free tumor DNA in blood plasma as a marker for circulating tumor cells in prostate cancer. *Clin. Cancer Res*. **15,** 1032–8 (2009).

62. Fleischhacker, M. & Schmidt, B. Circulating nucleic acids (CNAs) and cancer--a survey. *Biochim. Biophys. Acta* **1775,** 181–232 (2007).

63. Orozco, A. F. & Lewis, D. E. Flow cytometric analysis of circulating microparticles in plasma. *Cytometry. A* **77,** 502–14 (2010).

64. Cocucci, E., Racchetti, G. & Meldolesi, J. Shedding microvesicles: artefacts no more. *Trends Cell Biol*. **19,** 43–51 (2009).

65. Castells, a *et al*. K-ras mutations in DNA extracted from the plasma of patients with pancreatic carcinoma: diagnostic utility and prognostic significance. *J. Clin. Oncol*. **17,** 578–84 (1999).

66. Ryan, B. M. *et al*. A prospective study of circulating mutant KRAS2 in the serum of pateints with colorectal neoplasia: strong prognostic indicator in postoperative follow up. *Gut* **52,** 101–109 (2003).

67. Wang, S. *et al*. Potential clinical significance of a plasma-based KRAS mutation analysis in patients with advanced non-small cell lung cancer. *Clin. Cancer Res*. **16,** 1324–30 (2010).

68. Holdenrieder, S. *et al*. Nucleosomes in serum of patients with benign and malignant diseases. *Int. J. Cancer* **95,** 114–20 (2001).

69. Wimberger, P. *et al*. Impact of platinum-based chemotherapy on circulating nucleic acid levels, protease activities in blood and disseminated tumor cells in bone marrow of ovarian cancer patients. *Int. J. Cancer* **128,** 2572–80 (2011).

70. Cristofanilli, M. Circulating tumor cells, disease progression, and survival in metastatic breast cancer. *Semin. Oncol*. **33,** S9–14 (2006).

71. Steeg, P. S. Tumor metastasis: mechanistic insights and clinical challenges. *Nat. Med*. **12,** 895–904 (2006).

72. Gupta, G. P. & Massagué, J. Cancer metastasis: building a framework. *Cell* **127,** 679–95 (2006).

73. Cohen, S. J. *et al*. Relationship of circulating tumor cells to tumor response, progression-free survival, and overall survival in patients with metastatic colorectal cancer. *J. Clin. Oncol*. **26,** 3213–21 (2008).

74. Scher, H. I. *et al*. Circulating tumour cells as prognostic markers in progressive, castration-resistant prostate cancer: a reanalysis of IMMC38 trial data. *Lancet Oncol*. **10,** 233–9 (2009).

75. Veridex. www.cellsearchctc.com.

76. Armstrong, A. J. *et al*. Circulating tumor cells from patients with advanced prostate and breast cancer display both epithelial and mesenchymal markers. *Mol. Cancer Res.* **9,** 997–1007 (2011).

77. Punnoose, E. a *et al*. Molecular biomarker analyses using circulating tumor cells. *PLoS One* **5,** e12517 (2010).

78. Riethdorf, S. *et al*. Detection of circulating tumor cells in peripheral blood of patients with metastatic breast cancer: a validation study of the CellSearch system. *Clin. Cancer Res.* **13,** 920–928 (2007).

79. Rolle, A. *et al*. Increase in number of circulating disseminated epithelial cells after surgery for non-small cell lung cancer monitored by MAINTRAC(R) is a predictor for relapse: A preliminary report. *World J. Surg. Oncol.* **3,** 18 (2005).

80. Zieglschmid, V., Hollmann, C. & Böcher, O. Detection of disseminated tumor cells in peripheral blood. *Crit. Rev. Clin. Lab. Sci.* **42,** 155–96 (2005).

81. Castro, C. M. *et al*. Miniaturized nuclear magnetic resonance platform for detection and profiling of circulating tumor cells. *Lab Chip* **14,** 14–23 (2014).

82. Nagrath, S. *et al*. Isolation of rare circulating tumour cells in cancer patients by microchip technology. *Nature* **450,** 1235–9 (2007).

83. Raposo, G. *et al*. Accumulation of major histocompatibility complex class II molecules in mast cell secretory granules and their release upon degranulation. *Mol. Biol. Cell* **8,** 2631–45 (1997).

84. Heijnen, H., Schiel, A., Fijnheer, R., Geuze, H. & Sixma, J. Activation platelets release two types of membrane vesicles: microvesicles by surface shedding and exosomes derived from exocytosis of multivesicular bodies and alpha granules. *Blood* **94,** 3791–3799 (1999).

85. Taylor, D. D. & Black, P. H. Shedding of plasma membrane fragments. Neoplastic and developmental importance. *Dev. Biol. (N. Y. 1985)* **3,** 33–57 (1986).

86. Taylor, D. D., Bohler, H. C. & Gercel-Taylor, C. Pregnancy-linked suppression of TcR signaling pathways by a circulating factor absent in recurrent spontaneous pregnancy loss (RPL). *Mol. Immunol.* **43,** 1872–80 (2006).

87. Peinado, H. *et al*. Melanoma exosomes educate bone marrow progenitor cells toward a pro-metastatic phenotype through MET. *Nat. Med.* **18,** 883–91 (2012).

88. Shao, H. *et al*. Protein typing of circulating microvesicles allows real-time monitoring of glioblastoma therapy. *Nat. Med.* **18,** 1835–40 (2012).

89. Mathivanan, S. *et al*. Proteomics analysis of A33 immunoaffinity-purified exosomes released from the human colon tumor cell line LIM1215 reveals a tissue-specific protein signature. *Mol. Cell. Proteomics* **9,** 197–208 (2010).

90. Palazzolo, G. *et al*. Proteomic Analysis of Exosome-like Vesicles Derived from Breast Cancer Cells. *Anticancer Res.* **32,** 847–60 (2012).

91. Taylor, D. D. & Gercel-Taylor, C. MicroRNA signatures of tumor-derived exosomes as diagnostic biomarkers of ovarian cancer. *Gynecol. Oncol.* **110,** 13–21 (2008).

92. Skog, J. *et al*. Glioblastoma microvesicles transport RNA and proteins that promote tumour growth and provide diagnostic biomarkers. *Nat. Cell Biol.* **10,** 1470–6 (2008).

93. Nilsson, J. *et al*. Prostate cancer-derived urine exosomes: a novel approach to biomarkers for prostate cancer. *Br. J. Cancer* **100,** 1603–7 (2009).

94. Mack, M. *et al*. Transfer of the chemokine receptor CCR5 between cells by membrane-derived microparticles: a mechanism for cellular human immunodeficiency virus 1 infection. *Nat. Med.* **6,** 769–75 (2000).

95. Al-Nedawi, K. *et al*. Intercellular transfer of the oncogenic receptor EGFRvIII by microvesicles derived from tumour cells. *Nat. Cell Biol.* **10,** 619–24 (2008).

96. Valadi, H. *et al*. Exosome-mediated transfer of mRNAs and microRNAs is a novel mechanism of genetic exchange between cells. *Nat. Cell Biol.* **9,** 654–9 (2007).

97. Ciravolo, V. *et al*. Potential role of HER2-overexpressing exosomes in countering trastuzumab-based therapy. *J. Cell. Physiol.* **227,** 658–67 (2012).

98. Pritchard, C. C. *et al*. Blood cell origin of circulating microRNAs: a cautionary note for cancer biomarker studies. *Cancer Prev. Res. (Phila).* **5,** 492–7 (2012).

99. www.exosomedx.com. *Exosome Diagnostics*

100. Chen, C. *et al*. Microfluidic isolation and transcriptome analysis of serum microvesicles. *Lab Chip* **10,** 505–11 (2010).

101. Singh, A. B. & Harris, R. C. Autocrine, paracrine and juxtacrine signaling by EGFR ligands. *Cell. Signal.* **17,** 1183–93 (2005).

102. Wykosky, J. & Debinski, W. The EphA2 receptor and ephrinA1 ligand in solid tumors: function and therapeutic targeting. *Mol. Cancer Res.* **6,** 1795–806 (2008).

Chapter 2

Pro-apoptotic Activity in Conditioned Medium Culture

Abstract

In this chapter we describe an approach that simultaneously interrogates the factors secreted by diverse breast cancer cells, and the response of diverse breast cancer cells to secreted factors. We develop a conditioned medium exchange protocol that measures the effect of factors generated by 20 breast cancer cell lines on the same 20 cell lines, in all possible permutations. We measure two responses with important roles in cancer biology, proliferation and apoptosis, as outputs from this conditioned medium culture assay. We define producers as the cells that make the conditioned medium, and responders as the cells that respond to each medium with changes in proliferation or apoptosis. We generate 20x20 matrices for the effects of conditioned medium and analyze them to uncover trends in both secretion of active factors and cell line responses. We are able to separate conditioned media in groups, depending on the dominant phenotype they induce on multiple responder lines. These include groups that tend to promote growth in responders, as well as groups that tend to promote apoptosis. Additionally, we observe patterns in responder behavior. Two conditioned media emerge as strong apoptotic inducers. We undertake some basic biochemical characterization of the apoptotic activity, in the form of heat-shock, freeze/thaw, concentration and dilution series of the conditioned media. We develop the hypothesis that in addition to soluble proteins,

these cancer cells also secrete a membranous particulate fraction and proceed to isolate this fraction from both conditioned media and test it for apoptotic activity. The activity assay is performed both as an apoptotic luminescence-based assay as well as a live-cell timelapse microscope series, that allows for closer observation of conditioned media responder cells and phenotypic characterization of the apoptotic phenomenon.

2.1 Conditioned Medium Exchange: a Platform for Unveiling Paracrine Interactions in Breast Cancer.

This study is focused on the chemical cues secreted by breast cancer cells. More specifically, the aim of this study was to swap secreted protein cues between different cancer cells and observe how these impact cell fate decisions. In order to de-couple the chemical from the mechanical interactions between distinct breast cancer cells, we designed a conditioned medium (CM) cell culture assay. In this first large scale screen we sought to answer the following questions:

- ◊ Does culture in pre-conditioned medium affect the cell line that made it?
- ◊ How often do conditioned media cause an inhibitor or toxic effect on responder lines? How strong is this effect?
- ◊ Are there specific outlier cell lines that emerge from this screen, either as producers or responders? Do the culture media from some cell lines induce a strong effect on the majority of cancer cells tested?

Methods

The protocol for conditioned medium production required seeding the cells at a density of 10^6 cells/ml in T-150 culture flasks. Cells were allowed to adhere to flask surface, after which monolayers were washed twice with PBS and growth medium was replaced with serum-free RPMI, supplemented with 1% Penicillin-Streptomycin and buffered with 10mM Hepes. Conditioned medium was harvested 24hrs later and centrifuged 3min at 1,000g to exclude cell debris. It was subsequently immediately transferred on the receiver cell lines.

The receiver cell lines were seeded at a density of 10^4 cells/well in 96-well plates in triplicate wells. Seeding took place in regular growth medium. After 24hrs, cell monolayers were washed twice with PBS and switched to 100μl of conditioned medium. The chosen outputs for this assay were **proliferation** and **apoptosis**. EdU incorporation was employed as an indicator of cell proliferation. Therefore, 48hrs after switching the cells to CM culture, EdU was added in the wells at a final concentration of 10μM. After an additional 24hrs of EdU incubation, cells were fixed and permeabilized with a solution of 3.7% formaldehyde and 0.5% Triton-X. In total, the duration of live cell culture was 5 days.

For proliferative staining, EdU was coupled to fluorescent Alexa488 Azide by click chemistry. For apoptotic staining, plates were blocked in buffer containing 2% BSA and 0.3% TritonX, then incubated with cPARP mAb at 1:1000 ratio overnight at 4C. Primary antibody was washed out and cells were incubated for 2hrs at room

temperature with a solution of 1:5000 secondary 488 anti-mouse mAb as well 1ug/ml Hoescht, in order to obtain a total nuclear count. The plates were imaged and scored on an automated microscope at the ICCB screening facility at HMS.

The two outputs of the screen were: 1) proliferation, documented by using the synthetic thymidine analogue EdU in the last 24hrs of conditioned medium culture. This provided us with a measure of the fraction of the cell population that passed through S-phase of the cell cycle, and constitutes the **Proliferative Index (PI)** for that cell line in that particular culture condition. 2) Apoptosis, documented by cleaved-PARP monoclonal antibody staining of the fixed cultures. This constitutes the **Apoptotic Index (AI)** of the cell line in a particular culture condition. In addition to conditioned medium (CM) culture, each cell line is also cultured in serum-free (SF) medium and regular, FBS-supplemented growth medium (Serum), both conditions serving as comparative controls. Another endogenous control condition in this screen is the cell line's response to its own pre-conditioned medium (self-CM). Below we normalize and plot the data from this screen by this self-CM condition.

20x20 Conditioned Medium Matrices

The outcome of this double apoptotic and proliferative conditioned medium screen clearly demonstrates that the swapping of extracellular secretions is a potent regulator of cell fate. Some cell lines were as high as 27x more proliferative when grown is heterologous CM as opposed to growth in their own CM. Similarly some

CMs were able to induce 10-fold more apoptosis when compared to the control condition. One caveat of this screen was that cells were grown in 100% CM, with no addition of fresh medium. Also, in order to eradicate the strong proliferative signal supplied by fetal bovine serum in regular growth medium, the CMs were produced under serum-free culture conditions. Therefore, at the time of the screen the responder cell lines were grown in serum-free and nutrient-depleted media, which possibly sensitized them to the secreted factors in the CMs and amplified their responses. One concern regarding some of the high apoptotic counts recorded, is that the measured responses are a result of nutrient depletion rather than toxic factor addition in the CMs. This concern is addressed in the following section, where the pro-apoptotic nature of the CMs is confirmed by repeating some of the apoptotic assays in 50% CM / 50% SF culture conditions.

Furthermore, in accordance to our original expectation, the screen points to two outlier CMs that demonstrate strong pro-apoptotic effect in the majority of responder cell lines. CM HCC38 and CM BT20 were singled out since they were able to induce significant apoptosis in 15 and 16 out of the 19 cell lines respectively (fig2.1). Interestingly enough, CM HCC38 is not pro-apoptotic to BT20 cells and the opposite is also true: CM BT20 is not pro-apoptotic to HCC38 cells. A possible interpretation of this phenomenon is that the pro-apoptotic effect of both media is due to a common apoptosis-inducing secreted factor. Most cell lines are sensitive to the factor, yet the producer cell lines are resistant to autocrine stimulation in order to be able to grow and thrive in its presence.

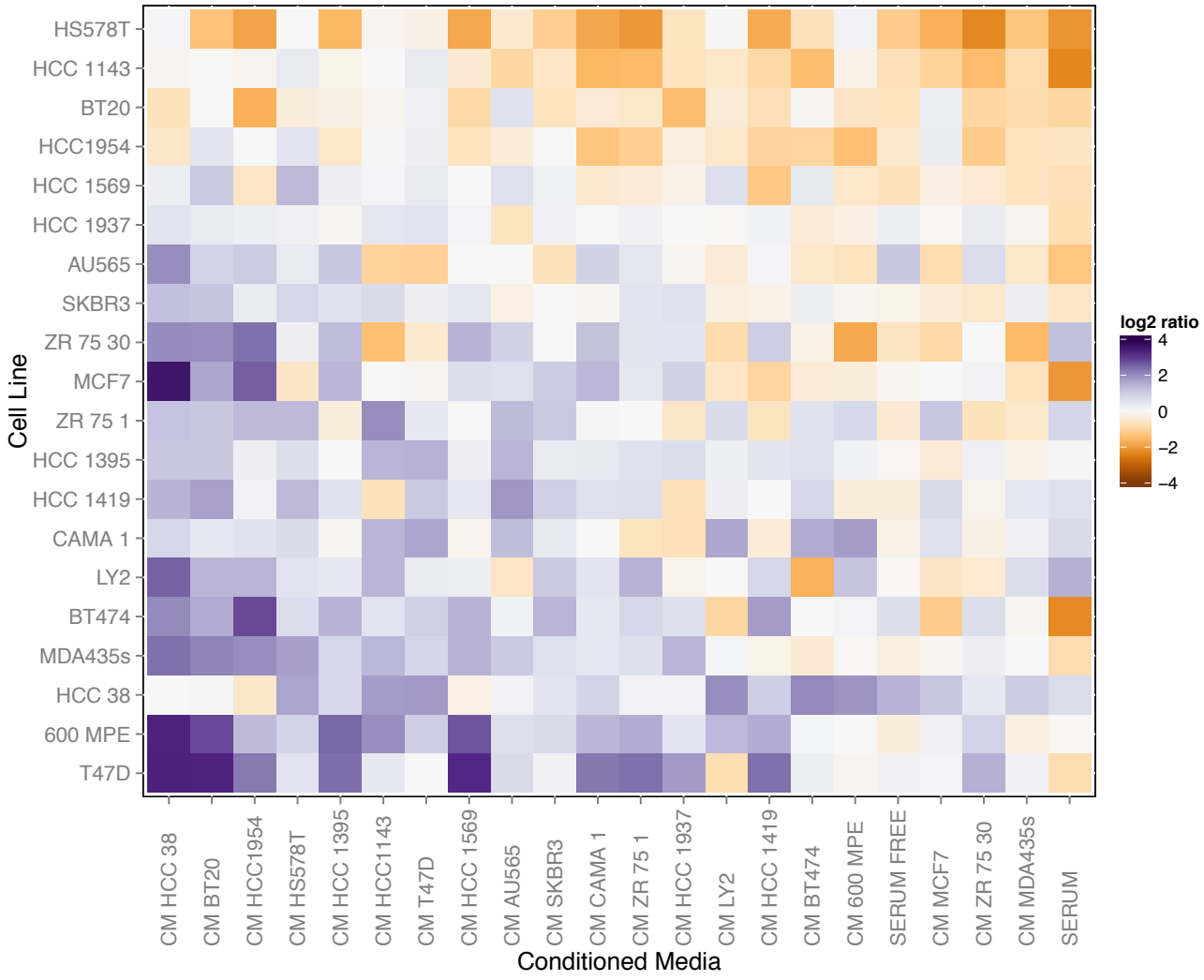

Figure 2.1: Apoptotic Index Heatmap.
Rows represent cell lines, while columns represent conditioned media. Each row has been normalized to the cell line's apoptotic response to its own pre-conditioned medium. On the heatmap, purple values represent apoptosis higher than control, while orange values represent apoptosis lower than control. Conditioned media were ranked from left to right according to their cumulative apoptotic index across all cell lines.

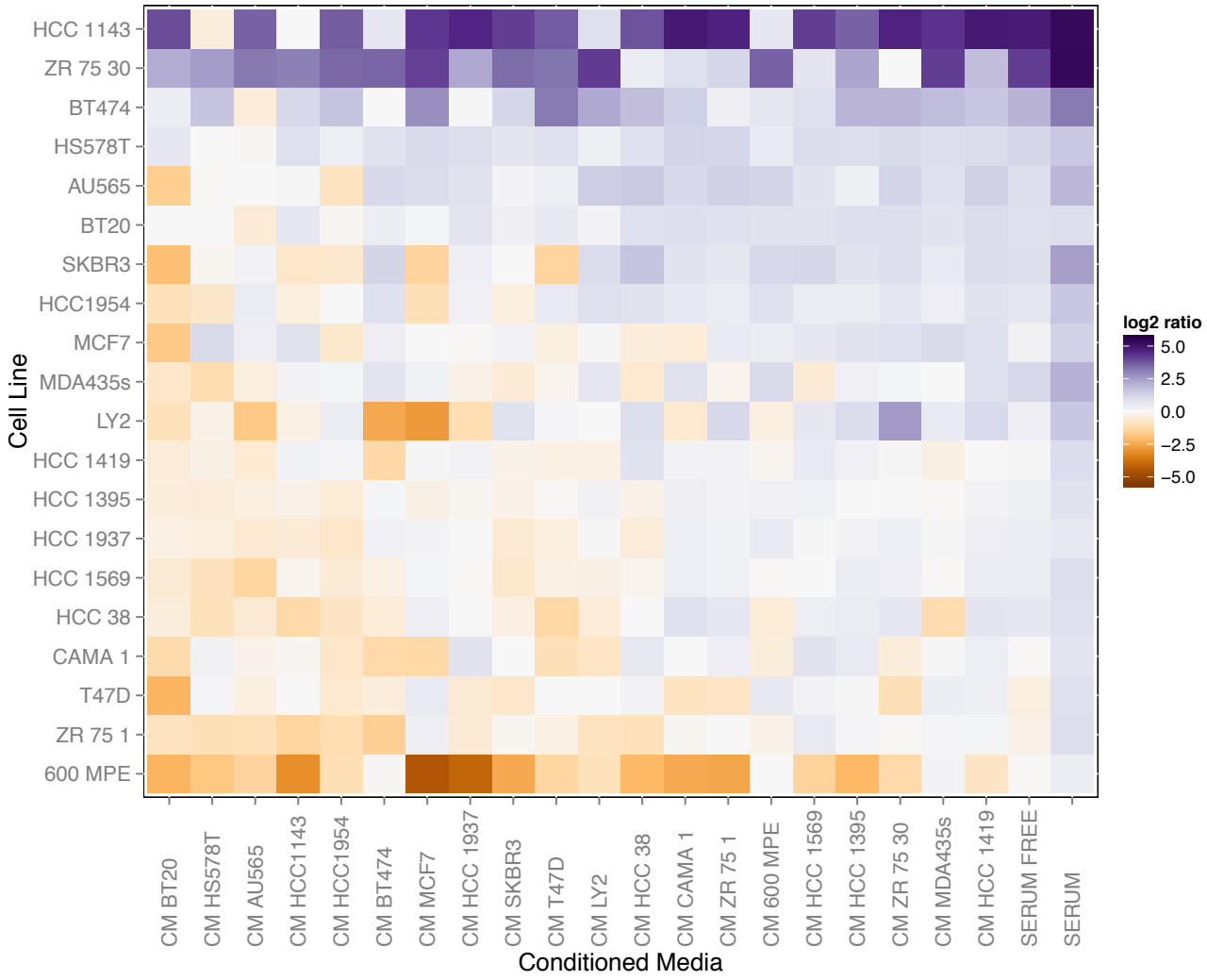

Figure 2.2: Proliferation Index Heatmap.
Rows represent cell lines, while columns represent conditioned media. Each row has been normalized to the cell line's proliferative response to its own pre-conditioned medium. On the heatmap, purple values represent proliferation that is higher than control, while orange values represent proliferation lower than control. Conditioned media were ranked from right to left according to their cumulative proliferative index across all cell lines.

In inspecting the clustergram of proliferative indices (fig2.2), we note that in addition to a strong pro-apoptotic effect, CM BT20 also demonstrates potent anti-proliferative activity in 15 out of the 19 cell lines tested, including HCC38 cells. In contrast, CM HCC38 boosts proliferation in the majority of cell lines tested (11 out of

19), including BT20 cells. While in the apoptotic dataset the two CMs behave similarly, the proliferative dataset implies that there are also differences in the mechanism of action of the two CMs.

CM Typing According to Dominant Phenotype Induction

When comparing the two data matrices, one surprising finding was that pro-apoptotic CMs are not necessarily endowed with anti-proliferative activity. Instead distinct CM-responder pairs scored all over the quadrants of low-proliferation/high apoptosis, low-proliferation/low-apoptosis, high-proliferation/low-apoptosis and high proliferation/high apoptosis, as demonstrated in figure 2.3. This is perhaps not as surprising when considering that in cancer cells the apoptosis and survival pathways are cross-wired. Figure 2.3 is a closer look at this phenomenon. Here the CMs are classified in different program categories depending on their apoptotic and proliferative readouts:

- ◊ The **growth program** is defined as a high proliferative index combined with a low apoptotic index, corresponding to 32% of responders.
- ◊ The opposite of this is the **death program**, defined by a low proliferative index matched by a high apoptotic index, corresponding to 34% of responders. In addition to these two programs of approximately equal prevalence in the 20x20 dataset, we also observe two hybrid states.
- ◊ The **acceleration program**, where both the proliferative and apoptotic indices are high, which amounted to 29% of responders. These are CMs that

stimulate a higher proliferation but also cause higher apoptosis in the responder cells. Interestingly enough this state is almost as prevalent as the more clear-cut growth and death programs in the dataset.

◊ Finally the **deceleration program**, defined as low proliferative and apoptotic indices. This program, at 5% occurrence, is the least frequent in the data. The biological significance of this program is potentially cell senescence.

In figures 2.3b to 2.3e CMs are grouped together according to their dominant phenotype induction based on the above model. It is noteworthy that no one CM is consistently able to induce the deceleration program. Instead, about half the CMs trigger the deceleration program is one or two cell lines at a time. Also of interest, the CMs that demonstrate high acceleration program counts (panel 2.3d), no deceleration activity was observed, which implies that in these CMs the two programs are mutually exclusive.

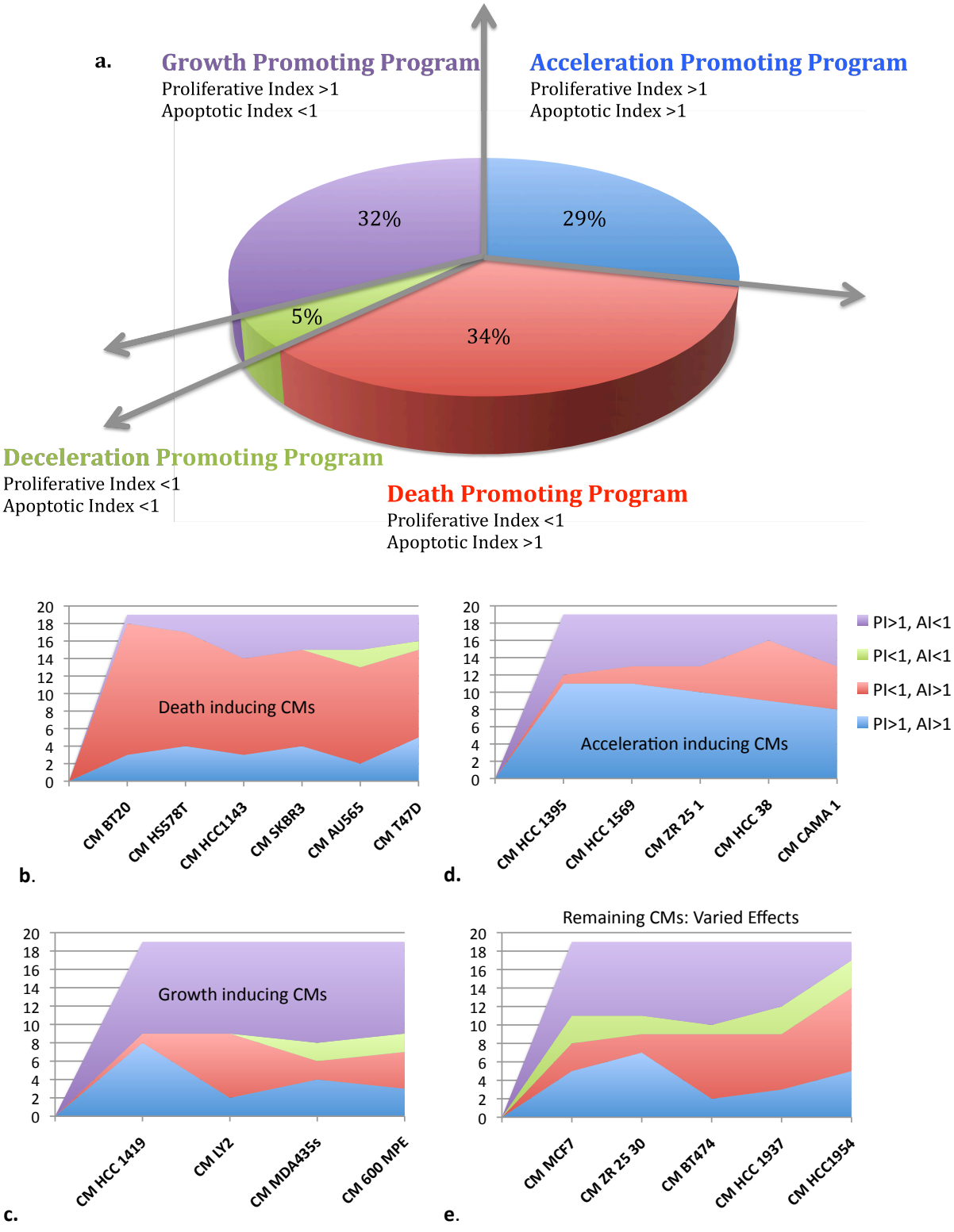

Figure 2.2: Cell fate programs induced by conditioned medium culture.
a) Our model assigns a program to a particular CM, based on the apoptotic and proliferative indices measured across the 19 responder cell lines. The pie chart indicates that when summing up all

apoptotic and proliferative readouts, the growth, acceleration and death programs were almost equal in their prevalence whereas the deceleration program occurred rarely in our dataset. b) This group of CMs demonstrates death-promoting activity in the majority of responder cell lines. c) In contrast, this group of CMs promoted growth in the majority of responders. d) This group of CMs induced an acceleration-promoting program in most responders tested. e) The remaining CMs are plotted together in this chart. There was no majoritary program induced in these cases, but instead the CMs had varied effects dependent on the responder cells.

The difference between the two most pro-apoptotic CM hits is salient in figure 2.3. CM BT20 induces a strong death phenotype in the majority of responder cell lines while a couple of cell lines score in the acceleration category under its influence. On the other hand, CM HCC38 is a mild player in the acceleration category, counting 9 accelerating responders. However, seven more responders commit to a death phenotype upon CM HCC38 stimulation. Both CMs induce growth in a small minority of responders. Based on this we expect the two strong pro-apoptotic CMs to share some similarities in content. Possibly a common set of toxic factors, yet at different concentrations, or a common strong toxic factor in combination with a diverse and different set of growth factors.

2.2 Correlation of Phenotypic Matrices to Cell Line Molecular Subtype

Breast cancer is classified into three categories, depending on expression of surface markers. Breast cancers which express the estrogen (ER) and progesterone (PR) receptors are known as luminal and are targeted by hormonal therapies. Cancers which show human-epidermal-growth-factor-receptor-2 amplification (HER2) are labeled as HER2+ and are clinically targeted by the monoclonal antibody Trastuzumab. Those which are negative for ER, PR and HER2 are known as triple negative breast cancers, and constitute a clinical challenge since there exists yet no

targeted molecular therapy for them. In table 1, the cell lines used in the 20x20 conditioned medium are classified according to the presence of these critical receptors[1,2]. The table and subsequent data analysis in this section excludes cell lines HCC1395 and HCC1419, since we were unable to identify the receptor status information of these cells in the literature.

Luminal (ER+/PR+)	HER2+	Triple Negative (ER-, PR-, HER2-)
MCF7	SKBR3	HCC1143
T47D	AU565	BT20
600MPE	BT474	HCC1937
ZR751	HCC1954	HS578T
LY2	HCC1569	HCC38
CAMA1	ZR7530	MDAMB435s

Table 2.1: Breast cancer cell line classification according to receptor status[1,2].

The analysis presented in this section aims to answer the following questions:

- ◊ On average, are there trends in how each cell line category responds to CM stimulation?
- ◊ Which CMs have the strongest effect in each category of responders? And inversely, how does each CM category affect each cell line?
- ◊ What are specific cell lines that respond strongest to triple negative CM stimulation, HER2+ stimulation or luminal stimulation?

Methods

To address each question we use slightly different strategies. We average over the proliferative/apoptotic indices for each cell line in each CM category. By plotting the bar chart of, for example, MCF7 response to CMs derived from luminal, HER2+ and triple negative cell lines we are able to distinguish which CM ensemble was on average more toxic to these cells and by how much. We omit the control condition of cell line response to its own CM, as the dataset has been normalized to that value and including it in the CM-ensemble would bias that ensemble's average towards the value of 1.

Next we want to investigate whether several cell lines within a receptor status group respond similarly to luminal/HER2+/triple negative CM stimulation. For this purpose we construct the correlation matrix that compares apoptotic/proliferative indices between two cell line responders for all cell line pair permutations within that group. The correlation function employed for these charts is:

$$Correlation(x,y) = \frac{\sum (x - \bar{x})(y - \bar{y})}{\sqrt{\sum (x - \bar{x})^2 \sum (y - \bar{y})^2}}$$

Where $\bar{x}$ and $\bar{y}$ are the average apoptotic/proliferative indices for cell line x and cell line y respectively.

Finally, after inspecting all correlation matrices we single out the datasets exhibiting highest correlation and plot the corresponding line charts of cell line response to CM stimulation. These line charts allow for a closer inspection of which CMs within the ensemble drive the response curves, as well as which cell lines in the set are the strongest responders.

Luminal Responders

Upon observation of the luminal responder panel (figure 2.4), we note that luminal cell lines are the most adversely affected by conditioned medium culture. When comparing figure 2.4a, to figures 2.5a and 2.6a it was observed that the average proliferative indices in luminal cell lines are lower that in HER2+ and in triple negative cells. We conclude that luminal cells are significantly dependent upon fetal bovine serum growth factors to proliferate in culture and are therefore more impacted by conditioned medium serum-free culture. Figure 2.4b indicates that for most luminal cells (with the exception of CAMA1 and LY2), luminal CMs were on average less apoptosis-inducing than HER2+ CMs and that moreover HER2+ CMs were less apoptosis-inducing than triple negative CMs. The pattern is completely reversed for CAMA1 cells.

The correlation matrices 2.4c and 2.4d do not indicate any coherence between the luminal cell responses to HER2+ CMs. However, we do observe a higher correlation of responses to triple negative CMs. The correlation is strongest in the apoptotic index matrix (figure 2.4f), but also present for the some of the same cell line pairs in

the proliferative matrix (figure 2.4e). The corresponding line charts (figure 2.4g and 2.4h) show that all luminal cell line responses converge to roughly the same proliferative and apoptotic index for CM HS578T. Proliferative indices also converge for in CM BT20 culture. In addition, CM BT20 and CM HCC38 are the top pro-apoptotic media for luminal cells, eliciting the highest apoptotic indices. MCF7, T47D and 600MPE are the most sensitive cell lines to these CMs, whereas LY2, ZR751 and CAMA1 also respond with heightened apoptosis but to a lesser extent.

HER2+ Responders

In the HER2+ panel, cell lines BT474 and ZR7530 are the strongest responders both in the apoptotic as well as the proliferative dataset (figure 2.5a and 2.5b). Luminal CMs are on average more proliferative and less apoptotic than HER2+ and triple negative CMs. This observation is somewhat surprising since it implies that permuting CMs within the group of HER2+ cells yields pro-apoptotic and anti-proliferative reactions. There appears to be a competitive mechanism in place between HER2+ cell lines. Particularly for BT474 and ZR7530, the HER2+CMs yield the highest apoptotic indices, whereas for the remainder of the HER2+ cell lines triple negative CMs take the apoptotic lead.

In inspecting the correlation matrices we note once again that the triple negative apoptotic matrix (figure 2.5f) is the one of highest correlation. We subsequently plot the CM-response line charts (figure 2.5g) and see that once again CM BT20 and CM HCC38 yield the highest apoptotic counts, with BT474, ZR7530 and SKBR3 being the

highest responders. In comparison to the luminal responders however, where the apoptotic indices were 10-fold higher than control, the HER2+ responders only climb up to 4-fold. There is one more similarity between figures 2.4h and 2.5g and that is the response to CM MDA435s: apoptotic indices converge for this CM on both luminal and HER2+ responder charts.

Triple Negative Responders

On this responder panel, HCC1143 is a clear outlier in the proliferation measurement (figure 2.6a). This cell line becomes 14-fold more proliferative in conditioned medium from any category of cells! It is unlikely that this indicates a high proliferative activity of every CM when used on HCC1143 cells. Rather we interpret this as a rare occasion when the normalizing condition of culturing the cells in their own pre-conditioned CM resulted in a very low proliferative count. All other triple negative cells exhibit very mild proliferative activity that is slightly higher when they are culture in luminal CMs.

The apoptotic bar chart (figure 2.6b) indicates that most triple negative cells remain unaffected by CM culture. Combined with the proliferative results this implies that triple negative cells are the least dependent on soluble environmental cues for proliferation and survival. They are located therefore on the opposite side of the spectrum from luminal cells, which as previously discussed were the most sensitized to environmental cues. Within the triple negative group, HCC38 and MDA435s cells exhibit the highest apoptotic counts.

The correlation heatmaps that follow indicate high correlation in the proliferative response of triple negative cells to HER2+ CMs (figures 2.6c and 2.6e). We plot the corresponding line chart, excluding the HCC1143 outlier, on figure 2.6f. All cell lines in the chart follow the same response pattern, with HS578T and BT20 being the strongest responders of the group, while CM ZR7530 and CM HCC1569 are the most proliferative stimulants.

As a final reflection on the 20x20 dataset, we asked the question of how did triple negative CMs affect triple negative cells. Particularly since it was previously observed that two triple negative CMs -CM BT20 and CM HCC38- yielded high apoptotic counts in HER2+ and luminal cells, we wanted to see how these fare when used to induce apoptosis in the more aggressive triple negative cell lines. For this purpose we construct figure 2.7, where the triple negative proliferative and apoptotic responses are charted on two different axes for four triple negative CMs. We observe that the pro-apoptotic CMs BT20 and HCC38 induce a similar response pattern on triple negative cells. Both CMs stimulate the proliferation of HCC1143 cells but beyond that did not exhibit any significant proliferative effect on the remaining charted cells. Interestingly, the apoptosis curves demonstrated that both CMs are mildly pro-apoptotic to HCC1937 cells and more strongly apoptotic to MDA435s cells. In the remaining triple negative cell lines, they do not induce and apoptotic effect and that includes a mutual apoptosis-proof relationship.

For comparative purposes we included the CM HS578T and CM HCC1143 responses on figure 2.7c and 2.7d respectively. Here we see a different trend. In addition to HCC1937 and MDA435s, HCC38 cells responded to both these CMs with high apoptotic indices, while BT20 are still at neutral apoptotic level. The trend is conserved in the proliferative curves, which to a great extent mirror the apoptosis curves. The lower the apoptotic count the higher the proliferative count and vice versa for these two CMs. More specifically, the BT20 proliferative response to CM HS578T is once again neutral, while the remainder of the cell lines are proliferatively suppressed by this CM. CM HCC1143 gives a proliferative boost to HS578T and BT20 cells, while it proliferatively suppresses HCC1937 and HCC38.

In conclusion, there is no single CM that successfully inhibits all triple negative cell lines. MDA435s cells were the most successfully inhibited triple negative cells and CM HCC38/ CM BT20 inhibited these more strongly than other triple negative CMs. In addition CM HCC38 and CM BT20 elicited a similar response pattern from triple negative cells, that was distinct from other triple negative CM patterns. This is yet another similarity that points to the possibility of common secreted factors in these two cell lines.

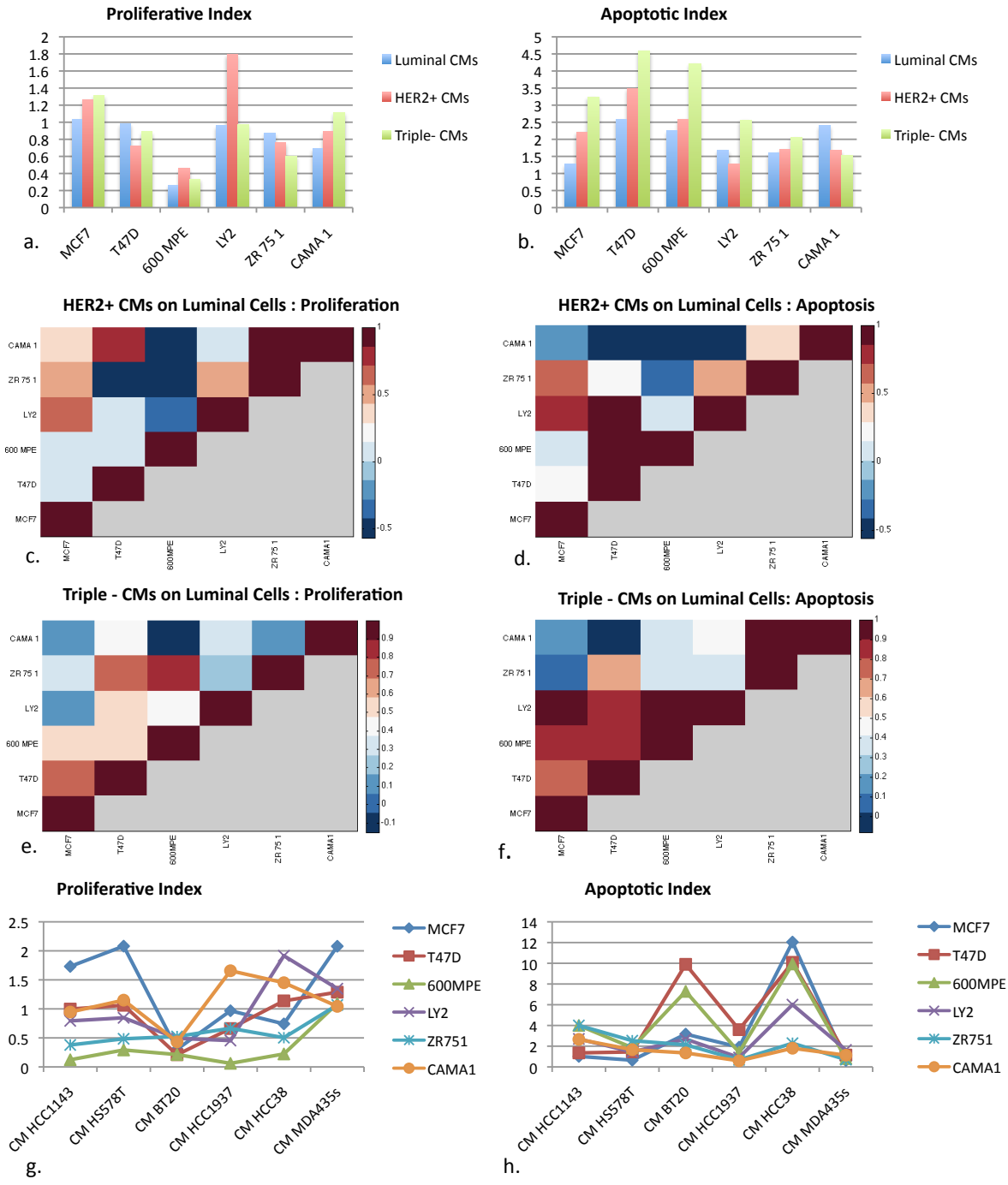

Figure 2.3: Luminal Responder Panel
a) Bar chart of proliferative responses of luminal cell lines over the average of luminal, HER2+ and triple negative CMs. b) Bar chart of apoptotic responses of luminal cell lines over the average of luminal, HER2+ and triple negative CMs. c) and d) Correlation matrices of proliferative and apoptotic indices respectively derived from luminal responders to HER2+ CM stimulation. e) and f) Correlation matrices of proliferative and apoptotic indices respectively derived from luminal responders to triple negative CM stimulation. g) and h) Line charts of proliferative and apoptotic indices respectively illustrating luminal response to triple negative CMs.

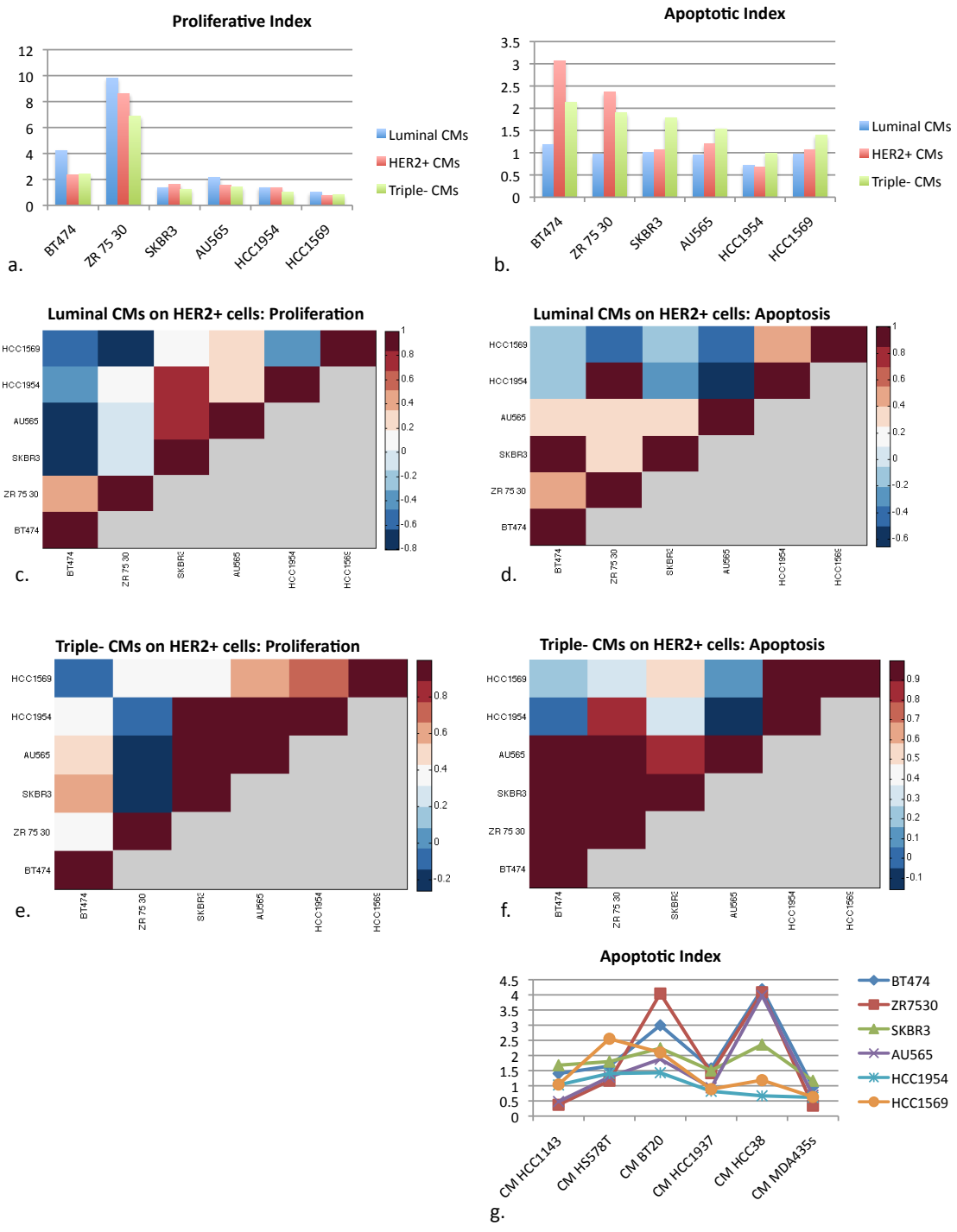

Figure 2.4: HER2+ Responder Panel
a) Bar chart of proliferative responses of HER2+ cell lines over the average of luminal, HER2+ and triple negative CMs. b) Bar chart of apoptotic responses of HER2+ cell lines over the average of luminal, HER2+ and triple negative CMs. c) and d) Correlation matrices of proliferative and apoptotic indices respectively derived from HER2+ responders to luminal CM stimulation. e) and f) Correlation matrices of proliferative and apoptotic indices respectively derived from HER2+ responders to

triple negative CM stimulation. g) Line chart of apoptotic indices illustrating HER2+ response to triple negative CMs.

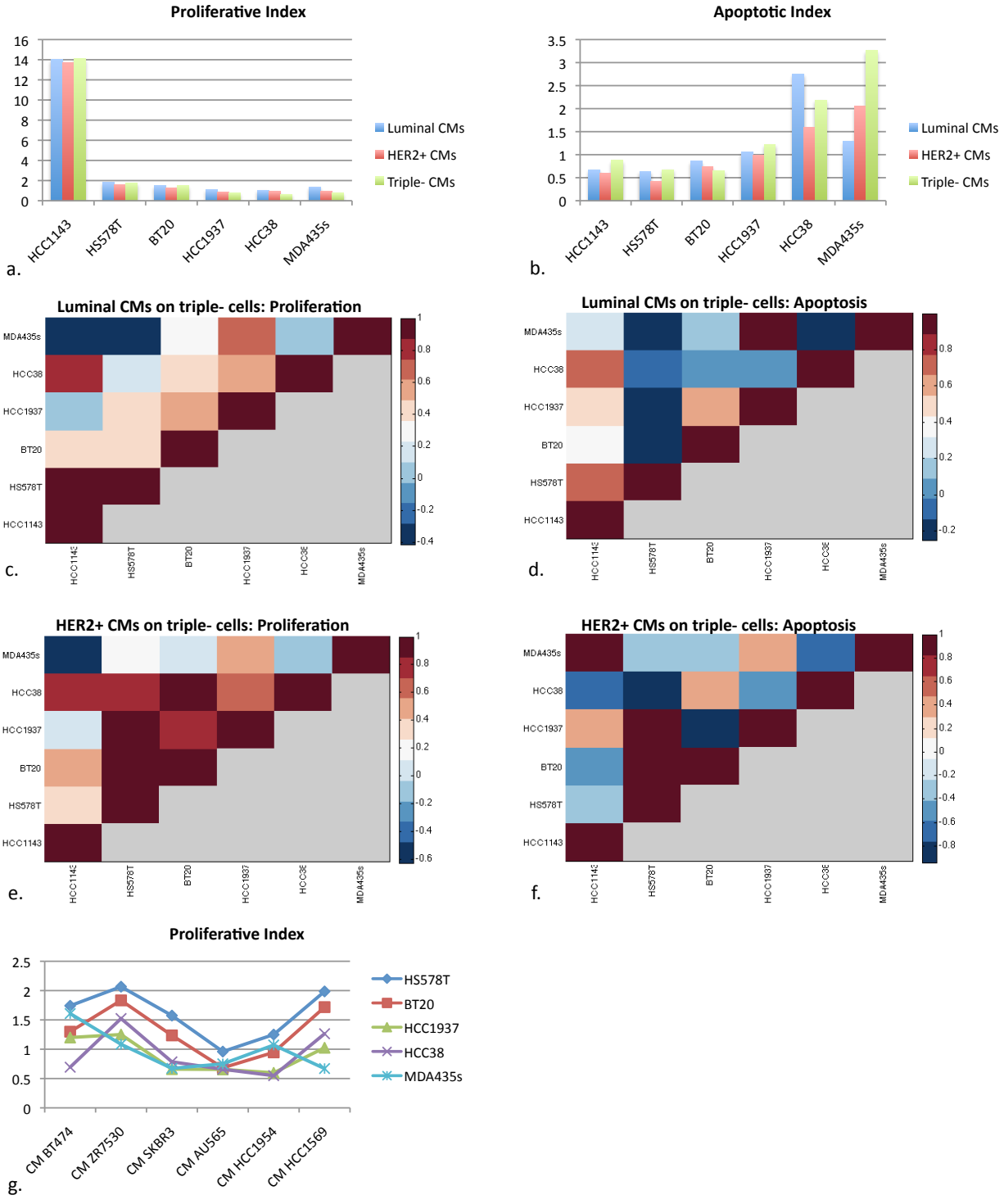

Figure 2.5: Triple Negative Responder Panel
a) Bar chart of proliferative responses of triple negative cell lines over the average of luminal, HER2+ and triple negative CMs. b) Bar chart of apoptotic responses of triple negative cell lines over the average of luminal, HER2+ and triple negative CMs. c) and d) Correlation matrices of proliferative

and apoptotic indices respectively derived from triple negative responders to luminal CM stimulation. e) and f) Correlation matrices of proliferative and apoptotic indices respectively derived from triple negative responders to triple negative CM stimulation. g) Line chart of proliferative indices illustrating triple negative response to luminal CMs. HCC1143 response is excluded from the chart due to being a strong outlier in the group.

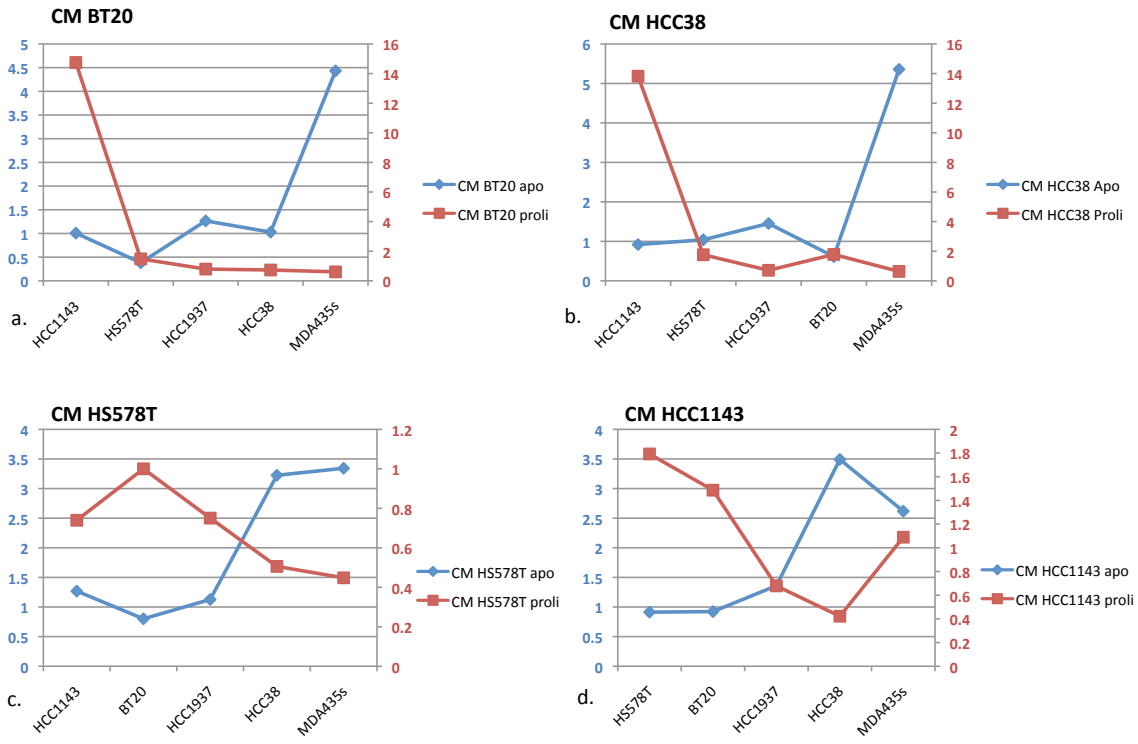

Figure 2.6: Triple Negative Response to Triple Negative CMs

Line charts of apoptotic and proliferative responses in the triple negative cell line ensemble. Proliferation is charted on the left y-axis (in blue) while apoptosis is charted on the right y-axis (in red). Each chart corresponds to a different triple negative CM.

2.3 Biochemical Characterization of Apoptosis-Inducing Conditioned Medium

This section examines the apoptotic effect induced by CM HCC38 more closely and seeks to identify the extent to which this effect can be concentrated and diluted. In addition we test whether the apoptotic effect is heat labile and whether it can be cryo-preserved. Finally, we fractionate CM HCC38 into large and small vesicular fractions then test all fractions for apoptotic activity.

Methods

M30 CytoDeath ELISA

The assay employed for apoptosis quantification in this section is the M30 CytoDeath ELISA (Peviva). This assay is founded upon the biological knowledge that caspases cleave various cellular proteins during apoptosis. In epithelial cells, one of those substrates is the intermediate filament protein keratin 18 (K18). The M30 antibody recognizes a neo-epitope exposed after caspase cleavage of K18 after the aspartic acid residue 396 [3]. Cleavage at this position occurs early during apoptosis by caspase-9 and during the execution phase by caspase-3 and caspase-7 [4]. The M30 CytoDeath ELISA measures the levels of soluble caspase-cleaved K18 (ccK18) fragments containing the K18Asp396 neo-epitope. After induction of apoptosis of epithelial cells, ccK18 increases are first observed in cell extracts. Release of antigen into the extracellular compartment occurs later and is due to secondary necrosis of apoptotic bodies. The ccK18 increase during apoptosis is inhibited by the caspase-inhibitor zVAD-fmk. The M30 capture antibody is a mouse monoclonal IgG2b antibody suitable for human, monkey and bovine cells.

Assay Procedure

For the purpose of this assay receiver cell lines MDAMB231 and MCF7 were seeded at a density of 10,000 cells/well in 96 well plates in duplicate. Cells were allowed to sediment and adhere to the plate bottom overnight, after which the culture medium was replaced with serum free RPMI and serum supplemented RPMI: the two negative controls in this assay. We employed a known apoptotic agent, staurosporine, as a positive control at a 2 μM final well concentration. We incubated cells with controls and experimental conditions for 48hrs. Cells were then lysed by the addition of 10 μL 10% NP-40 and shaking the plate at room temperature for 5min before proceeding with cell lysis and quantification of the CK18 substrate. 25 μL from each well were transferred on M30 mAb-coated ELISA plate and the incubations and washes were performed according to the assay manufacturer's instructions[5]. The absorbance at 450nm was measured on a Perkin Elmer microplate reader and converted to units/L of CK18 based on a recombinant CK18 calibration control curve.

Conditioned Medium Production

The conditioned medium for this assay was produced much like in chapter 1. HCC38 cells were seeded at a density of 10^6 cells/ml in T-150 culture flasks. Cells were allowed to adhere to flask surface, after which monolayers were washed twice with PBS and growth medium was replaced with serum-free RPMI, supplemented with 1% Penicillin-Streptomycin and buffered with 10mM Hepes. Conditioned medium was harvested 48hrs later and centrifuged 3min at 1,000g to exclude cell debris. For

the 1x CM HCC38 experimental condition, 100µL of CM were directly transferred on the receiver cell well.

Concentration and Dilution Series

For the CM concentration series, 100ml of CM HCC38 were passed through a 3K centrifugal filtration device, decanting and filtrate and conserving the concentrate, until the original CM volume was reduced down to 8ml. This constituted a 12x concentrated CM solution, 100 µL of which were transferred on the receiver cell wells. For the lower concentrations of 6x, 3x and 2x, we diluted the 12x concentrate with the appropriate amount of serum free RPMI. For the CM dilution series newly harvested CM HCC38 was diluted down 3x, 10x, 30x and 100x with serum free RPMI.

Freeze/Thaw and Heat Shock

For the freeze/thaw portion of the experiment, 120µL aliquots of 6x concentrated CM HCC38 were snap-frozen in liquid nitrogen and subsequently thawed and immediately transferred on receiver cell wells. For the heat shock portion of the experiment, 120µL aliquots of 6x concentrated CM HCC38 were heated at 95C for 10min then briefly centrifuged to bring condensation back in solution. The CMs were subsequently transferred on receiver cell wells.

Particulate Fractionation

For the fractionation portion of the experiment, a series of centrifugations was employed to differentially precipitate membranous particles of varied sizes out of the CM. The centrifugation method is extensively discussed in chapter 3. Briefly, 100ml of conditioned medium were harvested from cells and centrifuged at 300g for 10 min to remove cells, then at 2000g for 10min to remove apoptotic bodies. Conditioned medium was subsequently passed through a 3k centrifugal filtering device at 4000g for 30min in order to concentrate the large CM volume down to a few milliliters. The concentrated CM was ultra-centrifuged at 10,000g for 30min to pellet cell debris and large vesicles. The pellet from this step was conserved and re-suspended in 300µL of PBS. Each receiver cell well received 60 µL of this giant vesicle fraction (guv) in addition to 100 µL of serum free RPMI.

The supernatant from this centrifugation step was further ultra-centrifuged at 100,000g for 70min to pellet the exosomes. The exosomal pellet underwent a final wash step and, was re-suspended in 300 µL PBS. Similarly, each receiver cell well received 60 µL of this exosome fraction (exo) in addition to 100 µL of serum free RPMI. Finally, the supernatant (exosup) from the ultracentrifugation spin, which amounts to approximately a 12x concentrated CM, was conserved and 100 µL of it were transferred onto the receiver cell wells.

Statistical Analysis

For statistical analysis of MDAMB231 apoptotic results, all experimental conditions were compared to serum supplemented culture and statistical significance was determined by performing unpaired, two–tailed, homoscedastic t-tests. For the statistical analysis of MCF7 apoptotic results, all experimental conditions were compared to serum free culture since it was found to be significantly more apoptotic than the serum supplemented condition. Statistical significance was determined by performing unpaired, two–tailed, homoscedastic t-tests. In both cases P-values were computed. Results are graphically represented as average values over duplicate experimental conditions with error bars denoting the standard deviation from the mean.

Concentration and Dilution Series of CM HCC38

For both receiver cell lines, MDAMB231 and MCF7, the concentration series indicates that the apoptotic effect can indeed be concentrated in the conditioned medium (figures 2.8a and 2.8c). As mentioned in the methods section, concentration was achieved by centrifugal filtration through a 3,000kDa membrane. When comparing 3x and 2x concentrated CM HCC38 to 1x non-concentrated CM HCC38 we see that in both cases the concentration results in some loss of potency of the CM. We hypothesize that this is due to retention of small quantities of the active factor in the centrifugal device. By consequence, the 3x concentrated CM HCC38 is equivalent in apoptotic potency to the 1x unperturbed CM HCC38.

A closer look to MDAMB231 apoptotic response (figure 2.8a) reveals that staurosporine-induced apoptosis produces a lower concentration of cytokeratin18 fragments when compared to CM-induced apoptosis. This was a puzzling finding, particularly because after visual inspection of the staurosporine-treated wells we see that 2μM of staurosporine are quite effective at killing the entire cell content of the well within a few hours. One possible explanation of this phenomenon is that, particularly in MDAMB231 cells, staurosporine-induced cell death follows a different apoptotic pathway that is not as reliant in caspase 3, caspase 9 and caspase 7 –the three caspases that cleave cytokeratin18. In contrast, the data indicates that CM HCC38-induced apoptosis relies on this caspase-dependent, cytokeratin18-cleaving pathway.

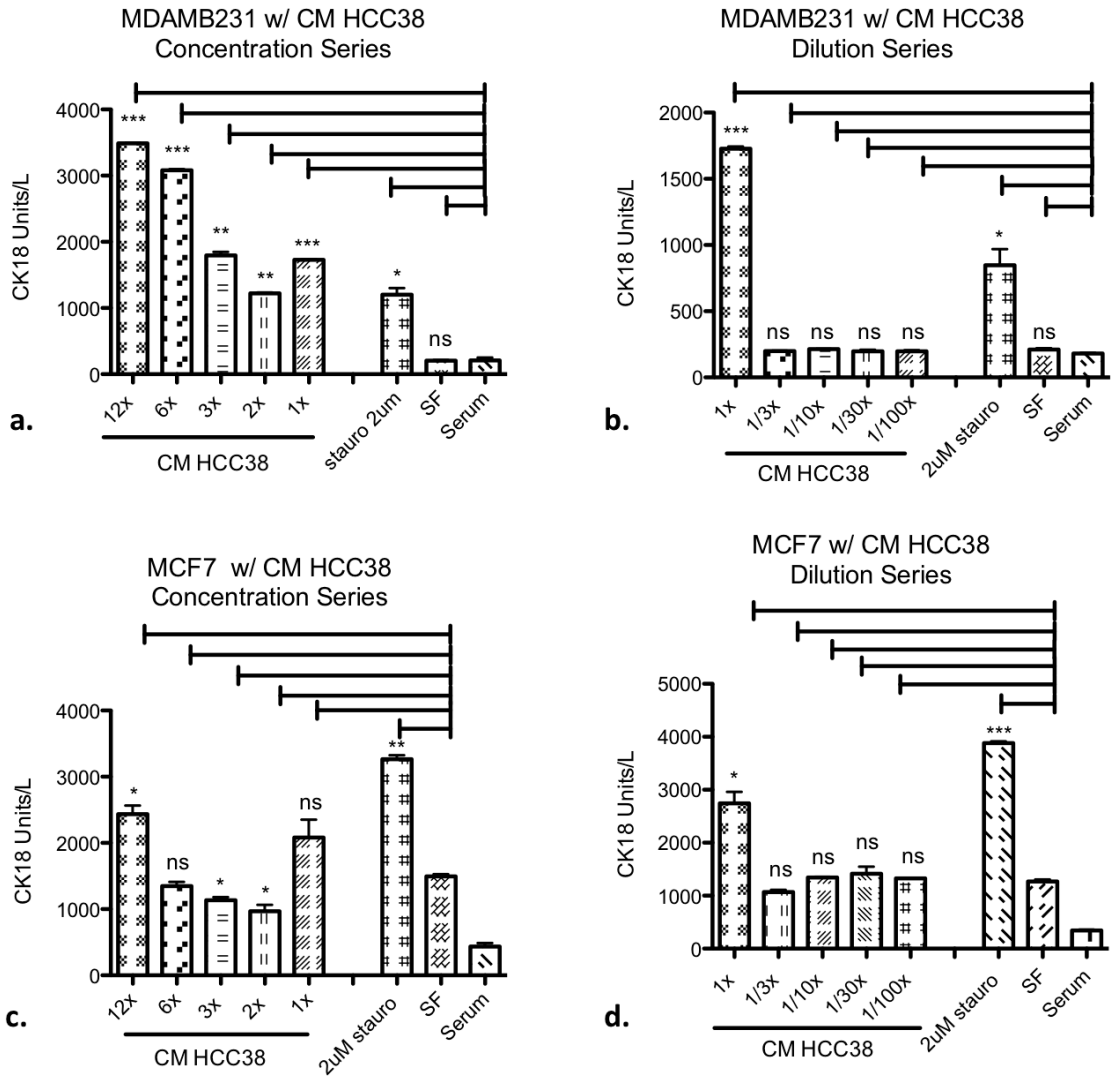

Figure 2.7: Concentration and dilution series of CM HCC38 using the M30 ELISA apoptotic readout assay. Bars denote average values over duplicate wells and error bars denote standard deviation from the mean. Statistical significant is determined by un-paired, two-tailed, homoscedastic T-tests. A single * denotes $P \leq 0.05$, a double ** denotes $P \leq 0.01$ a triple *** denotes $P \leq 0.001$ while ns stands for $P > 0.05$.

Upon inspection of MCF7 apoptotic response (figure 2.8c) we see that this cell type is apoptotically impacted simply by the absence of serum supplementation from the culture medium. Staurosporine has a strong apoptotic effect on MCF7 cells, while CM HCC38 has a moderate apoptotic effect that is lost at the 3x to 6x concentration

Finally on figures 2.8b and 2.8d we see that the CM HCC38-induced apoptotic effect cannot be diluted. Any attempt at diluting the newly-harvested CM HCC38 eliminates the apoptotic activity.

Freezing, heating and fractionation of CM HCC38

For both receiver cell lines, MDAMB231 and MCF7, the apoptotic assay indicates that snap-freezing in liquid nitrogen and subsequent thawing of CM HCC38 does not significantly affect its apoptotic potency (figures 2.9a and 2.9b). This finding suggests that the active factor in the CM can survive freezing –at least for short time periods. Denaturing the protein content of the CM by heating it at 95°C in both cases results in a slight boost of apoptotic activity. This result was puzzling to us. One possible interpretation is that heat shock denatures protective growth factors present in the CM, thus increasing its toxicity to receiver cells. The underlying implication is that heat shock does not irreversibly denature the toxic factor present in the CM, a viable possibility if the active factor is either a small molecule or a small peptide with heat labile tertiary structure. However we have already established that the active factor is retained by centrifugation of the CM through a 3,000kDa cutoff membrane. We can think of two scenarios that can reconcile these seemingly contradictory findings. The first scenario is that the active toxic factor is indeed a small heat labile peptide that is retained during filtration as part of a larger complex. The second scenario is that the active factor is in fact larger than 3000kDa, yet able to renature itself after boiling with the aid of molecular chaperones present in the

CM. Mass spectrometry analysis presented in the following chapter showed that CM HCC38 is rich in heat shock proteins and other molecular chaperones.

The final question we seek to answer in this series of quantitative apoptotic assays is whether the apoptotic factor is part of a particulate fraction in the CM HCC38. For this purpose we differentially centrifuge large membranous particles (guv) as well as small exosomes (exo) from the CM, as described in the methods section. We test these fractions for activity in addition to the supernatant from the final exosomal spin and the original non-fragmented 12x concentrated CM. As figures 2.9c and 2.9d show, the supernatant clearly retains the apoptotic potency for both receiver cell lines. In addition to that however, in MDAMB231 receiver cells the exosomes show a mild ($P \leq 0.05$) apoptotic activity whereas the guvs show no apoptotic activity. In the case of MCF7 receiver cells neither the exosomes nor the guvs show statistically significant apoptotic activity.

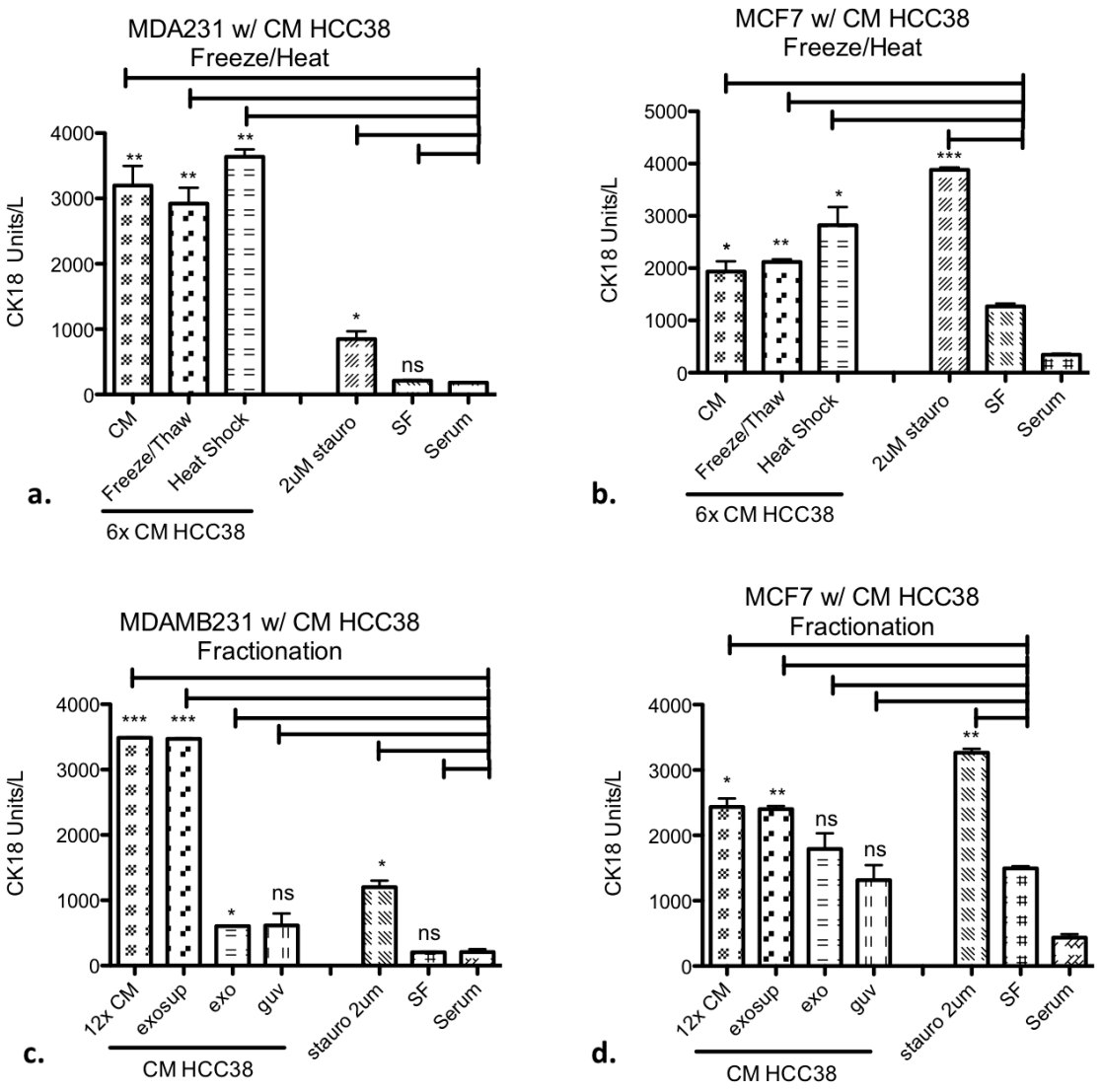

Figure 2.9: Freezing/Thawing, Heat Shock and Fractionation of CM HCC38 using the M30 ELISA apoptotic readout assay. Bars denote average values over duplicate wells and error bars denote standard deviation from the mean. Statistical significant is determined by un-paired, two-tailed, homoscedastic T-tests. A single * denotes $P \leq 0.05$, a double ** denotes $P \leq 0.01$ a triple *** denotes $P \leq 0.001$ while ns stands for $P > 0.05$

2.4 Live Cell Imaging of Apoptosis-Inducing Conditioned Media and Corresponding Exosomes

This section examines the apoptotic effect induced by both CM HCC38 and CM BT20 employing a direct live cell imaging approach over a period of 48 hours. We seek to elucidate the specific phenotype of the apoptotic effect and compare it to that of staurosporine treatment, a standard apoptotic agent. In addition, we are able to purify and fluorescently label CM-derived cancer exosomes and incubate them with receiver cell lines to visualize their uptake and potential apoptotic activity.

Methods

Assay Procedure

Cells were seeded in 12-well glass bottom Matek dishes at a density of 100,000 cells/well. Cells were allowed to sediment and adhere to the plate bottom overnight, after which monolayers were washed twice with PBS and the culture medium was replaced. Negative control wells received 1ml of serum free RPMI while positive apoptosis controls received 1ml of serum free RPMI supplemented with 2 μM staurosporine. For CM-cultured wells, culture medium was replaced with 1ml of CM. For exosome-cultured conditions, 20μl of concentrated exosome stock (comprising approximately 15% of a single exosome prep) was resuspended in 1ml of serum free RPMI. All wells also received 2.5 μM NucView488, a caspase-3 substrate routinely used for real time detection of apoptotic activity in live cells[6]. Cells were incubated and imaged for a total duration of 48hrs.

Conditioned Medium Production

HCC38 and BT20 cells were seeded at a density of 10^6 cells/ml in T-150 culture flasks. Cells were allowed to adhere to flask surface, after which monolayers were washed twice with PBS and growth medium was replaced with serum-free RPMI, supplemented with 1% Penicillin-Streptomycin and buffered with 10mM Hepes. Conditioned medium was harvested after 24hrs and centrifuged 3min at 1,000g to exclude cell debris. The CM was then passed through a 0.22 μm cutoff filter to rule out the presence of bacterial impurities.

Exosome Purification and Fluorescent Labeling

We purified exosomes out of tissue culture supernatant as described previously in section I of this chapter (Particulate Fractionation). For live cell imaging studies exosomes recovered by differential centrifugation were fluorescently labeled using the lipophilic dye PKH26. PKH-26 was designed as a live fluorescent probe of cell membrane, therefore the manufacturer's protocol had to be adapted for this application. Briefly, exosomes were resuspended in a solution of Diluent C (500μl) and PKH-26 dye (2μl). The exosomal/dye mixture was left to incubate for 5min at room temperature. Next the staining was halted by introducing 1ml of an aqueous solution of 1% BSA. Exosomes were recovered by ultracentrifugation and resuspended in 200ul serum-free medium, supplemented by 1% BSA.

Time Lapse Imaging

The 12-well glass bottom Matek dishes were mounted on the Prior Proscan III motorized custom built microscope stage, equipped with a 37°C-heated and 5% CO_2 incubation chamber.

All images were collected with on a Nikon Ti inverted microscope equipped with 10x Plan Fluor Phase1 0.3 NA objective lens and the Perfect Focus System for continuous maintenance of focus. For higher magnification, a 20x Plan Apo Phase2 0.75 NA was used for part of this study (as indicated in the figure captions). The microscope was equipped with a Lumencor SOLA fluorescence light source. Caspase-EGFP fluorescence was excited with the 480/30 nm excitation Chroma filter and RFP fluorescence was excited with the 560/40 nm excitation Chroma filter. Images were acquired with a Hamamatsu ORCA ER cooled CCD camera controlled with MetaMorph 7 software.

For timelapse experiments, images were collected either every 15 or 20 min (as indicated in the figure captions), using an exposure time of 500 ms and 2x2 binning, with illumination light shuttered between acquisitions. Brightness and contrast were adjusted on displayed images (identically for compared image sets) using MetaMorph 7 software.

Live Cell Imaging studies of Breast Cancer Cell Treatment with HCC38 and BT20-Derived Conditioned Media

To further elucidate the specific phenotype of conditioned medium-induced apoptosis in this section we present live cell timelapse microscopy images of three breast cancer cell lines treated with HCC38 and BT20-derived CMs. We observe that the degree of apoptosis as well as the time to apoptotic onset varies depending on the recipient cell line. At the same time, we are also able to discern some common apoptotic phenotypic traits between the three recipient cell lines.

Figure 2.10 monitors the activity of CM HCC38, CM BT20, staurosporine and serum free culture on **HCC1937** cells**.** Both CMs are the cause of total cell death in this cell line by 48hrs. However, in contrast to staurosporine-induced cell death that is immediate and unfolds in a period of approximately three hours after treatment, CM-induced apoptosis is incremental and slower to take place. In addition, we observe slight differences in the apoptotic phenotypes between the two CMs. By 14hrs several of the cells in both CM-treated wells are caspase-3 positive. However, in the CM BT20-treated well the majority of the culture has assumed a contracted rounded form, whereas in the CM HCC38-treated well apoptotic cells are interspersed between normal and elongated in appearance cells. By 24hrs in both wells the majority of cells are rounded, yet not all appear caspase-3 positive. Instead cells linger in this rounded pre-apoptotic stage, a phenotype that we recognize as a CM-induced response in other recipient cells as well. By 48hrs the NucView reporter is activated in all cells. The culture is now visibly apoptotic and accompanied by the

characteristic cell blebbing, an unequivocal sign of cell death. CM-treated wells look markedly different from the serum free-treated negative control where cells keep dividing and the monolayer keeps growing over the 48hr period.

Figure 2.11 presents the response of **HS578T** cells to the same set of culture conditions**.** This cell line appears significantly more resistant to CM-induced apoptosis than HCC1937 cells. In both CM-treated wells, cells keep dividing and the monolayer keeps growing albeit at a slower rate than the SF-treated negative control. We observe in this cell type as well the characteristic cell contraction and rounding that we saw in HCC1937 cells in response to CM treatment. SF-treated cells also round up by 48 hrs, however the essential difference between the three conditions is that CM-treated cells activate caspase-3 whereas SF-treated cells remain dark -an indicator of imminent mitosis rather than apoptosis.

Finally figure 2.12 presents the response of **MCF7** cells to CM HCC38 comparatively to controls. In this case again, CM treatment prolongs cell doubling time yet does not completely block cell division. Caspase-3 positive, apoptotic cells first appear in the interior of the cell island and by 48hrs the apoptotic effect spreads outward. However at the end of the experiment a significant fraction of the culture is still live. In contrast the entirety of the staurosporine treated cell island dies, with no events of cell division, extremely early in the culture. The SF control also presents a somewhat lower amount of apoptosis by 48hrs. This result agrees with ELISA findings presented in the previous section and complements that assay with a visual

image of the susceptibility of this cell type to cell death in serum free culture conditions.

Live Cell Imaging studies of Breast Cancer Cell Treatment with HCC38 and BT20-Derived Exosomes

Next we incubate receiver cell lines with exosomes isolated from the same CM-producing cell lines. The primary purpose of this experiment was to try and recapitulate some of the apoptotic activity by using solely the exosome fraction from the original conditioned media. A secondary end point was to examine exosome uptake by different breast cancer cell lines.

Figure 2.13 captures **MDAMB231** cells incubated with BT20-derived exosomes using a 10x magnification objective, while figure 2.14 represents the same cells this time incubated with HCC38-derived exosomes and imaged with a 20x magnification objective. Regarding exosome-induced cell death, neither HCC38 nor BT20 exosomes not appear to elicit significant cell death in the MDAMB231 cell culture. On figure 2.15 we present **MCF7** cells incubated with BT20 exosomes. Here too apoptosis incidence is identical in the control and exosome-treated wells.

One striking finding in this imaging dataset is the actual uptake of the exosomes by recipient cell lines. MDAMB231 cells appear to endocytose the exosome, which once internalized aggregate in the perinuclear region. The internalization of exosomes in this cell type appears to happen irrespectively of the cellular origin of the vesicles,

although more rigorous and quantitative study -which is beyond the scope of this project- would need to be undertaken to further qualify this statement. In contrast, exosome uptake is less efficient in MCF7 cells. Here exosomes seem to remain in the exterior of the cell membrane and drift in the extracellular space during the 48-hour imaging period.

A question open for investigation is whether exosome uptake is a prerequisite for any exosome activity on recipient cells. The precise mechanism of exosome uptake is unknown at this point. Moreover, it is unclear whether the uptake reflects a mechanistic matching between exosome ligand and recipient cell receptor or is instead solely due to the phagocytic aptitude of the recipient cell line.

A way of testing and differentiating between the two hypotheses would be to extrude biologically inert liposomes, matching the size of breast cancer exosomes, and monitor their uptake from recipient cell lines. A step further would be to embed ligands of known cell surface receptors on the liposomes and again quantify their uptake comparatively to the uptake of inert liposomes and exosomes in turn. However this type of investigation was not conducted since it strays from our primary area of research interest: the apoptotic factors present in the tissue culture supernatants of triple negative breast cancer cell lines.

Feng et al. have conducted interesting research pertinent to this question[7]. Their findings confirm that exosome internalization occurs primarily through a phagocytic

pathway. In testing a variety of different cell types for exosome uptake, they conclude that phagocytic cells, such as macrophages, are more efficient at internalizing exosomes than non-phagocytic cells. They further show that exosome phagocytosis is dependent upon actin and the PI3K pathway, while it is independent of the clathrin and caveolin cell trafficking pathways.

So far the data presented in this chapter indicate that apoptotic activity is contained and more efficiently delivered in the CM of HCC38 and BT20 cells. When pelleting out the exosome fraction, apoptotic activity still remains in the supernatant of the exosomal spin as shown in the previous section. These findings when taken together suggest that the active apoptotic factor is found in abundance in the CM and exosome-free CM fraction. Armed with this knowledge the next section will examine mass spectrometry results of HCC38 and BT20 exosomes and attempt to tease out proteins that are present in the CMs while being absent from the corresponding exosomes.

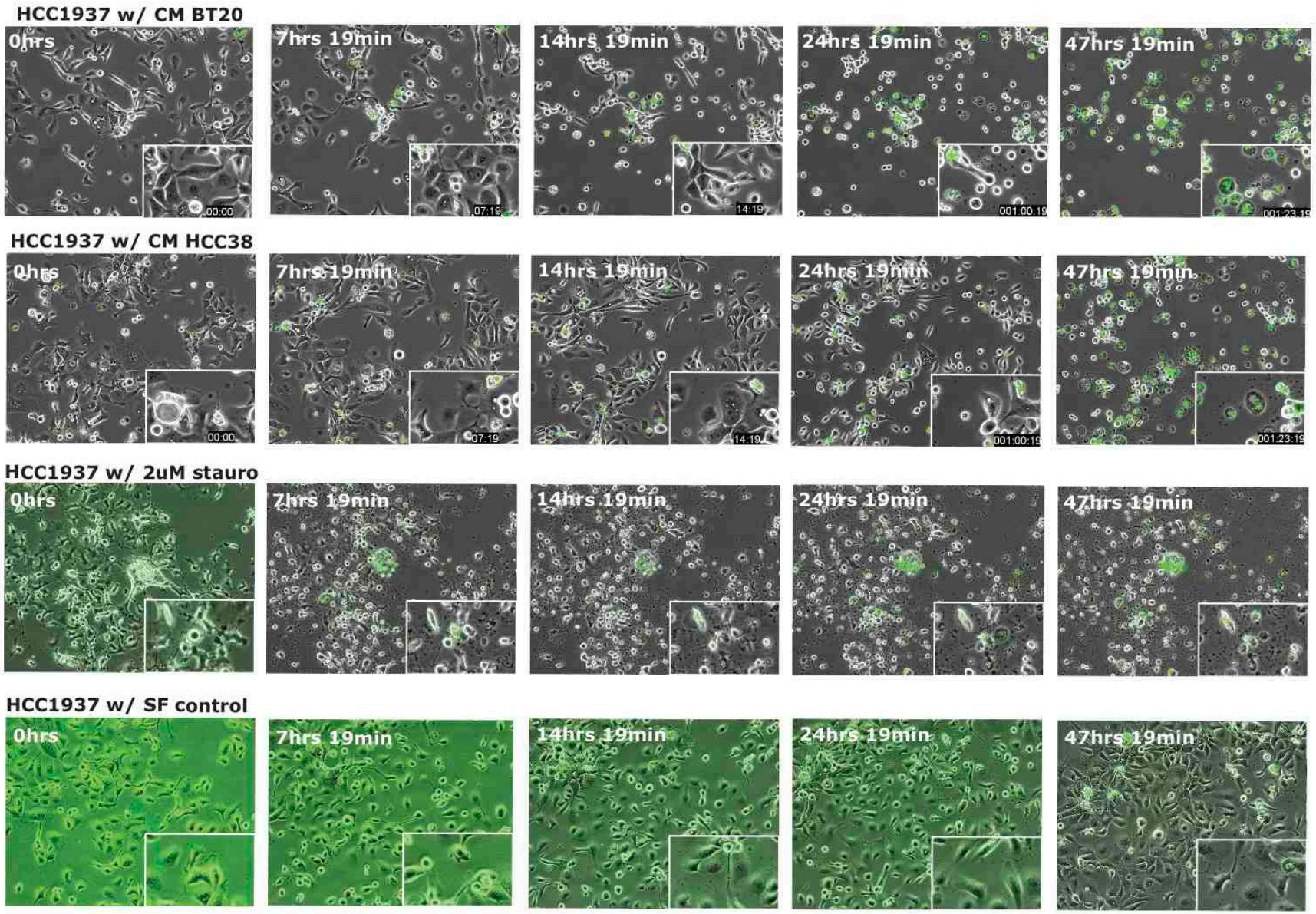

Figure 2.10 : Timelapse imaging series of HCC1937 cells in the presence of CM BT20, CM HCC38, 2μM staurosporine as a positive apoptosis control and serum-free RPMI culture as a negative apoptosis control. Cells were imaged for 48hrs, with a 20min timestep using a 10x magnification objective. All wells were incubated with 2.5μM of EGFP caspase-3 NucView apoptotic reporter.

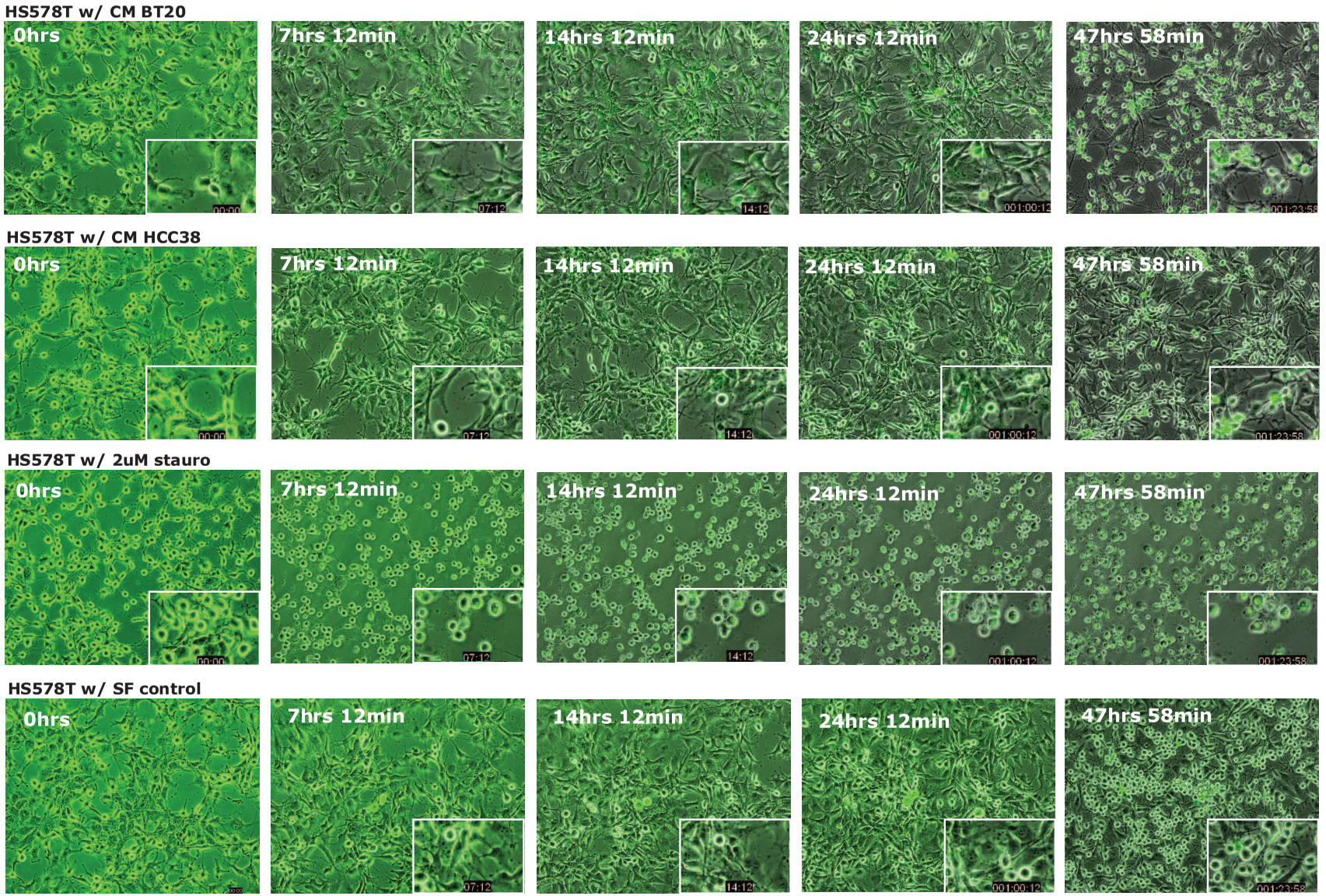

Figure 2.11: Timelapse imaging series of HS578T cells in the presence of CM BT20, CM HCC38, 2μM staurosporine as a positive apoptosis control and serum-free RPMI culture as a negative apoptosis control. Cells were imaged for 48hrs, with a 20min timestep using a 10x magnification objective. All wells were incubated with 2.5μM of EGFP caspase-3 NucView apoptotic reporter.

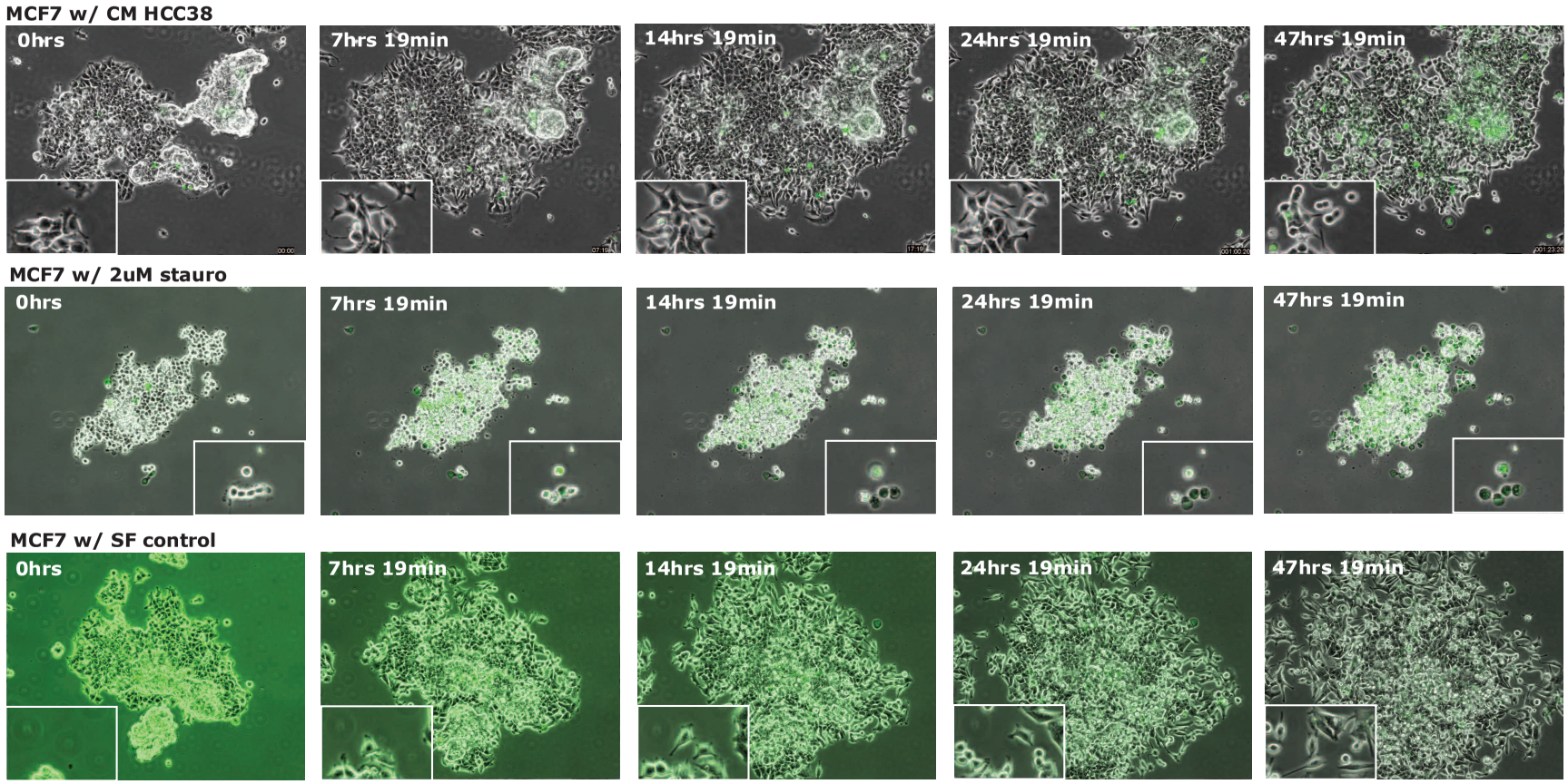

Figure 2.12: Timelapse imaging series of MCF7 cells in the presence of CM HCC38, 2μM staurosporine as a positive apoptosis control and serum-free RPMI culture as a negative apoptosis control. Cells were imaged for 48hrs, with a 20min timestep, using a 10x magnification objective. All wells were incubated with 2.5μM of EGFP caspase-3 NucView apoptotic reporter.

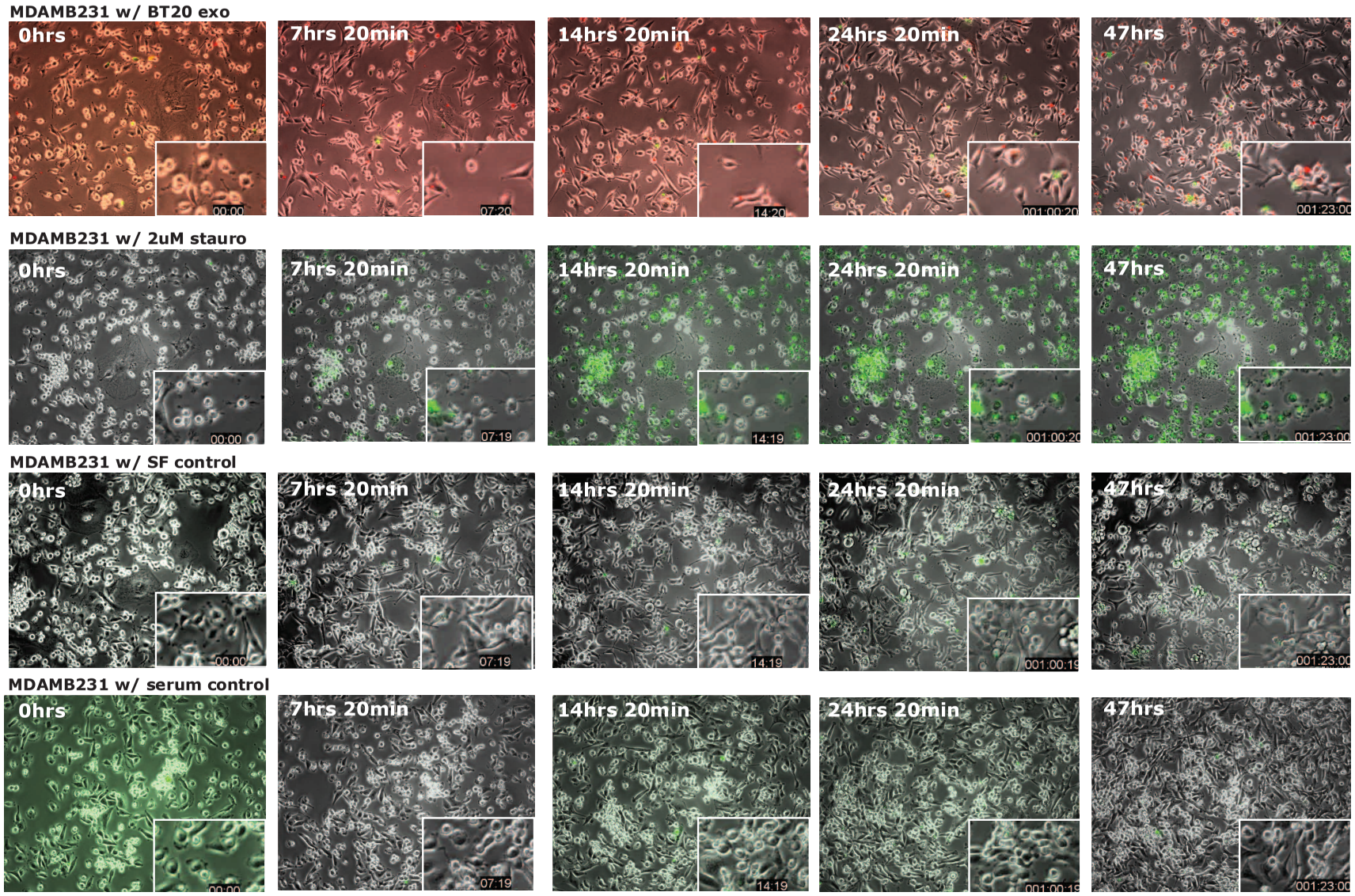

Figure 2.13: Timelapse imaging series of MDAMB231 cells in the presence of PKH26-labelled BT20-derived exosomes , 2μM staurosporine as a positive apoptosis control, serum-free RPMI and serum-supplemented RPMI culture as negative apoptosis controls. Cells were imaged for 48hrs, with a 15min timestep, using a 10x magnification objective. All were incubated with 2.5μM of EGFP caspase-3 NucView apoptotic reporter.

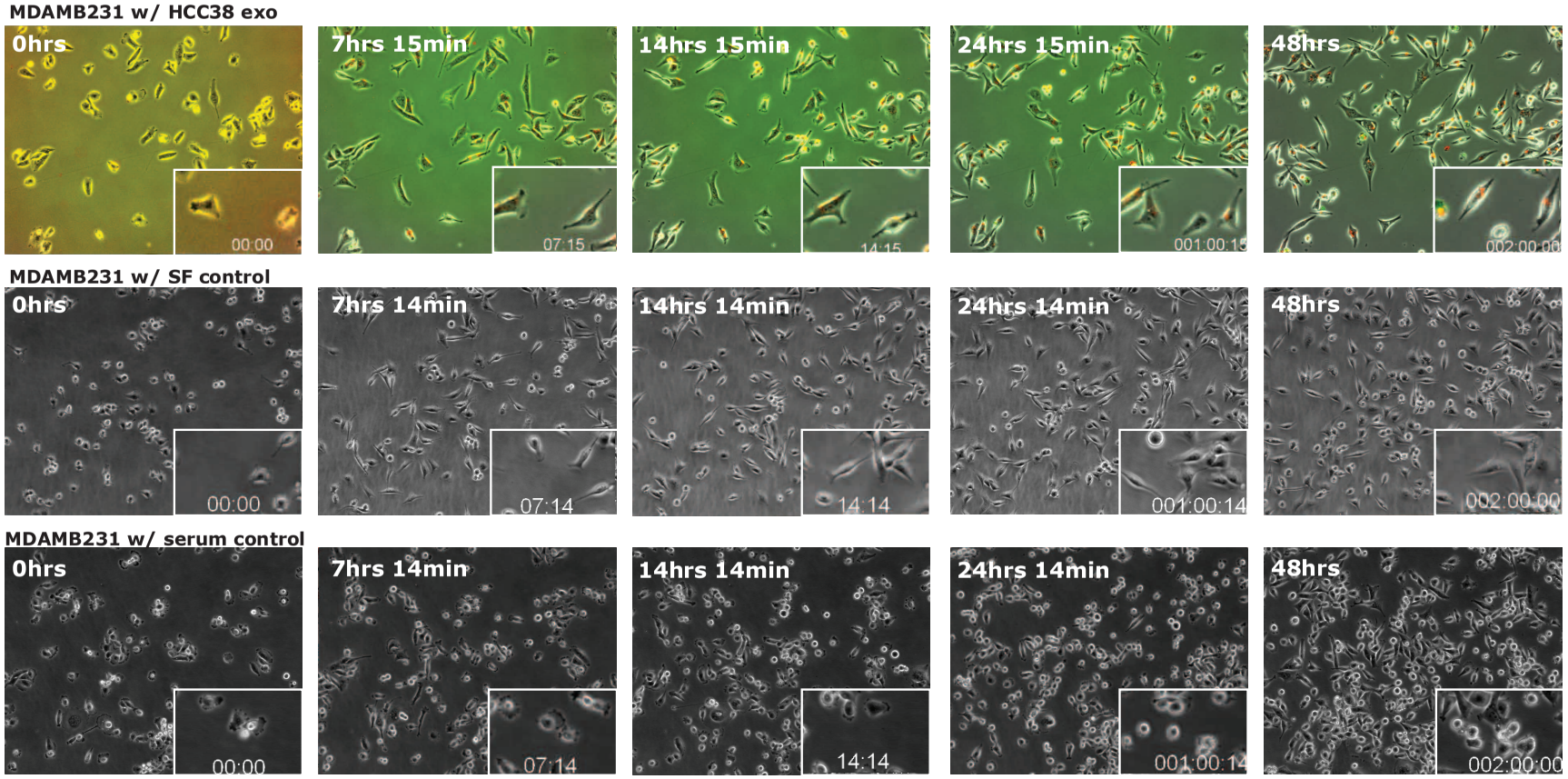

Figure 2.14: Timelapse imaging series of MDAMB231 cells in the presence of PKH26-labelled HCC38-derived exosomes , 2μM staurosporine as a positive apoptosis control and serum-free RPMI culture as a negative apoptosis control. Cells were imaged for 48hrs, with a 15min timestep, using a 20x magnification objective. Exosome containing wells were incubated with 2.5μM of EGFP caspase-3 NucView apoptotic reporter.

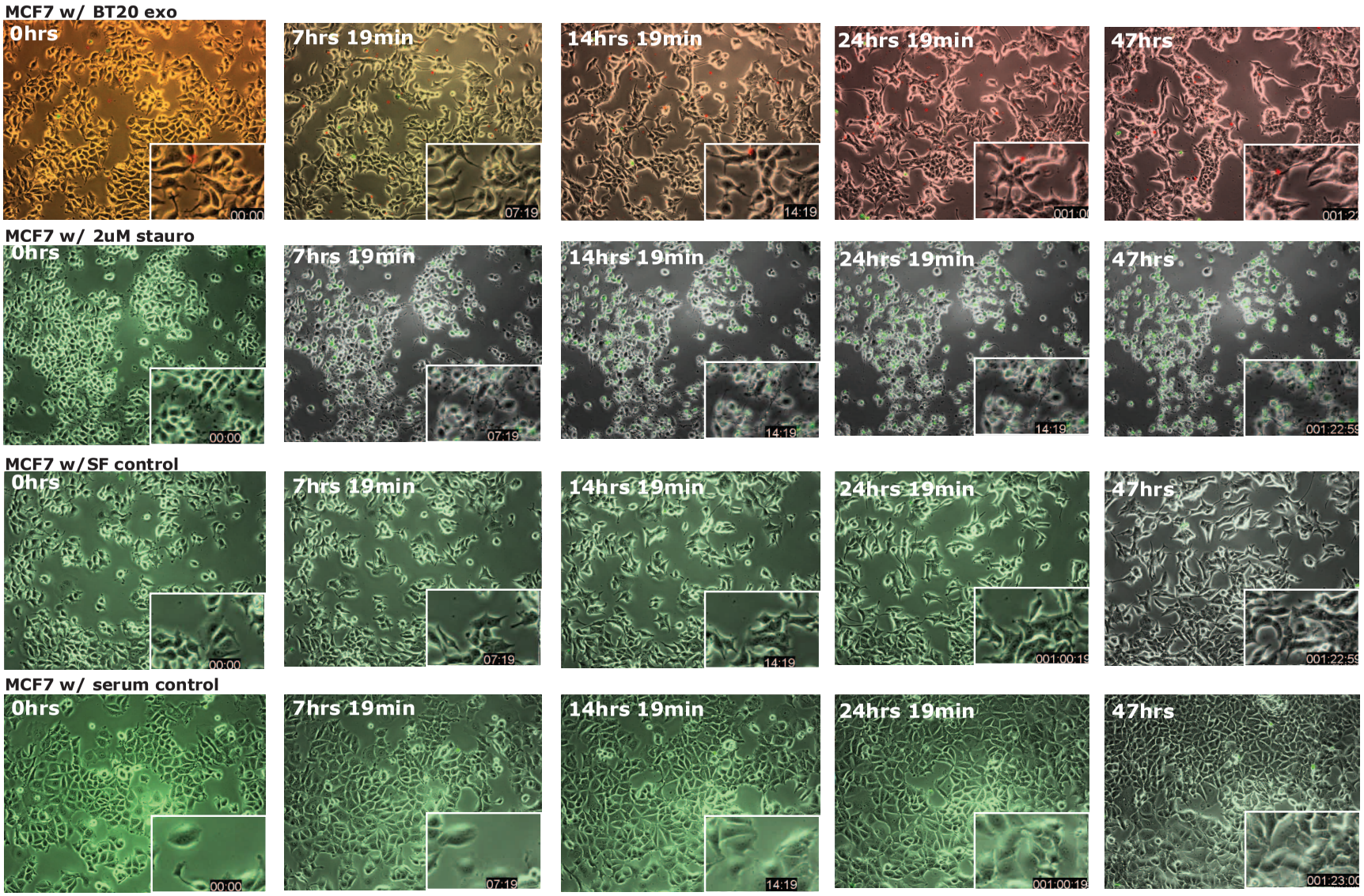

Figure 2.15: Timelapse imaging series of MCF7 cells in the presence of PKH26-labelled BT20-derived exosomes, 2μM staurosporine as a positive apoptosis control, serum-free RPMI and serum-supplemented RPMI culture as negative apoptosis controls. Cells were imaged for 48hrs, with a 20min timestep, using a 10x magnification objective. All wells were incubated with 2.5μM of EGFP caspase-3 NucView apoptotic reporter.

References

1. Neve, R. M. *et al.* A collection of breast cancer cell lines for the study of functionally distinct cancer subtypes. *Cancer Cell* **10,** 515–27 (2006).

2. Heiser, L. M. *et al.* Subtype and pathway speci fi c responses to anticancer compounds in breast cancer. (2011). doi:10.1073/pnas.1018854108/-/DCSupplemental.www.pnas.org/cgi/doi/10.1073/pnas.1018854108

3. Leers, M. P. *et al.* Immunocytochemical detection and mapping of a cytokeratin 18 neo-epitope exposed during early apoptosis. *J. Pathol.* **187,** 567–72 (1999).

4. Schutte, B. *et al.* Keratin 8/18 breakdown and reorganization during apoptosis. *Exp. Cell Res.* **297,** 11–26 (2004).

5. Peviva. M30 CytoDeath™ ELISA.

6. Cen, H., Mao, F., Aronchik, I., Fuentes, R. J. & Firestone, G. L. DEVD-NucView488: a novel class of enzyme substrates for real-time detection of caspase-3 activity in live cells. *FASEB J.* **22,** 2243–52 (2008).

7. Feng, D. *et al.* Cellular internalization of exosomes occurs through phagocytosis. *Traffic* **11,** 675–87 (2010).

Chapter 3

Transcriptomic and Proteomic Analysis of Conditioned Media

Abstract

We previously screened twenty breast cancer cell lines for apoptotic and proliferative response to twenty conditioned media (CM). This screen revealed that CM BT20 and CM HCC38 have strong pro-apoptotic activity on the majority of cell lines tested. As a systematic approach to uncovering molecular pathways underlying response to conditioned media, we proceed to correlate the phenotypic data matrices to transcriptomic data. This analysis identifies genes whose expression correlates strongly with the conditioned media matrices. Moreover we undertake mass spectrometry analysis of the two most apoptosis-inducing conditioned media, which reveals a list of common pro-apoptotic proteins in the two media. In addition to pro-apoptotic hits, the CM mass spectrometry dataset reveals a significant amount of cytoplasmic proteins as well as cell membrane receptors present in the extracellular space. We hypothesize that these molecules are expelled in the extracellular space as a result of a particulate secretory mechanism, and we proceed to purify this particulate fraction. The last section of this chapter covers the mass spectrometry analysis of the particulate fraction and compares it to the full CM in an attempt to shorten the list of candidate apoptotic molecules present in the CMs.

3.1 Correlation of Phenotypic Datasets to Transcriptional Gene Sets

In this part, we attempted to make a prediction as to the molecular nature of select conditioned media interactions, by correlating the phenotypic proliferative and apoptotic matrices to the transcriptional profiles of the cell lines.

Methods

Microarray gene expression data were obtained from a public database (http://cancer.lbl.gov/breastcancer/data), which contains the transcriptional characterization of 51 breast cancer cell lines. The authors of that work used an Affymetrix high-density oligonucleotide array human HG-U133A chip[1], and generated probe set based gene expression measurements from quantified Affymetrix image files (''.CEL'' files) using the BioConductor tool suite. All CEL files were analyzed simultaneously, creating a data matrix of probe sets by cell lines in which each value is the calculated log abundance of each probe set gene for each cell line.

From this file, containing information for 51 cell lines, we obtained the log transcriptional profiles of 18 cell lines involved in the conditioned medium experimental matrix. The file was annotated using IPA Ingenuity software. Gene set enrichment was also performed with IPA Ingenuity, to obtain two gene sets to be used in this correlative analysis: 'Proliferation of Breast Cancer Cell Lines' and 'Apoptosis of Breast Cancer Cell Lines'. These gene sets were further annotated so that the genes were separated into four localization categories: secreted, plasma

membrane, cytoplasmic, nuclear. Only the secreted and plasma membrane molecules were retained for this analysis.

For the purpose of correlation the two data sets, both the gene set as well as the phenotypic data set were normalized to a value between 0 and 1. This was achieved in the transcriptional data set by dividing each gene with by the maximum expression value that gene attains across all 18 cell lines. In turn, phenotypic data sets were normalized to the highest apoptosis/proliferative response of one cell line across all CM stimuli.

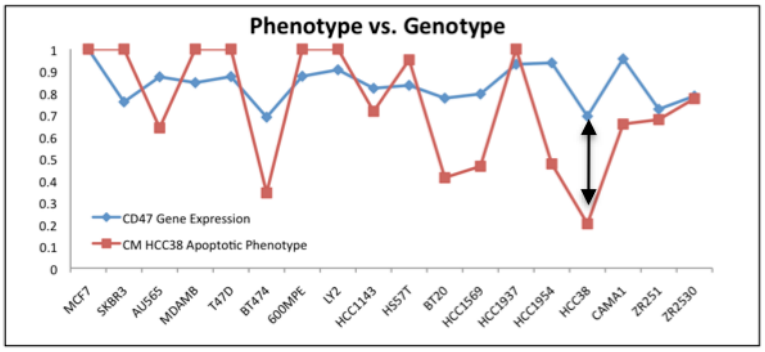

Figure 3.8: Correlation of phenotypic data set to transcription data set. Adding absolute distances over all cell lines.

Next, the absolute distances between the CM response and the gene expression value for a particular gene are calculated across all cell lines (figure 3.1). These distances are added up and constitute the 'Gene Score', of how well that particular gene correlates with the phenotypic profile that a CM causes across all cell lines:

$$GeneScore = \sum |x - y|$$

The lowest the score, the stronger the correlation. Seeing that several genes are represented by multiple gene probes in the data set, the correlation algorithm is repeated separately for each probe. Then, the probe displaying the closest

correlation is inserted into the final data matrix, while remaining probes are discarded.

Results of correlation to transcriptional gene sets

Repeating this for both gene sets gives rise to two correlation matrices. On the apoptosis correlative matrix (fig 3.2), we observe CM HCC38 and CM BT20 to cluster together and display a high correlation to most apoptotic genes. They are followed by CM HCC1954 and CM HS578T, which were also identified as pro-apoptotic CMs in the previous section. On the proliferation correlative matrix (fig 3.3), we observe CM BT20, which also has a strong anti-proliferative activity -as discussed previously- to correlate the least of all CMs to the proliferative gene set. Genes that had a strong correlation with the majority of conditioned media were singled out as hits, meriting further investigation. These are denoted with red boxes on the apoptotic and proliferative clusters.

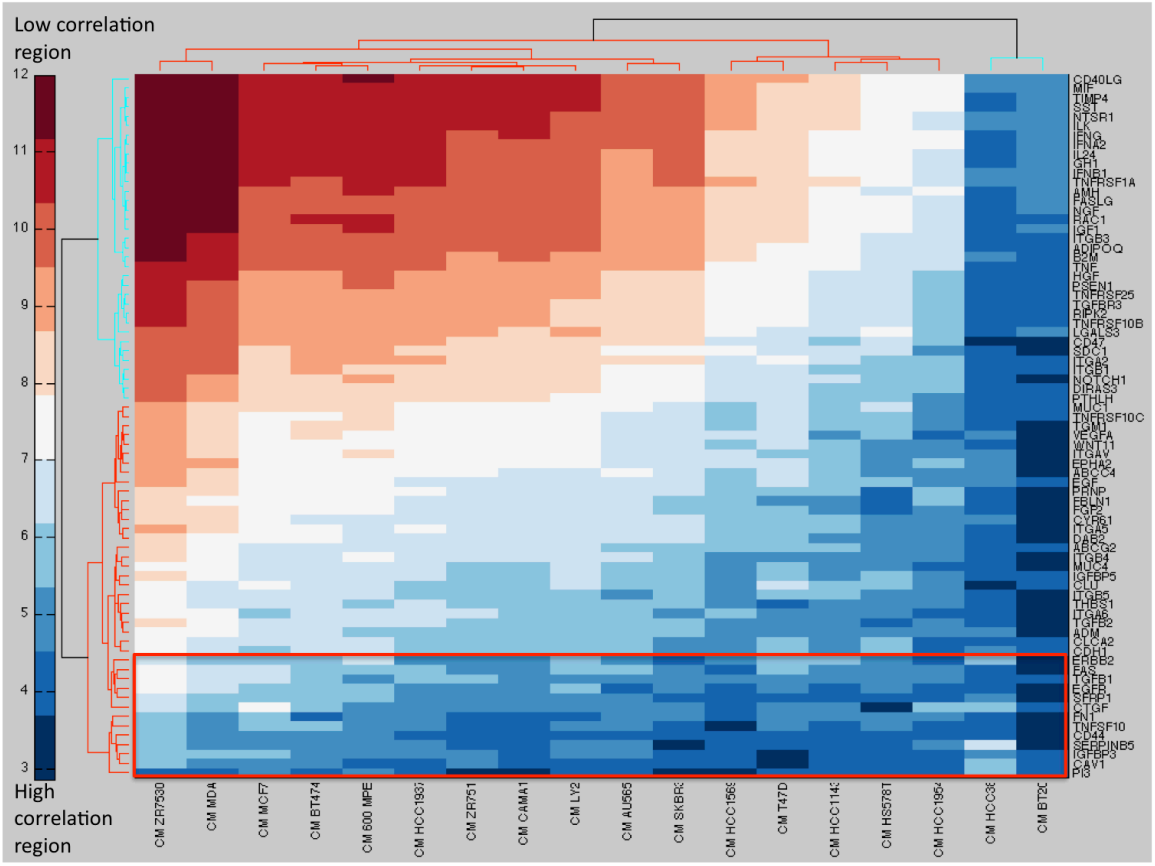

Figure 3.9: Correlation of apoptosis phenotypic dataset to apoptotic transcriptional gene set.

Next, the expression levels of hit genes is examined across all cell lines (fig 3.4 & fig 3.5). We make the simplifying assumption that genes whose expression level does not considerably fluctuate across cell lines, are most likely not responsible for the CM interactions, since their levels are the same in all CMs and subsequently cross them out on figure 3.4. In order to compare expression levels, we center the log values in the original transcriptional data set, by subtracting the median of a cell line across all genes from each gene's expression value. We compare expression levels for a particular hit gene by averaging over the multiple gene probes on figure 3.4. On

figure 3.5 we go even further in depth by comparing each gene probe separately in those hit genes that display great probe-to-probe variability.

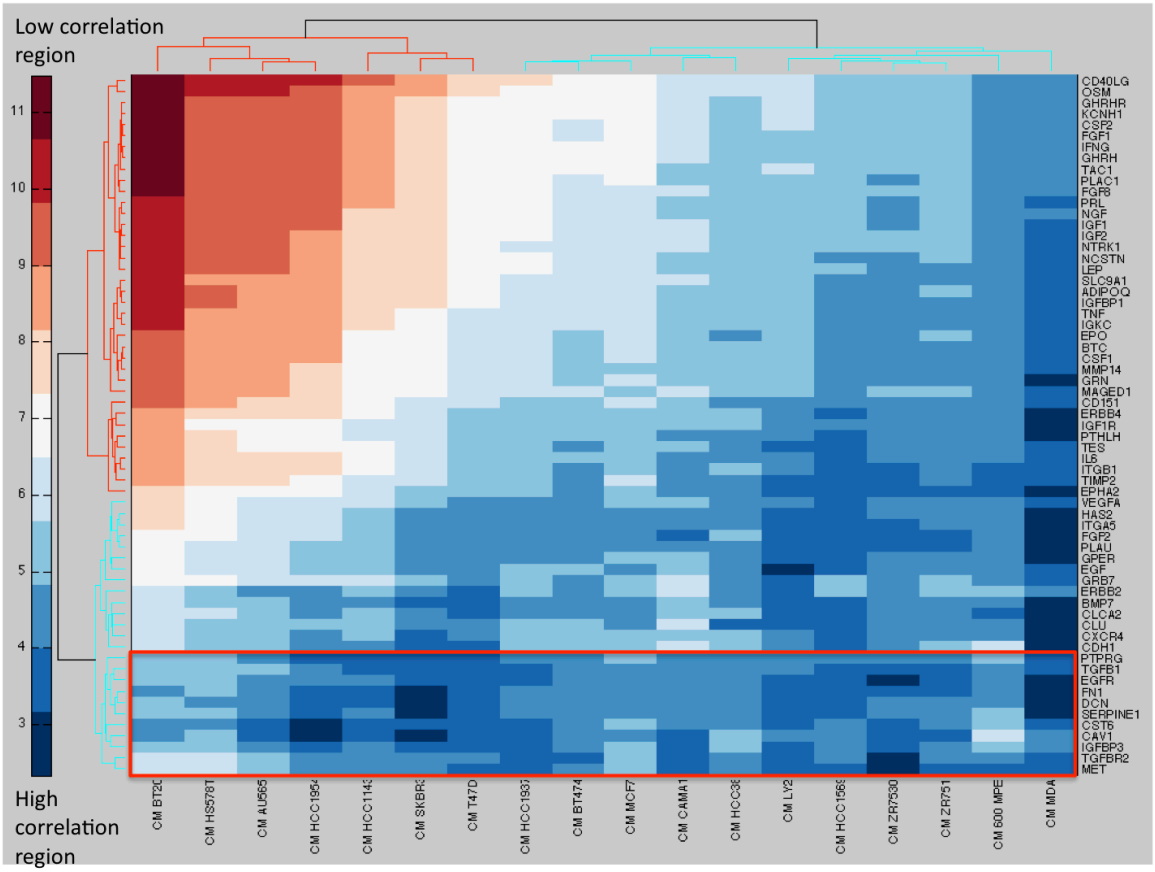

Figure 3.10: Correlation of proliferation phenotypic dataset to proliferative transcriptional gene set.

One application of this analysis is identifying overexpression of specific gene products in our pro-apoptotic CMs of interest: CM BT20 and CM HCC38. These are denoted on figure 3.4 & 3.5 by red arrows. The findings are summarized in table 3.2. Starting with HCC38 cells we observe that according to this correlative analysis, insulin **growth factor binding protein 3** (IGFBP3) and **fibronectin 1** (FN1) are over-secreted and set this CM apart from the majority of breast cancer cell lines. The

overexpression of IGFBP3 is a common trait in triple negative cells, since HCC1937, HCC1143 and HS578T also share it in varying amounts. The overexpression of FN1 is a rarer occurrence, also present in a single other cell line: HS578T cells. IGFBP3 is a documented antagonist of the IGF receptor and therefore a recognized apoptotic molecule. Exogenous IGFBP3 has been shown to inhibit proliferation of HS578T cells[2], as well as induce apoptosis in MCF7 cells[3]. However since other cell lines, that are producers of less toxic CMs, also feature an increased transcript of IGFBP3, this alone cannot explain the strong apoptotic activity of HCC38 CM. In addition to regulating IGF-ligand bioavailability, IGFBPs can also influence cell fate through IGF-independent mechanisms.

Fibronectin 1 on the other hand is only overexpressed in two considerably pro-apoptotic CM producers (HCC38 and HS578T). It is perhaps not surprising that these two triple negative breast cancer cell lines produce higher amounts of extracellular matrix, as that would improve their survival and migratory phenotypes as compared to less aggressive luminal cells. But how do cell lines of more epithelial phenotype react to culture in fibronectin-rich conditioned media? Soluble fibronectin can actually promote cell detachment and rounding in epithelial tissue culture monolayers[4]. Most importantly, in a study performed with HS578T cells, McCaig et al.[5] showed that soluble fibronectin interacts directly with IGFBP3 and IGFBP5 to modulate cell attachment. According to the transcriptional profiles, neither IGFBP3 of FN1 alone is sufficient to induce apoptosis. However the cocktail of the two combined can promote an anoikis phenotype in breast cancer cells.

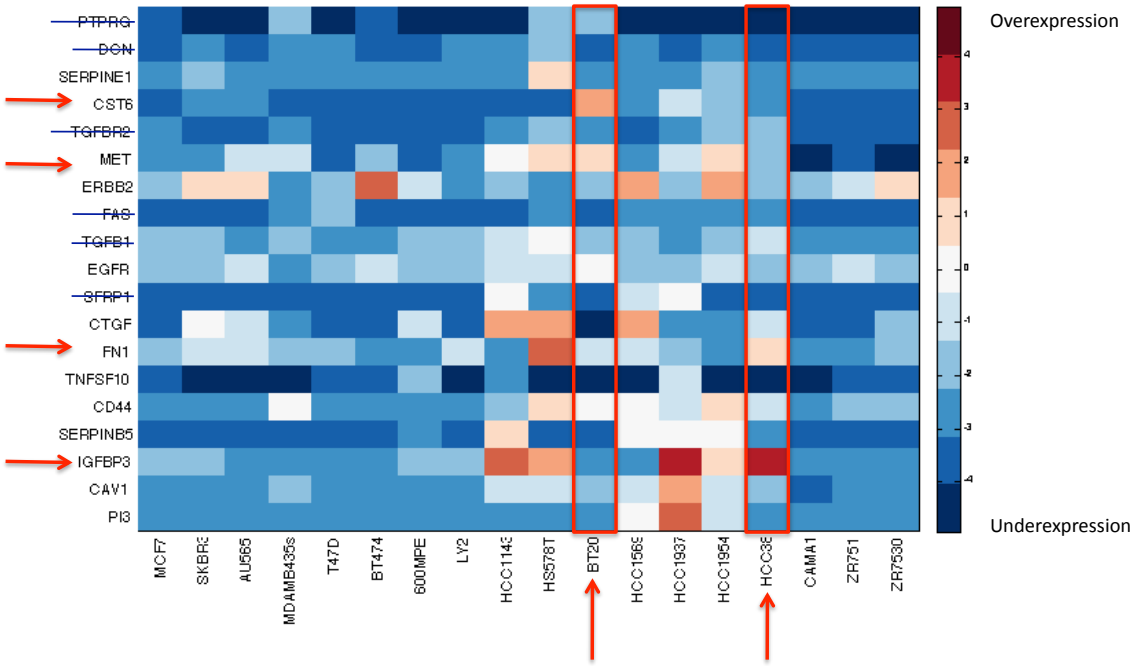

Figure 3.11: Heat map of expression levels of hit genes, averaged against all gene probes. Red boxes enclose the two cell lines producing the strongest apoptotic media. Red arrows indicate genes that are significantly overexpressed in these cell lines, in comparison to the rest. Crossed out genes in blue have relatively stable expression value across all cell lines and are therefore considered non-critical for the CM-interaction experiments.

Surprisingly there are no common secreted protein hits between our two pro-apoptotic media producing cell lines: BT20 and HCC38. The only secreted hit for BT20 cells is **cystatin M** (CST6), a secreted cysteine protease inhibitor that has been identified as a tumor suppressor gene that is epigenetically silenced during mammary tumorigenesis[6]. Cystatin M is a cathepsin inhibitor[7] –a protein class that we will touch upon in the following section of this chapter. According to the transcriptional dataset, BT20 cells are the only ones over-expressing this particular molecule.

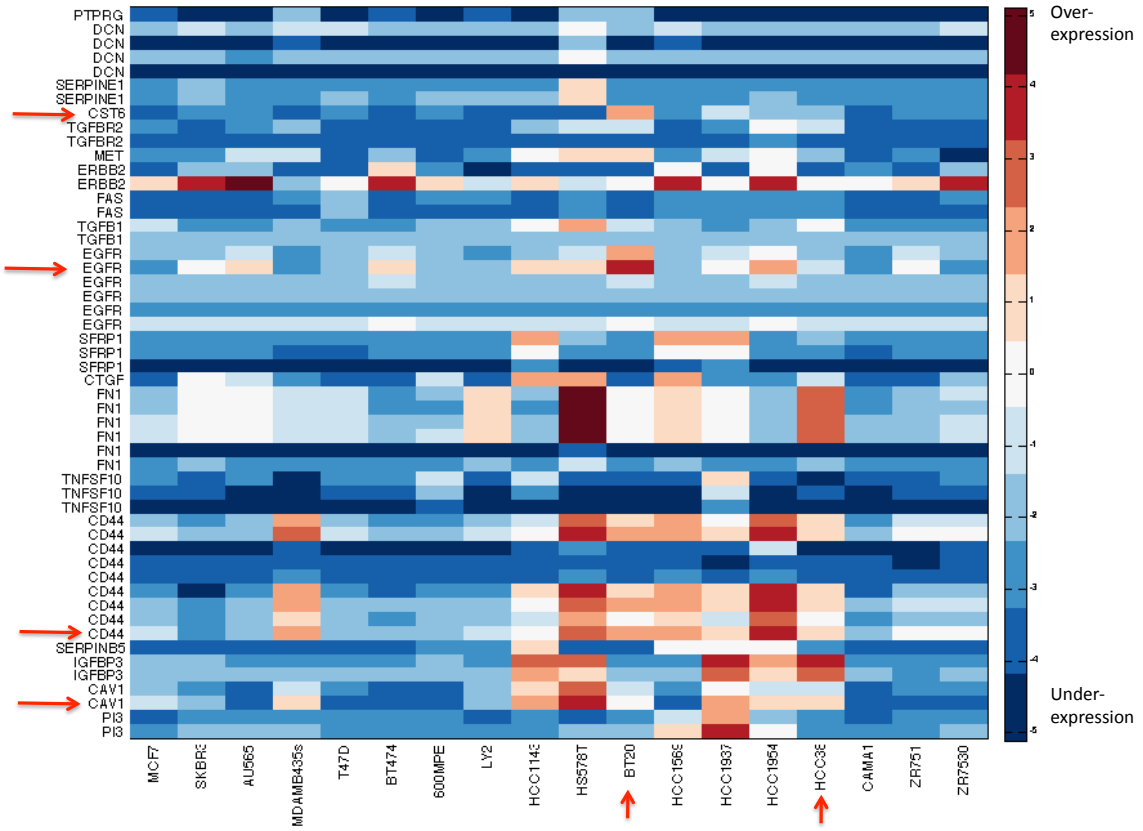

Figure 3.12: Heat map of expression levels of hit genes, showing individual gene probes. Vertical red arrows delineate the two cell lines producing the strongest apoptotic media. Horizontal red arrows indicate genes that are significantly overexpressed in these cell lines, in comparison to the rest.

In addition to secreted hits, the analysis identified plasma membrane receptors that are overexpressed in our two cell lines of interest. The underlying hypothesis here is that overexpression of a surface receptor on these cells can be depleting the media from vital growth factors at the time of CM production. One of these molecules - surface receptor for **hyaluronic acid** (CD44)- is common for both pro-apoptotic CMs. Once again this is a molecule associated with cell anchorage to the extracellular matrix, and as such related to cell survival rather than pro-apoptotic activity. The remaining plasma membrane hit for HCC38 cells is **caveolin1** (CAV1), a scaffolding

protein that couples integrins to various upstream tyrosine kinases. This gene is considered a tumor suppressor[8], and therefore is also unlikely to be involved in a pro-apoptotic activity. The remaining plasma membrane hits fro BT20 cells are the **epidermal growth factor receptor** (EGFR) and **hepatocyte growth factor receptor** (MET). Both of these are receptors of ubiquitous and multiple ligands and could very well be depleting the media from proliferative signals.

HCC38 Gene Hits	Full Name	Localization	Apoptotic Correlation	Proliferative Correlation	Single or multiple probe
IGFBP3	Insulin growth factor binding protein 3	Extracellular Space	✔	✔	Multiple 100%
FN1	Fibronectin 1	Extracellular Space	✔	✔	Multiple 71%
CAV1	Caveolin 1	Plasma Membrane	✔	✔	Single - 50%
CD44	Hyaluronate Receptor	Plasma Membrane	✔		Multiple 56%
BT20 Gene Hits	**Full Name**	**Localization**	**Apoptotic Correlation**	**Proliferative Correlation**	**Single or multiple probe**
CST6	Cystatin	Extracellular Space		✔	Single 100%
EGFR	Epidermal Growth Factor Receptor	Plasma Membrane	✔	✔	Multiple 33%
MET	Hepatocyte Growth Factor Receptor	Plasma Membrane		✔	Single 100%
CD44	Hyaluronate Receptor	Plasma Membrane	✔		Multiple 56%

Table 3.1: Hit gene candidates for HCC38 and BT20 cell lines.

One caveat of this analysis is that the gene set information for the breast cancer cell lines was acquired on the transcriptional level. However there are numerous biological events that can alter the expression of a final protein product after

transcription. To name a few: post-transcriptional regulation, alternative splicing, RNA degradation, translational inefficiency, protein modification and varied protein half-lives. Even though comparing the cell lines on the mRNA level is a good first step in visualizing their diverse genetic identities and yields some tentative predictions on the secreted content of the corresponding CMs, only proteomic analysis can irrefutably prove the presence of secreted proteins in the CM. In the following section we will do just that and examine how the proteomic makeup of select CMs compares to the transcriptional predictions.

3.2 Proteomic Analysis of HCC38 and BT20 Derived Conditioned Media

In this section we performed proteomic analysis of the HCC38 and BT20 derived conditioned media. We subsequently compare the resulting protein lists against each other and identified common pro-apoptotic hits present in both CMs as well as pro-apoptotic proteins unique to each CM. Finally we scanned both lists for the presence of the protein products predicted in the previously reported transcriptional analysis. For brevity and clarity we did not feature the complete list of mass spectrometry results in this section, but rather an abridged comparative version of it, focused on apoptosis associated molecules.

Methods

Cells were seeded at a density of 10^6 cells/ml in T-150 culture flasks and allowed to adhere to flask surface overnight. The monolayers were then washed twice with PBS and growth medium was replaced with serum-free RPMI, supplemented with 1% Penicillin-Streptomycin and buffered with 10mM Hepes. 12 ml of conditioned medium were harvested 24hrs later and centrifuged 3min at 1,000g to exclude cell debris. The CMs were then concentrated by centrifugation at 4,000g through a 3,000kDa membrane. 25ul of concentrate from the centrifugation were loaded and run halfway on an SDS-PAGE gel, using MOPS buffer. The gel was stained with Coomassie Blue and each gel lane was cut, under sterile conditions, into two sections. All sections were submitted for micro-capillary LC/MS/MS analysis at the Taplin Mass Spectrometry Facility of Harvard Medical School.

Excised gel bands were cut into approximately $1mm^3$ pieces. Gel pieces were then subjected to a modified in-gel trypsin digestion procedure. Gel pieces were washed and dehydrated with acetonitrile for 10 min. followed by removal of acetonitrile. Pieces were then completely dried in a speed-vac. Rehydration of the gel pieces was with 50 mM ammonium bicarbonate solution containing 12.5 ng/µl modified sequencing-grade trypsin (Promega, Madison, WI) at 4ºC. After 45 min., the excess trypsin solution was removed and replaced with 50 mM ammonium bicarbonate solution to just cover the gel pieces. Samples were then placed in a 37ºC room overnight. Peptides were later extracted by removing the ammonium bicarbonate solution, followed by one wash with a solution containing 50% acetonitrile and 1% formic acid. The extracts were then dried in a speed-vac (~1 hr). The samples were then stored at 4ºC until analysis.

On the day of analysis the samples were reconstituted in 5 - 10 µl of HPLC solvent A (2.5% acetonitrile, 0.1% formic acid). A nano-scale reverse-phase HPLC capillary column was created by packing 5 µm C18 spherical silica beads into a fused silica capillary (125 µm inner diameter x ~20 cm length) with a flame-drawn tip. After equilibrating the column each sample was loaded via a Famos auto sampler (LC Packings, San Francisco CA) onto the column. A gradient was formed and peptides were eluted with increasing concentrations of solvent B (97.5% acetonitrile, 0.1% formic acid).

As peptides eluted they were subjected to electrospray ionization and then entered into an LTQ Velos ion-trap mass spectrometer (ThermoFisher, San Jose, CA). Peptides were detected, isolated, and fragmented to produce a tandem mass spectrum of specific fragment ions for each peptide. Peptide sequences (and hence protein identity) were determined by matching protein databases with the acquired fragmentation pattern by the software program, Sequest (ThermoFisher, San Jose, CA). Spectral matches were manually examined and multiple identified peptides per protein were required.

Results

Figure 3.6 summarizes the results from the mass spectrometry analysis. The two conditioned media had 155 proteins in common, which in both cases corresponded to more than half of the total protein count. The list of common proteins was annotated for localization and function using IPA Ingenuity. This allowed us to bin the proteins in functional categories (figure 3.6b). The most salient feature of this analysis is that the majority of proteins in both conditioned media are of cytoplasmic origin. Next in abundance are extracellular proteins, followed by plasma membrane proteins. Finally, we observe a small percentage of nuclear proteins present in the CMs.

In terms of functional annotation, the largest functional group of proteins comprise - or associate with- the cell's cytoskeleton. That is not surprising, considering that these are high abundance proteins is cells. The next largest functional category is

glycolysis-associated proteins, followed by heat shock proteins. After that follows a large group of proteases/peptidases, extracellular matrix proteins, transcriptional and translational regulators and molecular chaperones. Most of these abundant protein categories, perhaps with the exception of proteases, are housekeeping in origin and cannot be readily associated with pro-apoptotic or anti-proliferative phenotypes. However, some of the less abundant proteins groups have more interesting functional characterization attached to them. Namely, we found kinase inhibitors, tumor suppressors, cytokines and inflammatory molecules within the common protein list.

In table (a) of figure 3.6, we list the common apoptosis-related molecules between CMs HCC38 and BT20. Among those we note a family of **kallikrein-related peptidases** characteristic of steroid-regulated cancers. Perhaps the most famous member of the kallikrein family is kallikrein 3, also known as prostate-specific antigen (PSA), a key diagnostic molecule in prostate cancer. While kallikrein 3 and 4 are androgen-regulated genes expressed almost exclusively in the prostate, kallikrein 5 (KLK5) and kallikrein 6 (KLK6) are estrogen-regulated and expressed in the breast and ovaries. In a study using human tissue samples, kallikrein genes 5 and 6 were found to be down-regulated in breast cancer relative to healthy mammary tissue[9]. It is presently unclear whether these proteases promote tumor progression or amount to a pro-apoptotic signal for the cancerous mass. However, what is known is that serpins are active inhibitors of kallikreins[10]. These two secreted protein groups can therefore interact in the extracellular space and

modulate the tumor environment. When considered within the scope of this study, different cancer cell lines express different amounts of serpins as shown in figure 2.4 for SERPINA1 and SERPINB5. In addition to that, our two pro-apoptotic CMs secrete varying amounts of KLK5 and KLK6. The interaction between the kallikreins of the donor cell line and the serpins secreted by the receiver cell line could very well contribute to the regulation of the receiver cell fate.

Among the proteases, **cathepsin D** (CTSD) is another common hit between the two CMs worth mentioning. This aspartic protease has been long identified as a clinical marker for poor prognosis in breast cancer patients[11]. Similarly to kallikreins, it is estrogen-regulated. However, in contrast to other proteases it only becomes activated under acidic pH conditions. Its potential role in apoptosis is ambiguous. When secreted, cathepsin D acts as a mitogen for cancer cells, either by directly binding unknown growth receptors on the cells or by proteolytic degradation of growth factor inhibitors or by proteolytic activation of growth factor receptors. However it has also been shown to enhance apoptotic cascades that were induced by apoptotic agents, including serum starvation or oxidative stress[12].

Quiescin (QSOX) is another common protein present in both CMs. Pernodet et al. have quantified expression levels of QSOX in different breast cancer cells and found MCF7 to express it more than MDA-MB-231 cells. Quiescin is therefore differentially expressed in different breast cancer cells. In the same study, the authors investigated the effect of exogenous quiescin over-expression in these cell lines.

They found that the QSOX-overexpressing clones proliferated less and were more dependent on extracellular matrix adhesion for survival[13].

In tables (c) and (d) of figure 3.6 we display the apoptosis-related hits that were unique to CM BT20 and CM HCC38 respectively. We note that both CMs contain additional yet different members of the cathepsin family. The same is true for proteasome subunits. In addition, CM BT20 contains **insulin-growth-factor-binding-protein 5 (IGFBP5)**, a secreted antagonist of the IGF receptor that captures and arrests IGF ligands. IGFBPs are well documented pro-apoptotic molecules shown to induce apoptosis of MCF7 cells in culture[3]. However their pro-apoptotic activity in the extracellular space can be curtailed by secreted kallikreins and cathepsins[14]. Once again the breast cancer conditioned media emerge as complex solutions of pro-apoptotic and pro-proliferative molecules that in addition to stimulating the receiver cells, are also actively interacting with each other.

a.

Symbol	Entrez Gene Name	BT20 CM Peptide count	HCC38 CM Peptide Count	Location
Tumor Supressors				
QSOX1	quiescin Q6 sulfhydryl oxidase 1	14.000	11.000	Cytoplasm
PDCD6IP	programmed cell death 6 interacting protein	3.000	3.000	Cytoplasm
Peptidases				
PDIA3	protein disulfide isomerase family A, member 3	10.000	6.000	Cytoplasm
CTSD	cathepsin D	14.000	4.000	Cytoplasm
PSMA4	proteasome (prosome, macropain) subunit, alpha type, 4	3.000	3.000	Cytoplasm
PSMA5	proteasome (prosome, macropain) subunit, alpha type, 5	3.000	3.000	Cytoplasm
CNDP2	CNDP dipeptidase 2 (metallopeptidase M20 family)	3.000	4.000	Cytoplasm
PSMA6	proteasome (prosome, macropain) subunit, alpha type, 6	3.000	4.000	Cytoplasm
GGH	gamma-glutamyl hydrolase (conjugase, folylpolygammaglutamyl hydrolase)	3.000	5.000	Cytoplasm
CFI	complement factor I	4.000	3.000	Extracellular Space
KLK5	kallikrein-related peptidase 5	4.000	3.000	Extracellular Space
KLK6	kallikrein-related peptidase 6	5.000	3.000	Extracellular Space
NPEPPS	aminopeptidase puromycin sensitive	6.000	6.000	Cytoplasm
Kinase Inhibitors/Regulators				
YWHAE	tyrosine 3-monooxygenase/tryptophan 5-monooxygenase activation protein, epsilon polypeptide	11.000	5.000	Cytoplasm
PEBP1	phosphatidylethanolamine binding protein 1	3.000	4.000	Cytoplasm
PPP2R1A	protein phosphatase 2, regulatory subunit A, alpha	3.000	5.000	Cytoplasm
SFN	stratifin	5.000	6.000	Cytoplasm
YWHAZ	tyrosine 3-monooxygenase/tryptophan 5-monooxygenase activation protein, zeta polypeptide	6.000	5.000	Cytoplasm

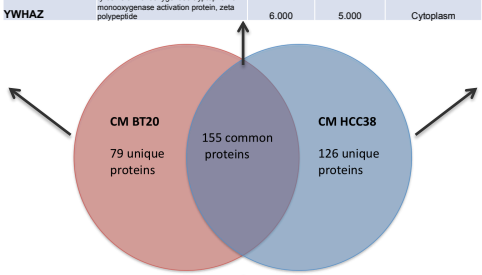

b.

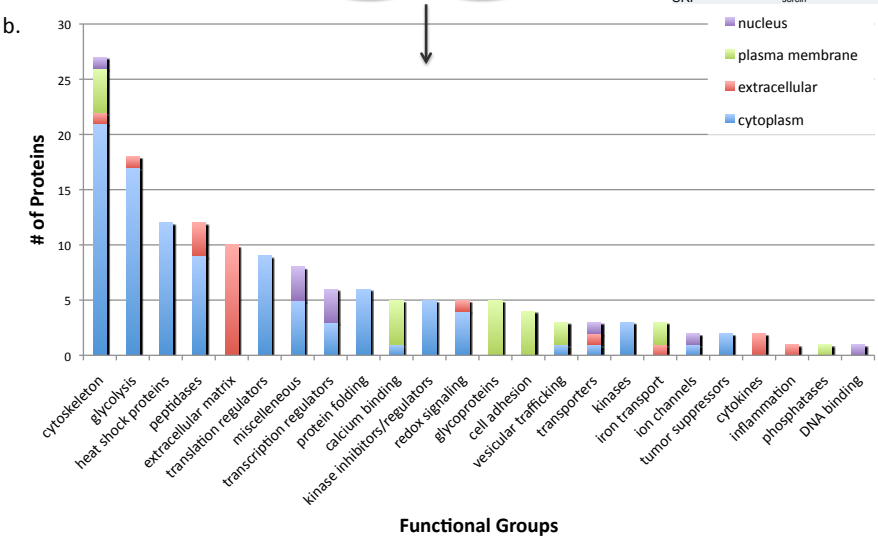

c.

Symbol	Entrez Gene Name	BT20 CM Peptide Count	Location
Proteases			
CPA4	carboxypeptidase A4	11.000	Extracellular Space
APEH	N-acylaminoacyl-peptide hydrolase	3.000	Cytoplasm
CTSH	cathepsin H	3.000	Cytoplasm
LGMN	legumain	3.000	Cytoplasm
PSMD5	proteasome (prosome, macropain) 26S subunit, non-ATPase, 5	3.000	Cytoplasm
CAPN1	calpain 1, (mu/l) large subunit	4.000	Cytoplasm
CTSA	cathepsin A	4.000	Cytoplasm
CTSL2	cathepsin L2	4.000	Cytoplasm
PSMA7	proteasome (prosome, macropain) subunit, alpha type, 7	4.000	Cytoplasm
PSME2	proteasome (prosome, macropain) activator subunit 2 (PA28 beta)	4.000	Cytoplasm
Growth Factor Binding			
IGFBP5	insulin-like growth factor binding protein 5	5.000	Extracellular Space

d.

Symbol	Entrez Gene Name	HCC38 CM Peptide Count	Location
Proteases			
ANPEP	alanyl (membrane) aminopeptidase	9.000	Plasma Membrane
C1S	complement component 1, s subcomponent	6.000	Extracellular Space
UCHL1	ubiquitin carboxyl-terminal esterase L1 (ubiquitin thiolesterase)	5.000	Cytoplasm
MMP7	matrix metallopeptidase 7 (matrilysin, uterine)	5.000	Extracellular Space
ACE	angiotensin I converting enzyme (peptidyl-dipeptidase A) 1	5.000	Plasma Membrane
PSMA3	proteasome (prosome, macropain) subunit, alpha type, 3	4.000	Cytoplasm
USP15	ubiquitin specific peptidase 15	4.000	Cytoplasm
C1R	complement component 1, r subcomponent	4.000	Extracellular Space
CTSB	cathepsin B	3.000	Cytoplasm
PSMD2	proteasome (prosome, macropain) 26S subunit, non-ATPase, 2	3.000	Cytoplasm
PSME1	proteasome (prosome, macropain) activator subunit 1 (PA28 alpha)	3.000	Cytoplasm
PSMB1	proteasome (prosome, macropain) subunit, beta type, 1	3.000	Cytoplasm
PSMB3	proteasome (prosome, macropain) subunit, beta type, 3	3.000	Cytoplasm
MMP2	matrix metallopeptidase 2 (gelatinase A, 72kDa gelatinase, 72kDa type IV collagenase)	3.000	Extracellular Space
Calcium Binding			
S100A11	S100 calcium binding protein A11	5.000	Cytoplasm
S100A6	S100 calcium binding protein A6	3.000	Cytoplasm
SRI	sorcin	3.000	Cytoplasm

Figure 3.6: Proteomic analysis of BT20 and HCC38 derived conditioned media.
The Venn diagram positioned in the middle indicates the number of overlapping proteins that were indentified in both CMs. a) The table contains select pro-apoptotic proteins that were identified in both CMs and their comparative peptide count. b) Following ontology and localization analysis of the common proteins between CM HCC38 and CM BT20, we plot the number of proteins found in each functional category. The bar color encodes for cellular localization: nucleus (purple), plasma membrane (green), extracellular (red) and cytoplasm (blue). c) Select pro-apoptotic proteins which are unique to CM BT20. d) Select pro-apoptotic proteins which are unique to CM HCC38.

Within CM HCC38 we identify two members of the **S100A** family: S100A11 and S100A6. These are intracellular calcium-binding proteins that regulate a wide range of cell functions, namely cytoskeletal dynamics, immune response and differentiation. A microarray study of pancreatic cancer identified S100A11 as a tumor suppressor that is upregulated in healthy tissue and the early stages of pancreatic carcinogenesis and decrease in expression during progression to cancer. Another study showed that intracellular S100A6 enhanced the sensitivity to apoptosis in hepatocellular carcinoma cells, via upregulation of caspase-3[15]. While there has been significant research elucidating intracellular functions of S100A proteins in cancer, it remains unclear whether these proteins have a functional role when found in the extracellular environment.

One additional advantage of this analysis is that it allows us to test the validity of the transcriptional dataset in terms of predicting the protein products in the extracellular and membranous fraction of the two cell lines. We construct table 3.2 for this purpose. Fibronectin (FN1) which was identified as a hit in the transcriptional analysis is actually present in both CMs, yet at larger quantity in CM HCC38. The remaining transcriptional hits for HCC38 cells (CAV1, CD44 and IGFBP3) were not actually present in the corresponding proteomic dataset. Instead we found IGFBP5, which was not transcriptionally predicted, present in CM BT20. In addition we see the growth factor receptors EGFR and MET to be present in the proteomic analysis of CM BT20, which again took us by surprise. Seeing that these

are receptors embedded in the plasma membrane we did not expect to find them in the secreted fraction of the CM, and yet they were present.

Symbol	Entrez Gene Name	CM BT20 Peptide Count	CM HCC38 Peptide Count	Location
FN1	fibronectin 1	7	46	Extracellular Space
IGFBP5	insulin-like growth factor binding protein 5	5	-	Extracellular Space
EGFR	epidermal growth factor receptor	7	-	Plasma Membrane
MET	met proto-oncogene (hepatocyte growth factor receptor)	5	-	Plasma Membrane
CD44	CD44 molecule (Indian blood group)	3	-	Plasma Membrane

Table 3.2: Hit overlap between transcriptional data set results (as summarized in table 2) and mass spectrometry analysis of conditioned media HCC38 and BT20.

Overall the proteomic analysis of the two CMs indicated that contrary to expectation, the extracellular medium of cultured breast cancer cells is not dominated by secreted protein products, but is instead rich in cytoplasmic and membrane proteins, including growth factor receptors and cell adhesion molecules. One possible interpretation of this finding is that during CM production apoptotic cells release their contents in the media or that during CM harvesting whole cells are lysed and cytosplasmic contaminants enter the CM. Another possibility is that cells actively shed or export part of their cytoplasm and plasma membrane in the extracellular space. The following chapter will further explore this possibility.

3.3 Proteomic Analysis of HCC38 and BT20 Exosome Fractions

In previous sections we established that breast cancer cells secrete exosome particles that we were able to successfully isolate from tissue culture supernatants. However, multiple apoptosis assays –both live cell imaging and M30 ELISA- showed that these microvesicles do not have significant apoptotic effect on recipient cells. In contrast our experiments indicate that the apoptotic activity is preserved in the supernatant of the exosome ultracentrifugation spin. In this section we perform mass spectrometry analysis of the HCC38 and BT20 exosome fractions. The purpose of this analysis is twofold. First, it is informative on the protein composition of exosomes. We will elaborate further on this point in the following chapter that is entirely dedicated to the characterization of exosome particles. Second, by comparing the mass spectrometry datasets of the exosome fraction to that of the full CM we are able to identify specific proteins unique to the CM fraction and by consequence narrow down the apoptotic candidate protein list.

Methods

LC/MS/MS Analysis

We purified exosomes out of tissue culture supernatant as described in the previous chapter. During the final ultracentrifugation step in the exosome purification process, the exosome pellet was resuspended in 25µl Laemmli buffer. The samples were heated at 95°C for 10min, then loaded and run halfway on an SDS-PAGE gel, using MOPS buffer. The gel was stained with Coomassie Blue and each gel lane was cut, under sterile conditions, into two sections. All sections were submitted for

micro-capillary LC/MS/MS analysis at the Taplin Mass Spectrometry Facility of Harvard Medical School and processed as described in the previous section.

Comparison of CM HCC38 and CM BT20 to corresponding exosomes

One overarching question we had when launching into this analysis was the size of the exosome protein content as compared to that of the full CM. In other words, are most proteins in the CM free-floating or are they organized in membrane-packaged exosomes? Figure 3.7a reveals that the majority of proteins from the mass spectrometry analysis are common between the exosome and full CM samples. In fact only 64 unique proteins in CM HCC38 were not identified in the corresponding exosomes. Of these, the majority were either of cytoplasmic or extracellular provenance, while there was also a smaller fraction of nuclear and plasma membrane proteins present (figure 3.7d).

Another relevant observation is that among these 64 unique protein hits, we identify both pro-apoptotic proteins (figure 3.7b) as well as pro-growth cytokines (figure 3.7c). The pro-apoptotic table contains a short list of proteases, many of which were already discussed in the proteomic analysis of the preceding section (figure 3.6). Specifically, the aspartic proteases, **cathepsin D** (CTSD) and **cathepsin B** (CTSB) that activate under acidic pH conditions, as well as the estrogen-regulated protease **kallikrein 6** (KLK6) were all discussed in the previous chapter.

In addition to the proteases we also identify a list of proteins related to inflammatory processes in cancer. **Vasorin** (VASN) is a transmembrane protein whose extracellular domain is cleaved and released in the extracellular environment in soluble form by the metalloprotease ADAM17. Malapeira et al.[16] recently showed that the soluble form of vasorin is capable of sequestering transforming growth factor beta (TGFβ) and in this way regulate epithelial-to-mesenchymal transitions in breast cancer. Their immuno-blots confirm the presence of the soluble form of vasorin is the condition media of multiple breast cancer cell lines (SKBR3, MDAMB416 and MDAMB631), while show that the protein is absent from MCF7 conditioned media.

Another pro-inflammatory hit is **pentraxin 3** (PTX3), a protein most commonly secreted by macrophages and dendritic cells in response to pro-inflammatory cytokines LPS, IL-1 and TNFα[17]. In a murine melanoma model, Leali et al.[18,19] showed that PTX3 is able to sequester fibroblast growth factor-2 (FGF2) and therefore suppress tumor growth and vascularization. Margheri et al. stably transfected breast cancer cell lines MCF7 and MDAMB231 with PTX3 and found that the PTX3-overexpressing clones showed powerful anti-FGF2 activity, particularly in an FGF2-dependent capillary morphogenesis assay[20]. The anti-angiogenic activity of PTX3 is well-documented in the literature, however no research has been conducted regarding pentraxin's 3 pro-apoptotic effect in cancer.

Among the cytokines that were uniquely identified in CM HCC38, **attractin** (ATRN) is a secreted cytokine associated with an invasive diagnostic signature in prostate cancer[21]. Particularly in glioma and malignant astrocytoma, Kwaja et al. found that attractin has promigratory activity on tumor cells[22].

b.

Symbol	Entrez Gene Name	HCC38 CM Peptide Count	Localization
Proteases			
GGH	gamma-glutamyl hydrolase	5	Cytoplasm
CNDP2	CNDP dipeptidase 2 (metallopeptidase M20 family)	4	Cytoplasm
CTSD	cathepsin D	4	Cytoplasm
USP15	ubiquitin specific peptidase 15	4	Cytoplasm
CTSB	cathepsin B	3	Cytoplasm
CFI	complement factor I	3	Extracellular Space
KLK6	kallikrein-related peptidase 6	3	Extracellular Space
Inflammation			
CHI3L1	chitinase 3-like 1 (cartilage glycoprotein-39)	4	Extracellular Space
VASN	vasorin	4	Plasma Membrane
PTX3	pentraxin 3, long	3	Extracellular Space

c.

Symbol	Entrez Gene Name	HCC38 CM Peptide Count	Localization
Cytokines			
SCG2	secretogranin II	8	Extracellular Space
ATRN	attractin	7	Extracellular Space
FAM3C	family with sequence similarity 3, member C	3	Extracellular Space

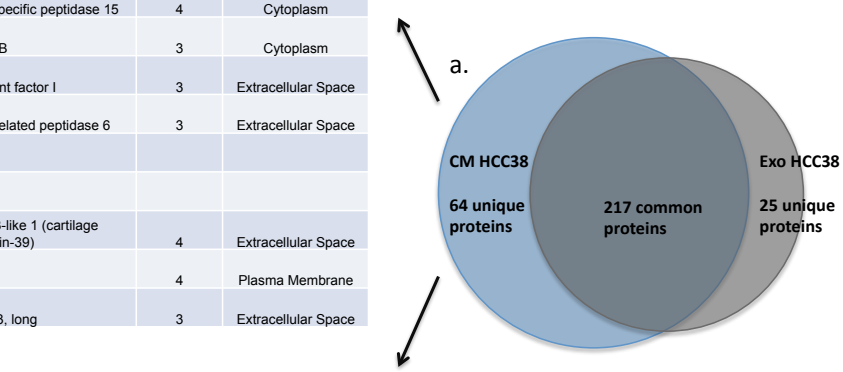

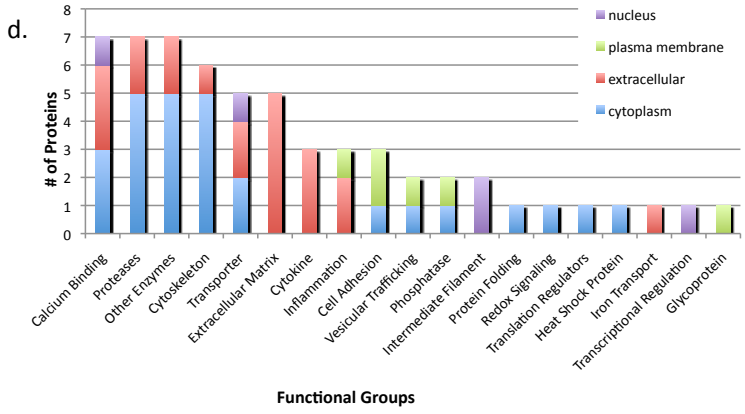

Figure 3.7: Comparative proteomic of HCC38 conditioned media and HCC38 exosomes.
a) The Ven diagram indicates thed number of unique proteins identified in CM HCC38. b) The table contains select pro-apoptotic proteins that were unique to CM HCC38. c) The table contains select pro-proliferative proteins unique to CM HCC38. d) Following ontology and localization analysis of the unique to CM HCC38 proteins, we plot the number of proteins found in each functional category. The bar color encoded for cellular localization: nucleus (purple), plasma membrane (green), extracellular (red) and cytoplasm (blue).

When comparing CM BT20 to its corresponding exosomes we see that the exosome proteomic dataset is larger than that of the CM's, possibly a consequence of the exosome fraction being more concentrated than the CM. Next, we observe a similar pattern as in the CM HCC38 comparison, that is the majority of CM BT20 proteins are alos identified in the exosomes and only a minority of 50 protein hits are unique to the CM. Annotation reveals that most of these proteins are of cytoplasmic cellular origin. There are approximately equal amounts of extracellular and plasma membrane proteins in the set and a small minority of nuclear proteins (figure 3.8d). Among these proteins we list a set possibly related to apoptosis (figure 3.8b) as well as a set of pro-proliferative hits (figure 3.8c).

In the apoptosis related hits, **legumain** (LGMN) stands out among the proteases. Legumain is an asparaginyl endopeptidase that was first identified in plant cells and later shown to be conserved among many mammalian cells. It has been recognized as a prognostic marker in breast cancer tumors by immunohistochemistry of patient neoplastic tissue sections[23]. In addition, it was shown that cancer cells overexpressing cytoplasmic legumain adopt an invasive and metastatic phenotype[24]. Another study has shown that legumain expression occurs in murine breast-tumor associated macrophages, while classical macrophages of the M1 phenotype, which perform key immune surveillance and antigen-presentation functions, do not express legumain[25]. No study has yet been conducted on secreted legumain and its potential functions.

In addition to proteases, we note the presence of kinase inhibitors in the unique CM BT20 protein hits. Particularly the **serine peptidase inhibitor Kunitz type 1** (SPINT1) is of interest to us, since the literature indicates it interacts with **hepatocyte growth factor** (HDGF), a growth-promoting factor also identified in the unique soluble protein hits of this analysis (figure 3.8c). In fact, the alternate name for SPINT1 is **hepatocyte growth factor activator inhibitor 1** (HAI-1) since it sequesters HDGF and curtails its activity[26]. Cheng et al showed that SPINT1-knockout clones of pancreatic cancer cells assumed an invasive and metastatic phenotype comparative to the wild-type control cells[26]. More specifically in breast cancer, Parr et al. showed that elimination of SPINT1 and SPINT2 expression in MDAMB231 breast cancer cells enhances the migratory and proliferative nature of these cells. They concluded that SPINT1 and SPINT2 serine protease inhibitors have strong therapeutic potential in the anti-HDGF cancer therapy arena[27].

Upon closer inspection we see that a third player in the hepatocyte growth factor signaling pathway is also present in the protein hit list. Indeed, the **hepatocyte growth factor receptor** (MET) itself is found in soluble form in the CM BT20 secretions (figure 3.8c). This was an unexpected finding, particularly because as we will be discussing in the following chapter, when tyrosine kinase receptors are found in the extracellular space, it is usually as part of the secreted exosome's membranes. However, there is precedence for this finding as Athauda et al.[28] using a sensitive electro-chemiluminescence immunoassay, confirmed c-MET ectodomain

shedding from breast cancer cells in culture and furthermore demonstrated that the shedding rate correlates with malignant potential.

b.

Symbol	Entrez Gene Name	BT20 CM Peptide Count	Localization
Protease			
CTSD	cathepsin D	14	Cytoplasm
CPA4	carboxypeptidase A4	11	Extracellular Space
NPEPPS	aminopeptidase puromycin sensitive	6	Cytoplasm
CNDP2	CNDP dipeptidase 2 (metallopeptidase M20 family)	3	Cytoplasm
GGH	gamma-glutamyl hydrolase (conjugase, folylpolygammaglutamyl hydrolase)	3	Cytoplasm
LGMN	legumain	3	Cytoplasm
Kinase Inhibitor			
PPP2R1A	protein phosphatase 2, regulatory subunit A, alpha	3	Cytoplasm
SPINT1	serine peptidase inhibitor, Kunitz type 1	3	Extracellular Space
Inflammation			
STIP1	stress-induced-phosphoprotein 1	3	Cytoplasm

c.

Symbol	Entrez Gene Name	BT20 CM Peptide Count	Localization
Tyrosine Kinase Receptor			
MET	met proto-oncogene (hepatocyte growth factor receptor)	5	Plasma Membrane
Growth Factor			
HDGF	hepatoma-derived growth factor	3	Extracellular Space
Cytokine			
ATRN	attractin	3	Extracellular Space

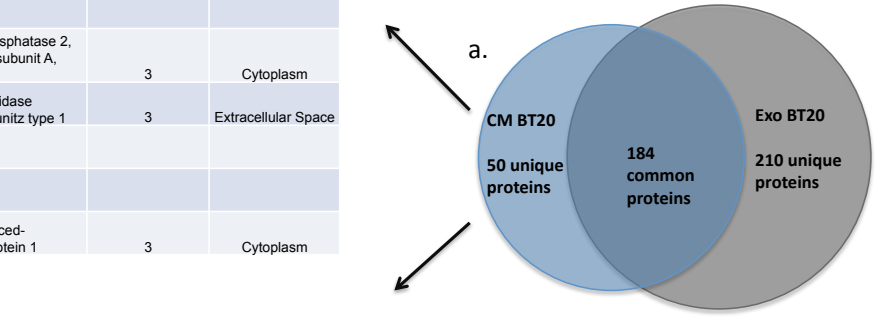

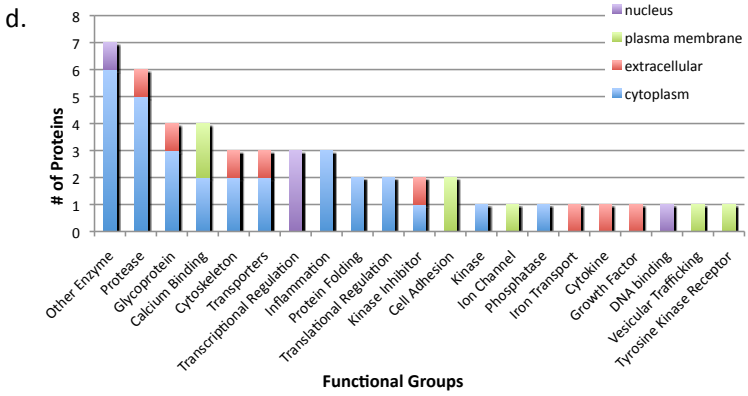

Figure 3.8: Comparative proteomic of BT20 conditioned media and BT20 exosomes.
a) The Ven diagram indicates thed number of unique proteins identified in CM BT20. b) The table contains select pro-apoptotic proteins that were unique to CM BT20. c) The table contains select pro-proliferative proteins unique to CM BT20. d) Following ontology and localization analysis of the unique to CM BT20proteins, we plot the number of proteins found in each functional category. The

bar color encoded for cellular localization: nucleus (purple), plasma membrane (green), extracellular (red) and cytoplasm (blue).

Within the scope of our study, it is extremely intriguing that both the hepatocyte growth factor receptor, the receptor's ligand as well as the ligand's active inhibitor are all found in the extracellular secretions of CM BT20. One question arising is whether the soluble form of the MET receptor can bind the ligand and therefore also act as an antagonist to the HDGF mitogenic signal. Another question relates to quantity of all three proteins: is the pro-growth signal of HDGF in abundance or is the SPINT1 inhibitor presence high enough to completely quench it? Certainly the presence of SPINT1 demonstrates a clear way that CM BT20 could be toxic to any recipient cell line dependent on a HDGF autocrine loop for it's proliferation. In the same vein, PTX3 that was identified in CM HCC38 is a clear mechanism of toxicity to any cell line dependent on FGF2 autocrine signaling. In addition, the elimination or inactivation of HDGF from CM BT20 will only increase this CM's pro-apoptotic activity on HDGF-dependent CM-recipient cells.

Finally on figure 3.9a we compare the unique proteins found in CM HCC38 and CM BT20 to each other and identify 16 common proteins between the two datasets. On figure 3.9b we proceed to group the proteins into functional categories, while comparing the peptide count recorded in each CM. Among the common proteases, **cathepsin D** (CTSD) stands out, while two other proteases are shared as well: **CNDP dipeptidase 2** and **gamma glutamyl hydrolase** (GGH). We also find the cytokine **attractin** (ATRN) shared between the two CMs. The remainder of the common

proteins are housekeeping in their function and unlikely to hold significant pro-apoptotic or pro-proliferative activity on CM-recipient cells.

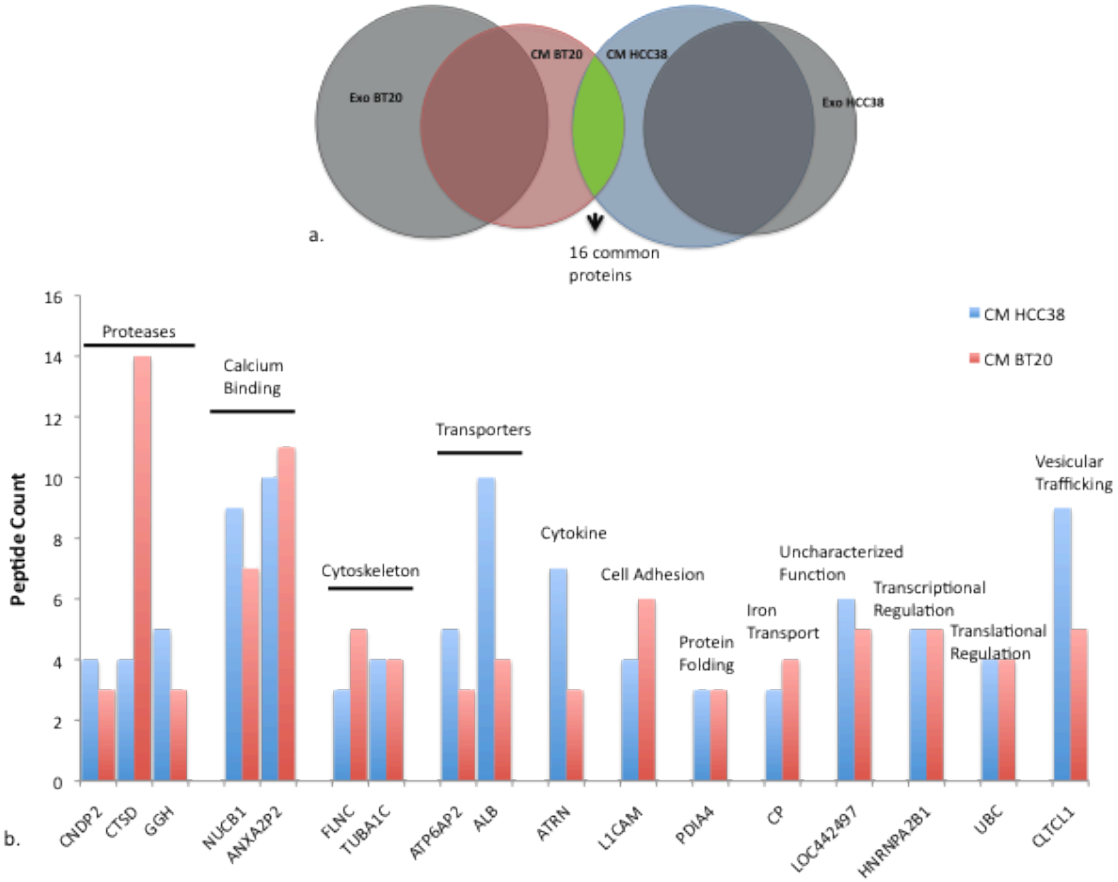

Figure 3.9: Comparative proteomic analysis of CM HCC38 and CM BT20 unique protein hits, excluding respective exosome protein content.
a) The Venn diagram indicates the common proteins between the two conditioned media. b) Following ontology and localization analysis we group the common proteins by function and plot the detected peptide count in each CM respectively. The clue bars indicate the CM HCC38 peptide count while red bars are for CM BT20.

Bibliography

1. Neve, R. M. *et al.* A collection of breast cancer cell lines for the study of functionally distinct cancer subtypes. *Cancer Cell* **10,** 515–27 (2006).

2. Gill, Z. P., Perks, C. M., Newcomb, P. V. & Holly, J. M. P. Insulin-like Growth Factor-binding Protein (IGFBP-3) Predisposes Breast Cancer Cells to Programmed Cell Death in a Non-IGF-dependent Manner. *J. Biol. Chem.* **272,** 25602–25607 (1997).

3. Nickerson, T., Huynh, H. & Pollak, M. Insulin-like growth factor binding protein-3 induces apoptosis in MCF7 breast cancer cells. *Biochem. Biophys. Res. Commun.* **237,** 690–3 (1997).

4. Hayman, E. G., Pierschbacher, M. D. & Ruoslahti, E. Detachment of cells from culture substrate by soluble fibronectin peptides. *J. Cell Biol.* **100,** 1948–54 (1985).

5. McCaig, C., Perks, C. M. & J.M.P., H. Intrinsic actions of IGFBP-3 and IGFBP-5 on Hs578T breast cancer epithelial cells: inhibition or accentuation of attachment and survival is dependent upon the presence of fibronectin. *J. Cell Sci.* **115,** 4293–4303 (2002).

6. Ai, L. *et al.* Epigenetic silencing of the tumor suppressor cystatin M occurs during breast cancer progression. *Cancer Res.* **66,** 7899–909 (2006).

7. Mohamed, M. M. & Sloane, B. F. Cysteine cathepsins: multifunctional enzymes in cancer. *Nat. Rev. Cancer* **6,** 764–75 (2006).

8. Fiucci, G., Ravid, D., Reich, R. & Liscovitch, M. Caveolin-1 inhibits anchorage-independent growth, anoikis and invasiveness in MCF-7 human breast cancer cells. *Oncogene* **21,** 2365–2375 (2002).

9. Yousef, G. M. *et al.* Kallikrein gene downregulation in breast cancer. *Br. J. Cancer* **90,** 167–72 (2004).

10. Borgoño, C. a & Diamandis, E. P. The emerging roles of human tissue kallikreins in cancer. *Nat. Rev. Cancer* **4,** 876–90 (2004).

11. Tandon A.K, Clark G.M., Chamness G.C., Chirgwin J.M., M. W. L. Cathepsin D and Prognosis in Breast Cancer. *N. Engl. J. Med.* **322,** 297–302 (1990).

12. Liaudet-coopman, E. *et al.* Cathepsin D: newly discovered functions of a long-standing aspartic protease in cancer and apoptosis. *Cancer Lett.* **237,** 1–17 (2006).

13. Pernodet, N. *et al.* High expression of QSOX1 reduces tumorogenesis, and is associated with a better outcome for breast cancer patients. *Breast Cancer Res.* **14,** R136 (2012).

14. Perks, C. M. & Holly, J. M. P. IGF binding proteins (IGFBPs) and regulation of breast cancer biology. *J. Mammary Gland Biol. Neoplasia* **13,** 455–69 (2008).

15. Joo, J. H. *et al.* S100A6 (calcyclin) enhances the sensitivity to apoptosis via the upregulation of caspase-3 activity in Hep3B cells. *J. Cell. Biochem.* **103,** 1183–97 (2008).

16. Malapeira, J., Esselens, C., Bech-Serra, J. J., Canals, F. & Arribas, J. ADAM17 (TACE) regulates TGFβ signaling through the cleavage of vasorin. *Oncogene* **30,** 1912–22 (2011).

17. Mantovani, A., Garlanda, C. & Bottazzi, B. Pentraxin 3, a non-redundant soluble pattern recognition receptor involved in innate immunity. *Vaccine* **21,** S43–S47 (2003).

18. Alessi, P. *et al.* Anti-FGF2 approaches as a strategy to compensate resistance to anti-VEGF therapy: long-pentraxin 3 as a novel antiangiogenic FGF2-antagonist. *Eur. Cytokine Netw.* **20,** 225–34 (2009).

19. Leali, D. *et al.* Fibroblast growth factor-2 antagonist and antiangiogenic activity of long-pentraxin 3-derived synthetic peptides. *Curr. Pharm. Des.* **15,** 3577–89 (2009).

20. Margheri, F. & Serratì, S. Systemic sclerosis-endothelial cell antiangiogenic pentraxin 3 and matrix metalloprotease 12 control human breast cancer tumor vascularization and development in mice. *Neoplasia* **11,** 1106–1115 (2009).

21. Cima, I. *et al.* Cancer genetics-guided discovery of serum biomarker signatures for diagnosis and prognosis of prostate cancer. (2011). doi:10.1073/pnas.1013699108/-/DCSupplemental.www.pnas.org/cgi/doi/10.1073/pnas.1013699108

22. Khwaja, F. W., Duke-Cohan, J. S., Brat, D. J. & Van Meir, E. G. Attractin is elevated in the cerebrospinal fluid of patients with malignant astrocytoma and mediates glioma cell migration. *Clin. Cancer Res.* **12,** 6331–6 (2006).

23. Gawenda, J., Traub, F., Lück, H. J., Kreipe, H. & von Wasielewski, R. Legumain expression as a prognostic factor in breast cancer patients. *Breast Cancer Res. Treat.* **102,** 1–6 (2007).

24. Liu, C., Sun, C. & Huang, H. Overexpression of Legumain in Tumors Is Significant for Invasion / Metastasis and a Candidate Enzymatic Target for Prodrug Therapy Overexpression of Legumain in Tumors Is Significant for Invasion / Metastasis and a Candidate Enzymatic Target for Prodrug T. 2957–2964 (2003).

25. Luo, Y. *et al.* Targeting tumor-associated macrophages as a novel strategy against breast cancer. **116,** (2006).

26. Cheng, H., Fukushima, T., Takahashi, N., Tanaka, H. & Kataoka, H. Hepatocyte growth factor activator inhibitor type 1 regulates epithelial to mesenchymal transition through membrane-bound serine proteinases. *Cancer Res.* **69,** 1828–35 (2009).

27. Parr, C. & Jiang, W. G. Hepatocyte growth factor activation inhibitors (HAI-1 and HAI-2) regulate HGF-induced invasion of human breast cancer cells. *Int. J. Cancer* **119,** 1176–83 (2006).

28. Athauda, G. *et al.* c-Met ectodomain shedding rate correlates with malignant potential. *Clin. Cancer Res.* **12,** 4154–62 (2006).

Chapter 4

Characterization and Functional Studies of Breast Cancer-Derived Exosomes

Abstract

The present chapter discusses the biology of exosomes, nanometer-sized particles secreted by most cell lines in culture. Exosomes form intracellularly by the inward budding of the limiting membrane of endocytic compartments, leading to vesicle-containing endosomes called multivesicular bodies. Multivesicular bodies fuse with the plasma membrane, releasing the endosomes –now termed exosomes- in the extracellular space. Although several studies address the composition and content of exosomes, their physiological roles both in healthy and diseased tissue remain vastly un-explored. We begin this study with a description of methods of purification and characterization of the exosomal fraction from tissue culture supernatants. We then discuss methods of quantitation and fluorescent labeling of particles. We next turn our attention to the protein content of exosomes. First we employ a proteomic approach to qualify the overall protein content of breast cancer-derived exosomes. Next we embark in a series of western blots which screen both cell lines and their corresponding exosomes for common diagnostic markers of breast cancer as well as drugable intracellular kinases. Following this screen we specifically focus on the EGFR tyrosine kinase and undertake functional studies of the receptor on the exosome membrane. Furthermore, we ask whether the phosphorylation status of EGFR reflects the phosphorylation status of the

exosome-producing cell line. Finally we attempt to uncover biological activity of exosomes, by incubating receptor-positive exosomes with receptor-negative cell types and observing whether receptor transfer takes place on the recipient cells.

4.1 Methods in Exosome Biology

Exosome Purification

There currently exist a variety of protocols for precipitating microvesicles from tissue culture supernatants and biological fluids. A size-cutoff filter can be employed to isolate vesicles in the size range of exosomes[1]. Alternatively polymer co-precipitation is a commercially proposed solution for speady recovery of exosomes[2]. However, the most popular and tested protocol for exosome recovery is differential ultracentrifugation proposed by Théry et al.[3]. The advantage of differential ultracentrifugation over other methods is the step-wise elimination of larger vesicles and fragments of shed membrane from the conditioned medium, preceding the isolation of the exosomal fraction. In this way fraction purity is ensured.

Differential ultracentrifugation, as described in figure 1, is our method of choice for exosome purification throughout this study. The exosome production protocol begins with a 48hr incubation of 80% confluent cell monolayers in serum-free RPMI medium. Serum-free medium is essential if exosomes will be purified from the resulting conditioned medium (CM), because fetal calf serum contains bovine microvesicle that can contaminate the purity of the exosomal fraction. At 48hrs conditioned medium is harvested from cells and centrifuged at 300g for 10 min to

remove cells, then at 2000g for 10min to remove apoptotic bodies. Conditioned medium is subsequently passed through a 3k centrifugal filtering device at 4000g for 30min in order to concentrate the large CM volume down to a few milliliters. The concentrated CM is subsequently ultra-centrifuged at 10,000g for 30min to pellet cell debris and large vesicles. The supernatant from this step is ultra-centrifuged at 100,000g for 70min to pellet the exosomes. The exosomal pellet undergoes a final wash step, is re-suspended in PBS and re-pelleted at 100,000g for 60min.

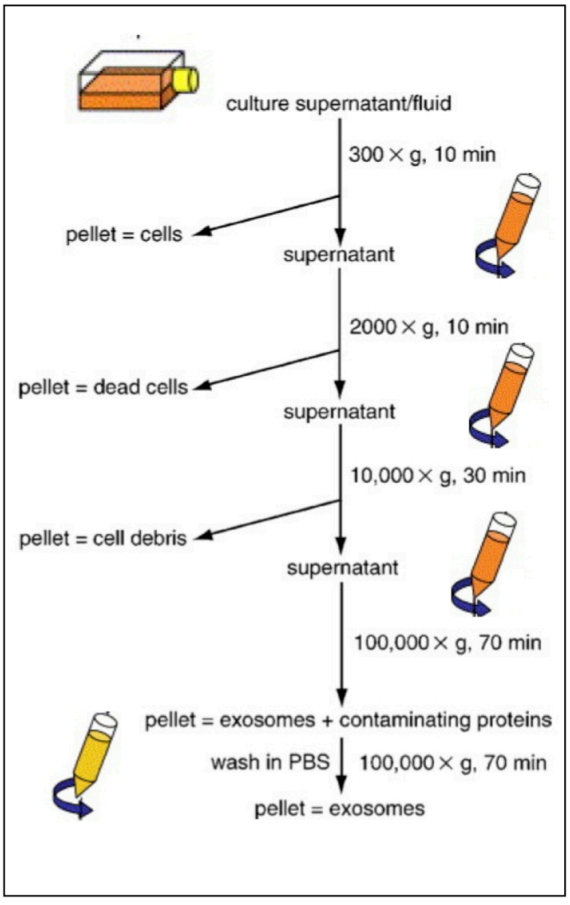

Exosome Purification Methods	Reference
1. Differential Centrifugation	Théry et al. 2006
2. Sucrose Gradient	Théry et al. 2006
3. Filtration	Wessleider et al. 2013
4. Polymer co-precipitation	Exoquick™ (www.systembio.com)

Figure 3.13: Methods of exosome purification. Left panel: purification by differential centrifugation. Right panel: all proposed methods of purification , with references.

Exosome Characterization

Following isolation, purity of the exosomal fraction can further be established by a) examining the protein composition of the exosomal membrane and b) sizing the purified particles. Due to the nanometer-scale size of exosomes, imaging of this biological structure is mostly limited to electron microscopy techniques. We employed both negative stain labeling as well as negative stain immunogold labeling to visualize and characterize exosomes for the purpose of this study.

The protocol followed for whole cell exosome mounting on Formvar-carbon coated grids and subsequent negative stain labeling preparation of samples for elecrtron microscopy analysis is the one introduced by Théry et al.[3]. Briefly, following ultracentrifugation the exosome pellet is fixed by re-suspension in 2% paraformaldehyde (PFA). 5ul of sample are adsorbed on Formvar-carbon coated grids. The grids are washed in PBS drops and subsequently dropped on a 1% glutaraldehyde solution. The grids are washed in distilled water and contrasted by incubation on a uranyl-acetate drop, for a minimum of 10min. Subsequently the grids are washed in distilled water and stored before imaging on electron microscope at 80kV.

For immunogold labeling exosomes were resuspended in PBS after ultracentrifugation. Fixation of exosomes was avoided here, since we found it to interfere with the structure and integrity of protein surface markers. Instead 5ul of 'live' exosomes were adsorbed on the Formvar-carbon coated grids, Following

adsorption, the grids were incubated with a succession of primary antibody – Protein A gold beads – bridging antibody – secondary antibody. Subsequently the grids were contrasted and embedded as described above.

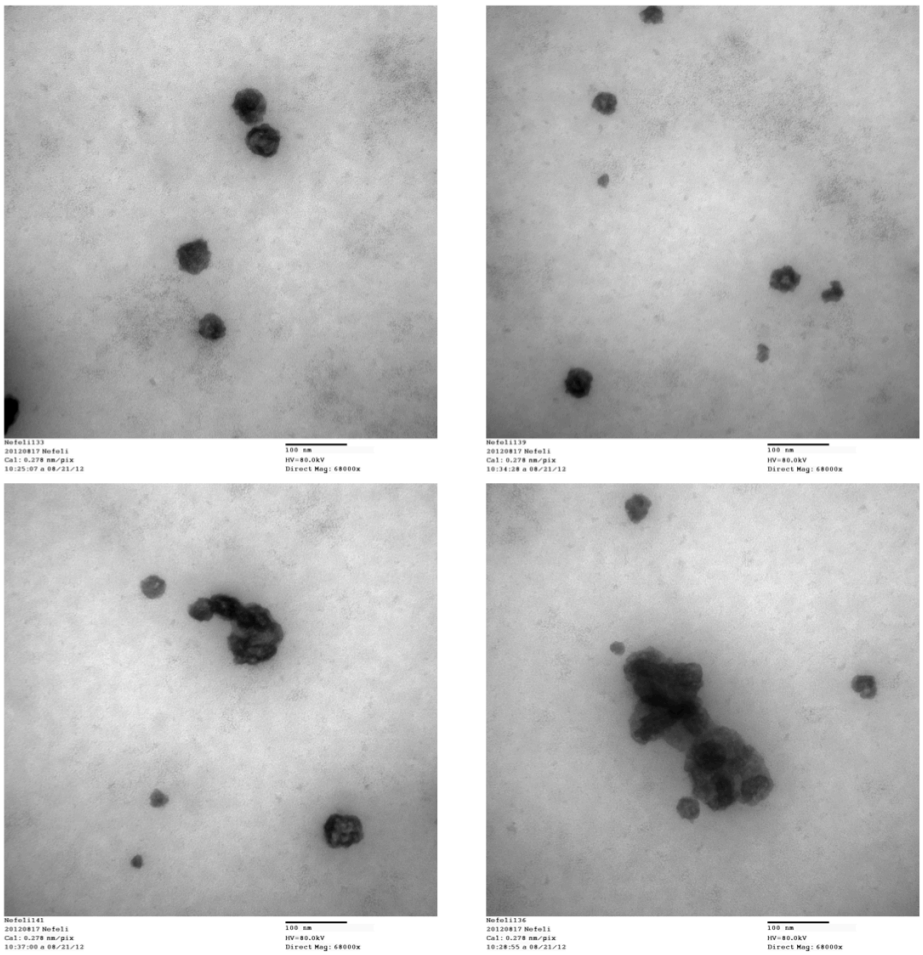

Figure 3.14: Negative stain electron microscopy of HCC38-derived exosomes.

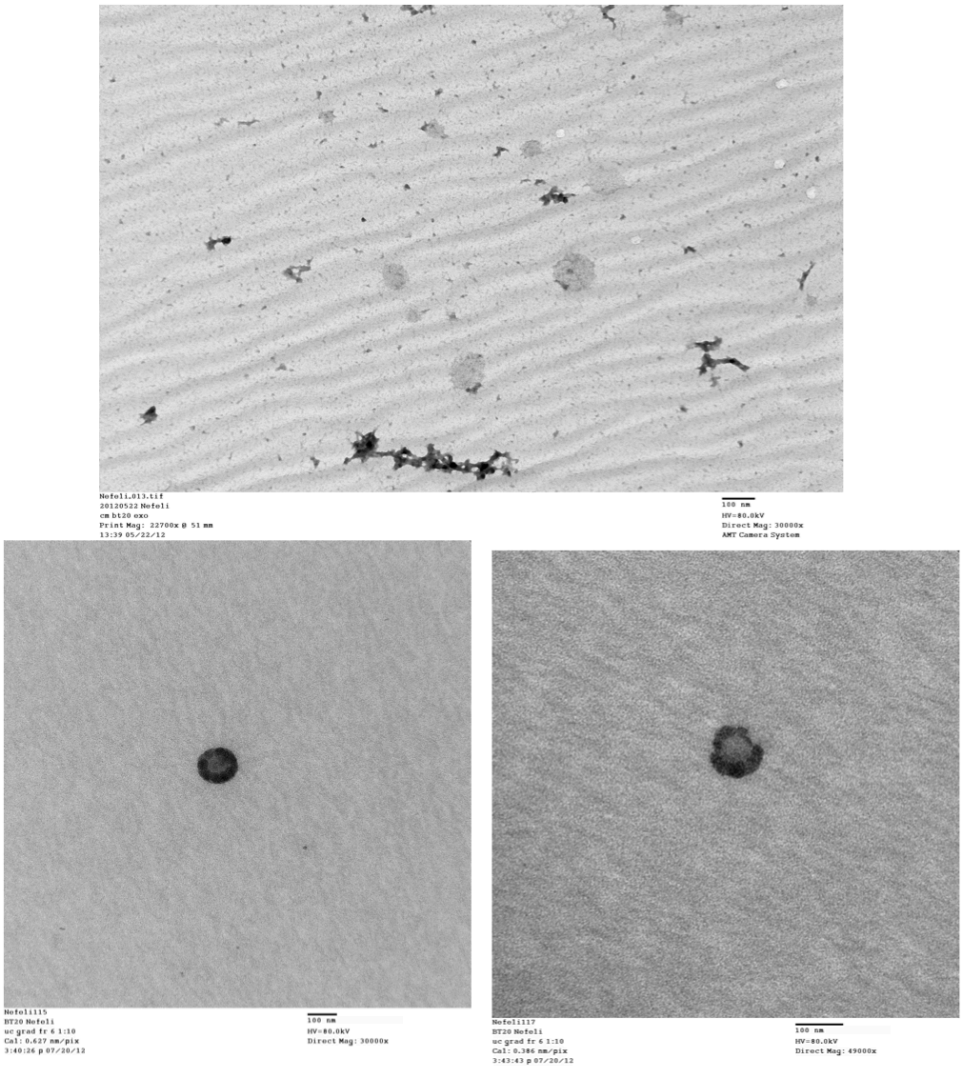

Figure 3.15: Negative stain electron microscopy of BT20-derived exosomes.

Proteins of the tetraspanin family are highly enriched in exosomes from virtually any cell type, as a result of the exosome biogenesis process[4]. Tetraspanins are membrane proteins with four transmembrane domains, involved in many different biological functions such as fusion, motility, immune stimulation, adhesion and protein sorting. In this study we blotted the exosomal fraction (exos), the supernatant from the exosomal ultracentrifugation (exosup) as well as the original

non-fractionated conditioned medium (CM) for tetraspanins CD63 and CD81. We show that in both HCC38 and BT20 derived exosomes, CD63 is present in the original CM and highly enriched in the exosomal fraction as compared to thsupernatant fraction (fig4&5). Additionally we observe a similar trend for CD81 in the case of HCC38-derived exosomes (fig4).

Another marker of exosomal presence is Major Histocompatibility Complex I (MHC I). MHC I is found in the extracellular space at full length (50kDa) when attached on exosomal membrane as well as at a cleaved (40kDa) soluble version. We show that whereas the CM and exosomal supernatant feature both MW-versions of MHC I, the exosome fractions contains solely the membrane bound full-length version of MHCI (figures 4&5).

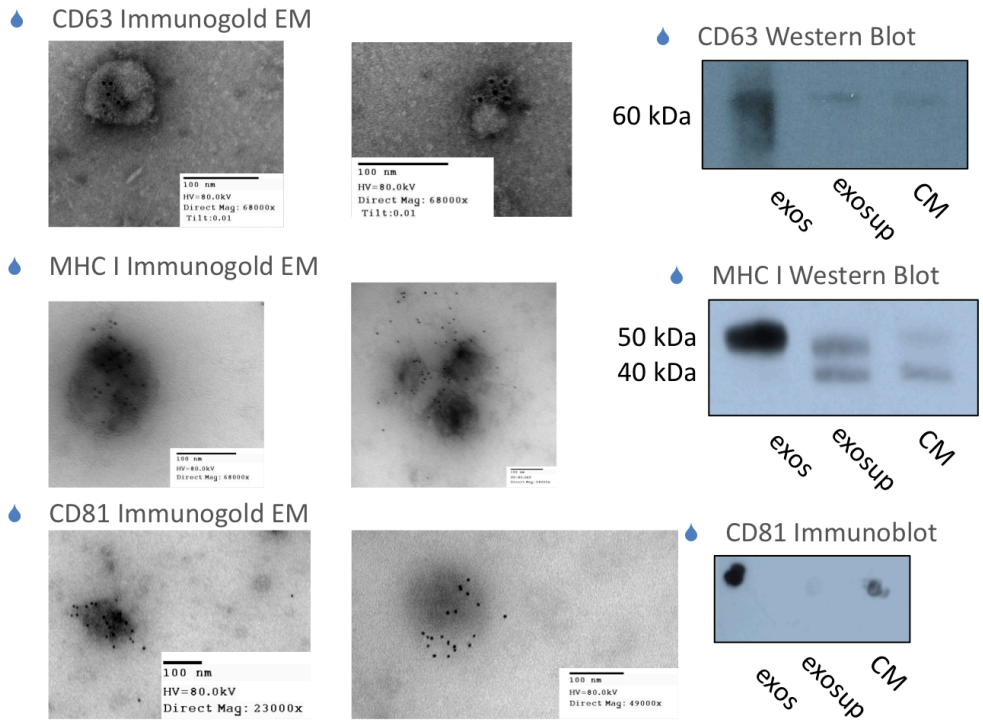

Figure 16: Negative stain immunogold labeling and confirmation by western blot of exosomal markers CD63, CD81 and MHC class I on the surface of HCC38-derived exosomes

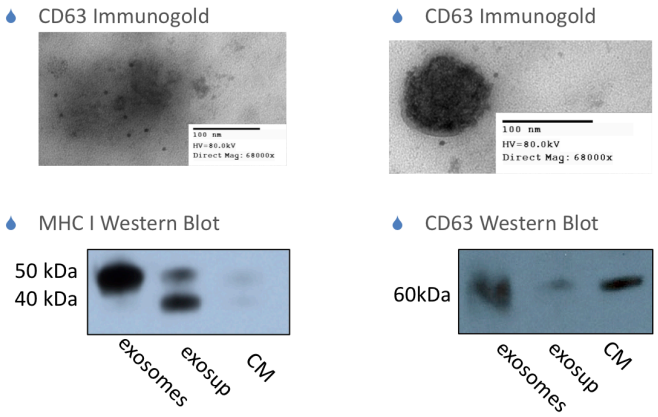

Figure 3.17: Negative stain immunogold labeling and confirmation by western blot of MHC class I and CD63 surface markers on BT20-derived exosomes.

Fluorescent Labeling of Exosomes

In order to temporary follow the endocytosis of exosomes by target cell lines, fluorescent labeling of the vesicles is necessary. There currently exist two ways by which to fluorescently label exosomes. The first is by cloning a GFP-CD63 variant into the genome of the exosome-producing cell line[5]. The alternative and more expedient way to fluorescent exosomes is direct labeling of the purified vesicles with the lipophilic dye PKH-26[6–8].

The PKH-26 dye was designed as a live fluorescent probe of cell membrane, therefore the manufacturer's protocol has to be adapted for this application. Briefly, exosomes are recovered by ultracentrifugation as previously described and resuspended in a solution of Diluent C (500ul) and PKH-26 dye (2ul). The exosomal/dye mixture is left to incubate for 5min at room temperature. Next the staining is halted by introducing 1ml of an aqueous solution of 1% BSA. Exosomes are recovered by ultracentrifugation and resuspended in 100ul serum-free medium, supplemented by 1% BSA.

Exosome Quantitation

Again, there are a variety of methods for quantifying number of exosomes in a solution. The golden standard for exosome quantitation is **NanoSight**, a microscopy based method of laser-assisted particle scattering that is able to determine not only concentration of particles, but also particle size, zeta potential and polydispersity of

the particulate solution (http://www.nanosight.com/). However due to high cost and limited accessibility to this equipment, alternate ways of quantifying exosomes had to be explored for the purpose of this study.

One alternative to particle number for sample quantitation was to measure instead the overall **protein concentration** of the exosome fraction. Exosome lysate was prepared by resuspension of the exosome ultracentrifugation pellet in 100ul MPER supplemented with 1x Roche protease inhibitor. The exosome lysate was incubated on ice for 30min and then centrifuged 15min at 14,000g to pellet membrane. The supernatant from the spin was recovered and protein levels were quantified following the protocol for a microBCA assay[9].

Another alternative for quantitation of exosome yield is measuring the overall **phosphate content** of the exosomal fraction, the phosphate serving as proxy for the amount of phospholipid present on the exosomal membrane. For the purpose of this assay the exosome pellet is re-suspended in 100ul of TBS buffer. A few microliters of sample are transferred in borosilicate test tubes and incubated with 10% sulfuric acid (H_2SO_4) at 200C for 1hr. A solution of 30% hydrogen peroxide (H_2O_2) is then added to the tubes and the samples are further heated for 40min. The tubes are cooled to room temperature and water is added to each one. Colorimetry is performed by adding a solution of 5% Ammonium Molybdate and 10% Ascorbic Acid to the samples, then incubating in a 45C water bath for 20min to develop color.

Absorbance is read at 820nm. A standard curve for the assay is prepared by titrating 0-10ul DOPC lipids.

This method is routinely used for phospholopid quantitation in liposome preparations, yet it is the first time it is used in the context of exosomes. Figure 6 demonstrates the efficiency of the assay in capturing the dose-dependent augmentation of phosphate in MDAMB231-derived exosomes. Also on figure 6, the ratio of phosphate to protein is plotted for exosomes derived from five distinct breast cancer cell lines. We observe significant variability of protein to phosphate content in exosomes, dependent on the cell line of origin. HCC38-derived vesicles feature 100-fold more phosphate than protein, BT20 and T47D exosomes feature a 1 to 1 ratio, whereas SKBR3 and MCF7 exosomes feature more protein than phosphate.

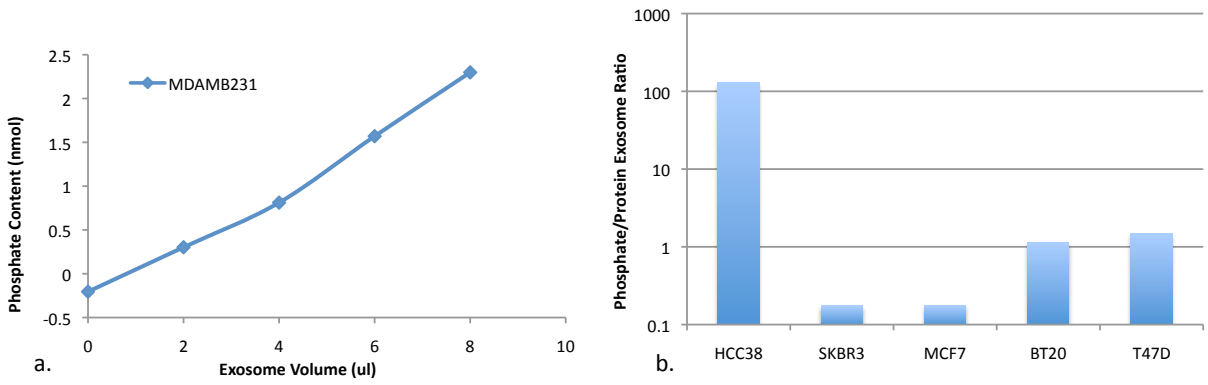

Figure 3.18: a) Dose-dependent augmentation of phosphate content in MDAMB231 exosomes. b) Ratio of phosphate (measured with phosphate assay) to protein (measured with microBCA assay) for five different types of breast cancer exosomes.

4.2 Mass Spectrometry Analysis of BT20 and HCC38-derived exosomes.

The purpose of this analysis is to get an idea of the overall protein content within cancer-derived exosomes. Immunoblots presented in the following section allowed us to probe specifically for therapeutically relevant molecules, whereas proteomic analysis supplies us with broader insights on breast cancer-derived exosome composition.

The purification of exosomes and micro-capillary LC/MS/MS analysis protocols followed are described in chapter 3, section 3. The exosome dataset presented is the same as in chapter 23 however here we proceed to analyze the HCC83 and BT20 exosome proteomic contents alone.

On figure 3.7a we see that BT20 and HCC38 exosomes have in total 572 protein hits in common. For the purpose of this analysis we used the entire list of proteins including those of low peptide count as we found that exosome markers appeared in the dataset at very low peptide counts (1 or 2 peptides detected). In terms of the cellular provenance of the exosome's common 572 proteins, we find that the majority of proteins –about 60%- are of cytoplasmic origin. When compared to the mass spectrometry list of common proteins between the two CMs, that number is almost equal. The main difference between the two is that plasma membrane proteins appear enriched in the exosome fraction as compared to the full CM, while extracellular proteins are depleted (figure 3.7c). Finally nuclear proteins are also

more abundant in exosomes compared to the corresponding CMs. These observations are in line with expectations based on exosome biology. Cytoplasmic proteins are shuttled in the extracellular space by being packaged in microparticles. These microparticles conserve most membrane proteins present in the plasma membrane. They also encapsulate microRNAs, which explains the higher representation of nuclear proteins in the exosomes.

In terms of functional characterization of the 572 common proteins we see, as in the corresponding CM analysis, an abundance of cytoskeletal proteins as well as a variety of other functional categories that are housekeeping in their nature such as transporters, translational regulators, calcium binding and heat shock proteins. Particularly the presence of a high number (approximately 45) of glycolytic enzymes and regulators raises the question of whether exosomes have an intact glycolytic pathway and are able to convert extracellular glucose to ATP[10]. Accordingly, the fact that exosomes carry multiple cell adhesion molecules, the list ranging from a variety of integrins to epithelial-specific CAMs, raises the question of whether these proteins are functional on the surface of exosomes and help anchor the vesicles to recipient cells. Moreover can these exosomal adhesion molecules be uptaken by recipient cells and alter their phenotype? These are fascinating questions about exosome function in the extracellular space that remain vastly unanswered in the literature at present.

Beside the predictable housekeeping protein sets we also find some surprising protein categories on figure 3.7c. The high abundance of ribosomal proteins is one such surprise. In fact, proteomic studies of exosomes derived from a variety of cell types and a range of biological fluids feature ribosomal proteins[11]. The presence of intact ribosomes encapsulated in exosomes is unlikely, since these cellular structures of 20nm in size are marginally smaller than the 100nm-sized exosomes. One possibility is that ribosomes co-precipitate with the exosomes during the purification process and are simply a contaminant. Another interpretation is that ribosomal proteins associate with RNA strands packaged in the exosomes and are therefore encapsulated in the vesicles.

Another surprising finding is the presence of a variety of histones in the microvesicles. This finding is surprising yet not unprecedented. Peng et al. confirm the presence of histone H2A in exosomes isolated from the ascites of ovarian cancer patients, while they note that they do not know whether the histone can be found within the vesicle or rather teathered on the outside of the vesicle's membrane as an extracellular contaminant[12]. The later is also the position of Mathivanan on the issue who notes that extracellular histones are a result of apoptotic blebs that co-precipitate with exosomes during purification[11].

Another functional category of interest is the one labeled 'oncogene' on figure 3.7b. It consists mainly of RAB-proteins, of the RAS oncogene family. These are GTPases involved in membrane trafficking, vesicle formation, vesicle movement and

membrane fusion. Mathivanan et al. make a similar observation of RAS protein enrichment while conducting proteomic analysis of human colon tumor cell line LIM1215-derived exosomes[13]. Thus, the presence of RAS onco-proteins could potentially be a specific marker of tumor-derived exosomes. Along with the category 'G protein regulation' these proteins imply that there is some intact component of G protein signaling taking place within exosomes.

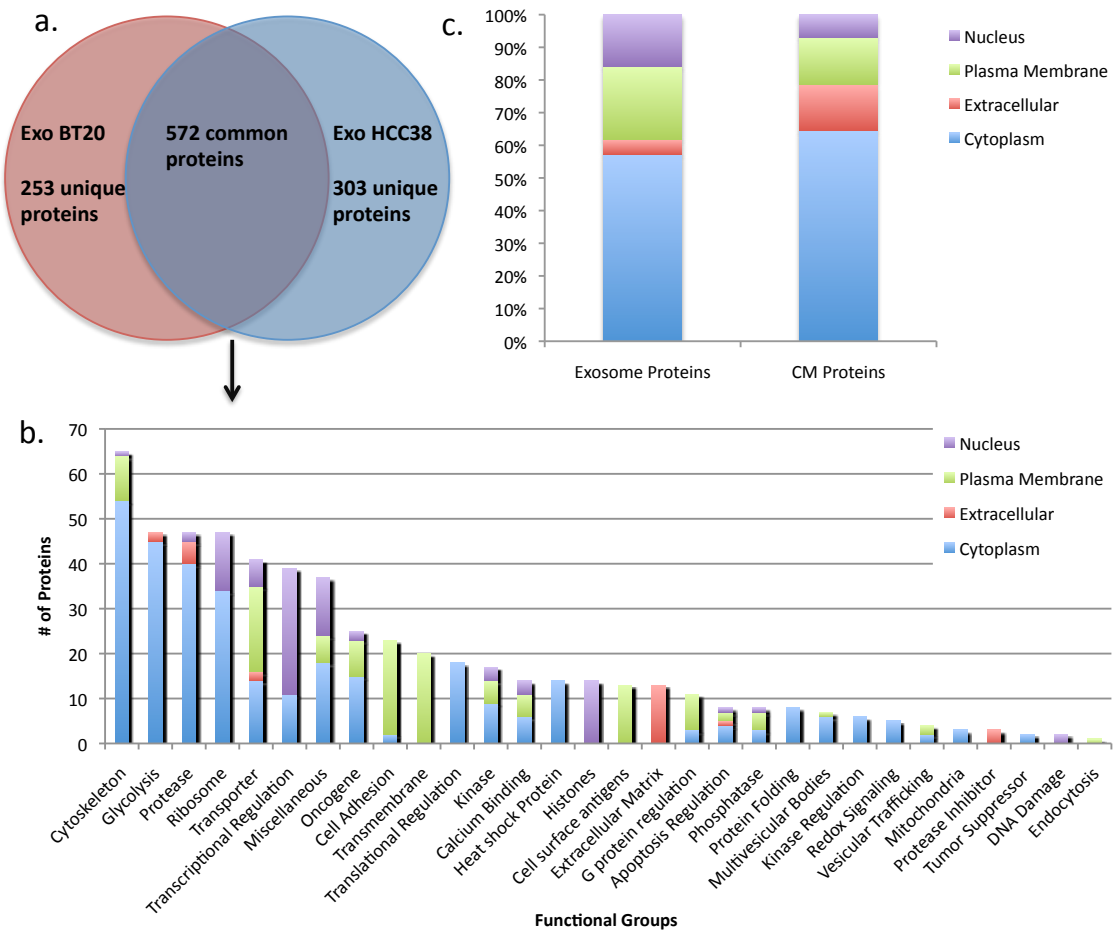

Figure 3.7: Comparative proteomic analysis of HCC38 and BT20-derived exosomes. a) The Venn diagram indicates the number of common proteins identified between HCC38 and BT20 exosomes. b) The bar charts compares the common protein composition between the exosome proteomic group and conditioned medium (CM) proteomic group. c) Following ontology and localization analysis of

the common proteins between the two types of exosomes, we plot the number of proteins found in each functional category. The bar color encodes for cellular localization.

On table 3.1a we list exosome markers that we identified by mass spectrometry analysis of HCC38 and BT20-derived exosomes, along with their respective peptide count. Among these we find the tetraspanins C9, CD81 and CD63 as well as multiple proteins from the heat shock protein-70 family (HSP70). We also find three antigens of the major histocompatibility complex I (MHC I) family and multiple proteins pertaining to multivesicular bodies, the cellular compartment where exosome biogenesis takes place. Finally we identify flotillin1 (FLOT1), a component of membrane lipid rafts whose presence has been previously reported on extracellular vesicles[11].

Other than the exosomal markers common to both types of exosomes, we also see that each proteomic dataset contains cell-type specific protein markers which we list in table 3.1b. The epidermal growth factor receptor (EGFR) is identified in both HCC38 and BT20 exosomes, a finding that further validates immunoblots results presented in the following section (figure 3.8 and 3.9). We also see two members of the transmembrane claudin family (CLDN3 and CLDN4) present in both types of exosomes. This is particularly useful, since in the absence of efficient antibodies we previously were not able to confirm claudin presence on cancer exosomes. Claudins have emerged as significant biomarkers in breast cancer[14] and by consequence their presence in cancer exosomes holds the promise of diagnostic application.

Alongside to common cancer-specific proteins found in the two types of exosomes we also find tyrosine kinases specific to HCC38 exosomes, MAPK being among them, as well as IGFBP5 a growth factor antagonist specific to BT20 exosomes. Finally we list the RAS-oncoproteins in table 3.1b since as discussed previously they are specific and unique to tumor-derived exosomes.

In table 3.2 we list proteins indicative of different cellular compartments and functions present in the exosomes. First comes a long list of metabolic enzymes. Among these GADH ALDOA, ALDOC, ENO1, FASN and MDH1 are of common occurrence in a variety of exosomes and have been previously reported in exosome proteomic studies[11]. Next we list various members of the actin and tubulin protein familes, as representatives of the cell cytoskeleton. Among plasma membrane markers we find the transferrin receptor (TFRC) as well as a variety of integrins and cell adhesion molecules. Particularly the presence of E-cadherin (CDH1) and epithelial cell adhesion molecule (EpCAM) is of diagnostic value since it can be exploited in immuno-affinity exosome capturing technologies in order to specifically isolate tumor-derived epithelial exosomes from complex biological fluids. These molecules are also featured in the immunoblots below so that once again the proteomic analysis confirms and validates these findings. Finally, we list multiple members of the histone protein family, a possible indicator of nuclear protein presence within the exosomes.

a.

Exosome Markers	Entrez Gene Name	HCC38 exo Peptide Count	BT20 exo Peptide Count	Localization
Tetraspanins				
CD9	CD9 molecule	4	4	Plasma Membrane
CD81	CD81 molecule	1	2	Plasma Membrane
CD63	CD63 molecule	2	2	Plasma Membrane
HLA antigens class I				
HLA-A	major histocompatibility complex, class I, A	7	3	Plasma Membrane
HLA-B	major histocompatibility complex, class I, B	3	4	Plasma Membrane
HLA-G	major histocompatibility complex, class I, G	1	1	Plasma Membrane
Multivesicular Body				
CHMP2A	charged multivesicular body protein 2A	2	7	Cytoplasm
CHMP4B	charged multivesicular body protein 4B	1	4	Cytoplasm
CHMP5	charged multivesicular body protein 5	1	2	Cytoplasm
CHMP6	charged multivesicular body protein 6	1	1	Cytoplasm
MVB12A	multivesicular body subunit 12A	1	5	Cytoplasm
CHMP1B	charged multivesicular body protein 1B	2	1	Plasma Membrane
CLU	clusterin	5	4	Cytoplasm
Heat shock Protein 70 kDa				
HSPA1L	heat shock 70kDa protein 1-like	13	9	Cytoplasm
HSPA5	heat shock 70kDa protein 5 (glucose-regulated protein, 78kDa)	8	5	Cytoplasm
HSPA8	heat shock 70kDa protein 8	21	20	Cytoplasm
HSPA1A/ HSPA1B	heat shock 70kDa protein 1A	12	8	Cytoplasm
HSPA2	heat shock 70kDa protein 2	4	4	Cytoplasm
HSPA4	heat shock 70kDa protein 4	5	2	Cytoplasm
HSPA4L	heat shock 70kDa protein 4-like	1	1	Cytoplasm
Lipid Raft Marker				
FLOT1	flotillin 1	9	2	Plasma Membrane

b.

Cell-Type Specific Markers	Entrez Gene Name	HCC38 exo Peptide Count	BT20 exo Peptide Count	Localization
Tyrosine Kinase Receptor				
EGFR	epidermal growth factor receptor	10	17	Plasma Membrane
Tyrosine Kinase				
PTK7	protein tyrosine kinase 7	4	7	Plasma Membrane
NTRK2	neurotrophic tyrosine kinase, receptor, type 2	1	-	Plasma Membrane
BTK	Bruton agammaglobulinemia tyrosine kinase	1	-	Cytoplasm
MAPK1	mitogen-activated protein kinase 1	3	-	Cytoplasm
Claudin				
CLDN3	claudin 3	2	1	Plasma Membrane
CLDN4	claudin 4	1	1	Plasma Membrane
Growth Factor Binding				
IGFBP5	insulin-like growth factor binding protein 5	-	7	Extracellular
Oncogene				
RAB14	RAB14, member RAS oncogene family	4	4	Cytoplasm
RRAS2	related RAS viral (r-ras) oncogene homolog 2	3	4	Plasma Membrane
RHOA	ras homolog family member A	3	4	Cytoplasm
RBBP4	retinoblastoma binding protein 4	1	1	Nucleus
RAP2B	RAP2B, member of RAS oncogene family	1	1	Plasma Membrane
RAP1A	RAP1A, member of RAS oncogene family	4	5	Cytoplasm
RAN	RAN, member RAS oncogene family	4	3	Nucleus
RALA	v-ral simian leukemia viral oncogene homolog A (ras related)	2	7	Cytoplasm
RAC1	ras-related C3 botulinum toxin substrate 1 (rho family, small GTP binding protein Rac1)	3	3	Plasma Membrane
RAB7A	RAB7A, member RAS oncogene family	9	10	Cytoplasm
RAB5C	RAB5C, member RAS oncogene family	4	6	Cytoplasm
RAB5B	RAB5B, member RAS oncogene family	1	3	Cytoplasm
RAB5A	RAB5A, member RAS oncogene family	3	2	Cytoplasm
RAB35	RAB35, member RAS oncogene family	2	5	Cytoplasm
RAB33B	RAB33B, member RAS oncogene family	1	1	Cytoplasm
RAB2A	RAB2A, member RAS oncogene family	2	2	Cytoplasm
RAB23	RAB23, member RAS oncogene family	1	1	Cytoplasm
RAB1A	RAB1A, member RAS oncogene family	2	3	Cytoplasm
RAB18	RAB18, member RAS oncogene family	2	2	Cytoplasm
RAB11A	RAB11A, member RAS oncogene family	4	5	Cytoplasm
NRAS	neuroblastoma RAS viral (v-ras) oncogene homolog	1	1	Plasma Membrane
HRAS	Harvey rat sarcoma viral oncogene homolog	4	3	Plasma Membrane

Table 3.1: Proteomic analysis of HCC38 and BT20-derived exosomes. a) List of common exosome markers identified in both proteomic datasets. b) List of cell-type specific markers, demonstrating uniqueness of exosomes to cell type of origin.

a.

Cellular Markers	Entrez Gene Name	HCC38 exo Peptide Count	BT20 exo Peptide Count	Localization
Metabolic Enzymes				
AKR1B1	aldo-keto reductase family 1, member B1 (aldose reductase)	2	4	Cytoplasm
ALDH16A1	aldehyde dehydrogenase 16 family, member A1	4	4	Cytoplasm
ALDH1A3	aldehyde dehydrogenase 1 family, member A3	9	1	Cytoplasm
ALDH9A1	aldehyde dehydrogenase 9 family, member A1	1	3	Cytoplasm
ALDOA	aldolase A, fructose-bisphosphate	17	11	Cytoplasm
ALDOC	aldolase C, fructose-bisphosphate	2	1	Cytoplasm
ASS1	argininosuccinate synthase 1	1	7	Cytoplasm
BLVRB	biliverdin reductase B (flavin reductase (NADPH))	1	3	Cytoplasm
CAD	carbamoyl-phosphate synthetase 2, aspartate transcarbamylase, and dihydroorotase	3	2	Cytoplasm
CBR1	carbonyl reductase 1	3	5	Cytoplasm
CNP	2',3'-cyclic nucleotide 3' phosphodiesterase	5	9	Cytoplasm
DARS	aspartyl-tRNA synthetase	1	8	Cytoplasm
DERA	deoxyribose-phosphate aldolase (putative)	4	2	Cytoplasm
ENO1	enolase 1, (alpha)	21	14	Cytoplasm
EPRS	glutamyl-prolyl-tRNA synthetase	6	7	Cytoplasm
FASN	fatty acid synthase	68	50	Cytoplasm
FKBP1A	FK506 binding protein 1A, 12kDa	1	1	Cytoplasm
G6PD	glucose-6-phosphate dehydrogenase	5	15	Cytoplasm
GANAB	glucosidase, alpha; neutral AB	3	1	Cytoplasm
GAPDH	glyceraldehyde-3-phosphate dehydrogenase	19	15	Cytoplasm
GPI	glucose-6-phosphate isomerase	6	5	Extracellular Space
HPRT1	hypoxanthine phosphoribosyltransferase 1	3	1	Cytoplasm
IARS	isoleucyl-tRNA synthetase	9	4	Cytoplasm
IDH1	isocitrate dehydrogenase 1 (NADP+), soluble	3	10	Cytoplasm
KARS	lysyl-tRNA synthetase	1	4	Cytoplasm
LDHA	lactate dehydrogenase A	14	7	Cytoplasm
LOXL2	lysyl oxidase-like 2	1	4	Extracellular Space
MARS	methionyl-tRNA synthetase	3	4	Cytoplasm
MDH1	malate dehydrogenase 1, NAD (soluble)	4	3	Cytoplasm
ME1	malic enzyme 1, NADP (+)-dependent, cytosolic	1	2	Cytoplasm
MTHFD1	methylenetetrahydrofolate dehydrogenase (NADP+ dependent) 1, methenyltetrahydrofolate cyclohydrolase, formyltetrahydrofolate synthetase	11	8	Cytoplasm
NQO1	NAD(P)H dehydrogenase, quinone 1	3	7	Cytoplasm
P4HB	prolyl 4-hydroxylase, beta polypeptide	2	2	Cytoplasm
PAICS	phosphoribosylaminoimidazole carboxylase, phosphoribosylaminoimidazole succinocarboxamide synthetase	8	4	Cytoplasm
PDIA6	protein disulfide isomerase family A, member 6	1	2	Cytoplasm
PGD	phosphogluconate dehydrogenase	5	4	Cytoplasm
PHGDH	phosphoglycerate dehydrogenase	6	11	Cytoplasm
PLOD1	procollagen-lysine, 2-oxoglutarate 5-dioxygenase 1	9	7	Cytoplasm
PLOD3	procollagen-lysine, 2-oxoglutarate 5-dioxygenase 3	1	2	Cytoplasm
PPIA	peptidylprolyl isomerase A (cyclophilin A)	6	9	Cytoplasm
PPIB	peptidylprolyl isomerase B (cyclophilin B)	2	10	Cytoplasm
PYCRL	pyrroline-5-carboxylate reductase-like	2	2	Cytoplasm
RARS	arginyl-tRNA synthetase	4	2	Cytoplasm
TALDO1	transaldolase 1	3	5	Cytoplasm
TKT	transketolase	4	8	Cytoplasm
TPI1	triosephosphate isomerase 1	10	9	Cytoplasm
UGP2	UDP-glucose pyrophosphorylase 2	4	4	Cytoplasm

b.

Cellular Markers	Entrez Gene Name	HCC38 exo Peptide Count	BT20 exo Peptide Count	Localization
Cytoskeleton – Cytoplasmic Marker				
ACTBL2	actin, beta-like 2	2	2	Nucleus
ACTB	actin, beta	8	9	Cytoplasm
ACTN1	actinin, alpha 1	31	7	Cytoplasm
ACTN4	actinin, alpha 4	30	12	Cytoplasm
TUBA1A	tubulin, alpha 1a	15	16	Cytoplasm
TUBA4A	tubulin, alpha 4a	3	2	Cytoplasm
TUBA4B	tubulin, alpha 4b (pseudogene)	1	1	Cytoplasm
TUBB	tubulin, beta class I	4	3	Cytoplasm
TUBB1	tubulin, beta 1 class VI	5	5	Cytoplasm
TUBB3	tubulin, beta 3 class III	9	4	Cytoplasm
TUBB2A	tubulin, beta 2A class IIa	14	8	Cytoplasm
TUBB4A	tubulin, beta 4A class IVa	4	4	Cytoplasm
TUBB4B	tubulin, beta 4B class IVb	1	1	Cytoplasm
Plasma Membrane Marker (Iron Transport)				
TFRC	transferrin receptor	17	5	Plasma Membrane
Cell Adhesion – Epithelial Cell Markers				
CDH1	cadherin 1, type 1, E-cadherin (epithelial)	2	6	Plasma Membrane
EPCAM	epithelial cell adhesion molecule	4	4	Plasma Membrane
ICAM1	intercellular adhesion molecule 1	6	4	Plasma Membrane
ITGA2	integrin, alpha 2 (CD49B, alpha 2 subunit of VLA-2 receptor)	16	21	Plasma Membrane
ITGA3	integrin, alpha 3 (antigen CD49C, alpha 3 subunit of VLA-3 receptor)	23	16	Plasma Membrane
ITGA6	integrin, alpha 6	12	18	Plasma Membrane
ITGB1	integrin, beta 1 (fibronectin receptor, beta polypeptide, antigen CD29 includes MDF2, MSK12)	18	17	Plasma Membrane
ITGB4	integrin, beta 4	11	20	Plasma Membrane
ITGB5	integrin, beta 5	3	10	Plasma Membrane
ITGB6	integrin, beta 6	2	1	Plasma Membrane
Histone – Nuclear Marker				
H1F0	H1 histone family, member 0	3	3	Nucleus
H2AFV	H2A histone family, member V	2	2	Nucleus
H2AFY	H2A histone family, member Y	2	9	Nucleus
H2AFY2	H2A histone family, member Y2	2	2	Nucleus
HIST1H1A	histone cluster 1, H1a	4	4	Nucleus
HIST1H1B	histone cluster 1, H1b	4	5	Nucleus
HIST1H1C	histone cluster 1, H1c	2	3	Nucleus
HIST1H2AA	histone cluster 1, H2aa	3	2	Nucleus
HIST1H2BA	histone cluster 1, H2ba	3	4	Nucleus
HIST1H2BB	histone cluster 1, H2bb	6	6	Nucleus
HIST1H4A (includes others)	histone cluster 1, H4a	12	12	Nucleus
HIST1H4G	histone cluster 1, H4g	1	1	Nucleus
HIST2H2BE (includes others)	histone cluster 2, H2be	2	2	Nucleus
HIST3H3	histone cluster 3, H3	3	4	Nucleus

Table 3.2: Proteomic analysis of HCC38 and BT20-derived exosomes. a) List of metabolic enzymes identified in both proteomic datasets. b) List of other cellular markers identified in both proteomic datasets.

4.3 Diagnostic Significance of Breast Cancer Derived Exosomes

Having established that exosomes are rich in protein content, a logical continuation of this research is to gear experiments toward obtaining a comprehensive protein profile for breast cancer exosomes relative to their cell lines of origin. The primary question we want to answer is whether receptor tyrosine-kinases, which are routinely used to determine stage and molecular subtype of tumor biopsies, are present in breast cancer exosomes. There is limited literature reporting advances on this front. Ciravolo et al.[15] confirmed the presence of the HER2 receptor on exosomes derived by HER2-overexpressing breast cancer cell lines SKBR3 and BT474. In addition, they showed that the exosome-localized HER2 was successful in binding Trastuzumab, the monoclonal antibody inhibitor of this receptor. A more systematic study investigating glioblastoma cell lines has shown that in addition to the tetraspanin and MHC I markers characteristic of exosomes, the glioblastoma-derived exosomes also carried popular glioblastoma markers: EGFR, EGFRvIII, PDPN, PDGFR and EphA2[16].

A secondary question up for investigation is whether upstream cytolasmic protein kinases are also present in breast cancer exosomes and if so, to what extent. Along the same lines, we are interested in characterizing the protein content in exosomes

and seeing whether, in addition to cell membrane receptors, exosomes are able to export cytoplasmic and nuclear proteins in the extracellular space.

In addition to documenting the presence of receptor tyrosine-kinases in the exosomes, we are also interesting in interrogating the functionality of these receptors and their upstream effector pathways in these extracellular vesicles. A separate objective of ours is to identify whether the phosphorylation patterns of these proteins are conserved on the exosomes when the producing cell lines are challenged with growth factor and tyrosine-kinase inhibitors.

Finally, after documenting specific receptor signatures in different types of breast cancer exosomes, we ask whether incubation of cell lines with heterologous exosomes results in the transfer of exosome-specific receptors to the recipient cell line. The experiments that are presented below aim to answer this multitude of questions by characterizing the content and function of breast cancer-derived exosomes.

Methods

Quantitative Comparison of Exosomes to Cell Lines of Origin

Exosome lysates for six breast cancer cell lines –MCF7, T47D, MDAMB231, SKBR3, HCC38 and BT20- were prepared as described above by resuspension of the exosome ultracentrifugation pellet in 100ul MPER supplemented with 1x Roche protease inhibitor. Cell lysates were prepared by scraping cell monolayers and

resuspension of cells in PBS. The solution was centrifuged at 400g for 3min in order to pellet cells. Subsequently the cells were also resuspended in the same lysis buffer: MPER supplemented with 1x Roche protease inhibitor. Both exosome and whole cell lysates were incubated on ice for 30min and then centrifuged 15min at 14,000g to pellet insoluble fragments. The supernatants from the spin were recovered and protein levels were quantified following the protocol for a microBCA assay[9].

Following quantitation, 10ug of each protein extract were supplemented with Laemmli buffer and denatured at 95C for 10min. Lysates were loaded on a polyacrylamide gel and separated by electrophoresis in the presence of MOPS running buffer. The gels were transferred onto hydrophobic polyvinylidene difluoride membranes (PVDF), probed with primary and secondary fluorescently tagged goat anti-mouse Ig (1:5,000) or donkey anti-rabbit Ig (1:5,000). Signals were detected using the LI-COR Odyssey fluorescent western blot imager.

Treatment of Breast Cancer Exosomes with EGF, Lapatinib, Glucose and Phosphatase Inhibitors

For the purpose of these experiments eight T-150 culture flasks of cancer cells were cultured in serum-free RPMI medium for 48hrs. Following collection, the pooled supernatants amounting to 100ml of conditioned medium (CM) were spun 10min at 300g to pellet whole cells followed by 20min at 2,000g to pellet large cell debris. The CMs were concentrated 20-fold through a 3k filtration device centrifuged at 4,000g.

In the experiment that examined EGF and Lapatinib activity on breast cancer exosomes, the concentrated CMs were divided into four equal volume fractions that received respectively 1ml of DMEM supplemented with a) no treatment, b) 200ng/ml recombinant EGF, c) 10μM Lapatinib or d) 200ng/ml recombinant EGF and 10μM Lapatinib. All samples were incubated 1 hour at room temperature with gentle shaking. Following incubations, exosomes were pelleted down from all CM samples according to previously described differential ultracentrifugation protocol. The pelleted exosomes were resuspended in 30μL Laemmli running buffer supplemented with Roche protease inhibitor and Sigma Cocktail 2 phosphatase inhibitor. The exosome lysates were heated at 95C for 10min and loaded on two (15μL each) polyacrylamide gels. A standard western blotting protocol was employed thereafter. Membranes were probed with anti-rabbit EGFR, anti-rabbit pEGFR and anti-mouse beta-actin monoclonal antibodies. Following quantitation of protein bands, the ratio of pEGFR to EGFR was plotted for all treatment conditions. The experiment was repeated in duplicate and statistical analysis calculated unpaired, two-tailed, homoscedastic T-tests comparing all treatment conditions to the untreated control condition.

In the experiment that examined glucose, phosphatase inhibitor and Lapatinib activity on breast cancer exosomes, we began with the same process for production of 100ml of conditioned medium, clarification by centrifugation followed by 20-fold concentration. Next, the concentrated CMs were divided in to four equal volume

fractions that received respectively a) 1ml of PBS (no treatment) b) 10μM Lapatinib in1ml of PBS, c) 1ml of glucose/orthovanadate buffer d) 10μM Lapatinib in 1ml of glucose/orthovanadate buffer. The glucose/orthovanadate buffer consisted of 25mM glucose, 100mM NaCl, 1mM CaCl2, 1mM MgCl2, 50mM Hepes pH7.5 and 100mM orthovanadate activated at 90C for 5min. All samples were incubated 1 hour at room temperature with gentle shaking. Following incubations, exosomes were pelleted down from all CM samples according to previously described differential ultracentrifugation protocol. The pelleted exosomes were resuspended in 30μL Laemmli running buffer supplemented with Roche protease inhibitor and Sigma Cocktail 2 phosphatase inhibitor. The exosome lysates were heated at 95C for 10min and loaded on two (15μL each) polyacrylamide gels. A standard western blotting protocol was employed thereafter. Membranes were probed with anti-rabbit EGFR, anti-rabbit pEGFR, anti-rabbit AKT, anti-rabbit pAKT and anti-mouse beta-actin monoclonal antibodies. Following quantitation of protein bands, the ratios of pEGFR to EGFR as well as pAKT to AKT were plotted for all treatment conditions. The experiment was repeated in triplicate for HCC38 exosomes and quatruplicate for BT20 exosomes and statistical analysis calculated unpaired, two-tailed, homoscedastic T-tests comparing all treatment conditions to the untreated control condition.

Collection of Exosomes from EGF and/or Lapatinib Treated Cells

For the purpose of this experiment eight T-150 culture flasks of cancer cells were seeded and allowed to reach 80% confluence. The cells were then serum starved in

serum-free RPMI culture overnight. The next day the media was replaced with fresh serum-free RPMI supplemented with a) no treatment, b) 100ng/ml EGF and 1:1000 phosphatase inhibitor, c) 100ng/ml EGF, 1:1000 phosphatase inhibitor and 10μM Lapatinib and d) 10μM Lapatinib. Each treatment condition was applied in two flasks of cells. The cells were incubated with treatment for 24hrs, after which the supernatants were collected for each condition and exosomes were pelleted following according to previously described differential ultracentrifugation protocol. The pelleted exosomes were resuspended in 30μL Laemmli running buffer supplemented with Roche protease inhibitor and Sigma Cocktail 2 phosphatase inhibitor. The exosome lysates were heated at 95C for 10min and loaded on two (15μL each) polyacrylamide gels. A standard western blotting protocol was employed thereafter. Membranes were probed with anti-rabbit EGFR, anti-rabbit pEGFR, anti-rabbit AKT, anti-rabbit pAKT and anti-mouse beta-actin monoclonal antibodies. Following quantitation of protein bands, the ratios of pEGFR to EGFR as well as pAKT to AKT was plotted for all treatment conditions.

In order to perform the corresponding in-cell control experiment, cancer cells were seeded in 6-well plates and allowed to reach 80% confluence. The same protocol as above was followed. After treatment we waited 3 hrs and proceeded to lyse the cells with 2x Laemmli buffer. The cell lysates were heated at 95C for 10min and 15μL of each condition were loaded on polyacrylamide gels. A standard western blotting protocol was employed thereafter. Membranes were probed with anti-rabbit EGFR, anti-rabbit pEGFR, anti-rabbit AKT, anti-rabbit pAKT and anti-mouse beta-actin

monoclonal antibodies. Following quantitation of protein bands, the ratios of pEGFR to EGFR as well as pAKT to AKT were plotted for all treatment conditions.

Receptor Transference from Receptor-Positive Exosomes to Receptor-Negative Cell Lines

Donor cell lines MCF7 and T47D were seeded at 80% confluence in eight T-150 culture flasks. Supernatants were collected after 48hrs of culture in serum-free RPMI and exosomes were purified employing the to the previously described serial ultracentrifugation protocol. Exosome pellets were resuspended in PBS and stored at 4C. Recipient cell lines MDAMB231 and SKBR3 were seeded at a density of 100,000 cells/well in 6-well plates and allowed to adhere to the culture plate overnight. Then the media was switched to serum free RPMI and cell monolayers were serum starved for 24hrs. We then proceeded to add half the volume of each exosomes preparation to each cell line, while the untreated control received an equal volume of blank PBS. The cells were incubated with the exosomes for 6hrs after which the supernatants were discarded and the monolayers were washed twice in PBS to remove any unbound vesicles. Next the monolayers were lysed using 100μL 2x Laemmli buffer. Finally 15μL of each sample were heated at 95C for 10min, then loaded in a standard polyacrylamide gel. A standard western blotting protocol was employed thereafter. Membranes were probed with anti-rabbit CDH1, anti-rabbit EpCAM and anti-mouse beta-actin monoclonal antibodies. Following quantitation of protein bands, the ratios of CDH1 to beta-actin as well as EpCAM to beta-actin were plotted for all treatment conditions.

Results

Quantitative Comparison of Exosomes to Cell Lines of Origin

The first set of results aims to compare exosomes to their cell lines of origin by loading equal amounts of both lysates on polyacrylamide gels and blotting for a variety of cell membrane proteins. The ensuing western blots are displayed in figure 3.8 and feature eight cell surface receptors. The majority of receptors tested are of diagnostic and therapeutic importance in breast cancer: the epidermal growth factor receptors 1 (EGFR) as well as 2 (HER2), the hepatocyte growth factor receptor (MET), the insulin-like growth factor receptor (IGF1R), the major histocompatibility complex I and finally cadherin-1 (CDH1). The first four are receptor tyrosine kinases that are clinical targets for monoclonal antibody therapies. The last one, cadherin-I or E-cadherin, is an epithelial cell-cell adhesion glycoprotein. The loss of E-cadherin has been implicated in cancer progression and metastasis. Absence of E-cadherin in breast tumor clinical histology sections indicates an invasive cancer phenotype. In addition to these we also probed for the epithelial cell-adhesion molecule (EpCAM) and proto-oncogene tyrosine-protein kinase SRC. We probed for EpCAM since it is a common molecule used in affinity-capture diagnostic technologies that aim to purify circulating cells of epithelial origin from blood samples. We probed for SRC because in contrast to EGFR and HER, it is a non-receptor tyrosine kinase and wanted to establish if the protein receptor TRKs patterns observed in exosomes also extend to non-receptor TRKs.

On figure 3.8 we observe that when a protein is featured in the whole cell lysates, it can also be found in the corresponding exosomes. This fact alone establishes exosomes as a strong diagnostic molecule in breast cancer.

On figure 3.9 we quantitatively compare the western blot findings by normalizing all cell lysates to the maximum fluorescent intensity value in each receptor group. We repeat this process for the corresponding exosomes. The question we pose is whether exosomes accurately reflect the cell line that is overexpressing the receptor in each group. We find that exosomes accurately predict that SKBR3 cells are HER2 over-expressers and that BT20 cells are EGFR over-expressers. We also see that exosomes reflect the fact that MCF7 cells are IGF1R over-expressers and that T47D cells have the highest amount of CDH1. In addition, we find that exosomes in most cases accurately reflect the lowest expressers in the group. MDAMB231 exosomes are negative for CDH1, as are MDAMB231 cells. Similarly MDAMB231 and HCC38 cells are negative for IGF1R much like the corresponding cells. In the middle of the expression spectrum we see some fluctuations in the exosome pattern as compared to the cell lysate profile of expression. When differences in expression levels become small between two cell lines, exosomes predictions blur. This is evident in IGF1R receptor, where cell lysates show that BT20 cells contain more IGF1R that T47D cells, yet exosomes indicate the opposite.

Upon closer inspection of the western blot images on figure 3.8 we are able to note subtleties on the state of the blotted proteins in the exosomes versus the cell lysates.

Notably, MET cell lysates feature a secondary band at 170kDa that corresponds to pro-MET, most visible in the high MET expresser cell lines BT20 and MDAMB231. The band is absent from the exosomal MET version, in both cases. In contrast, in MCF7 cells the pro-IGF1R subunit of 200kDa weight can be found in MCF7-derived exosomes but is absent in the whole cell lysate.

We also see that while some receptors are found in exosomes in comparable quantities to their cellular amounts, others are significantly enriched or depleted in the exosomes. Specifically EpCAM is significantly enriched in all exosomes as compared to the cell lines of origin. While we have no biological explanation for this finding, it is nevertheless convenient from a diagnostic perspective. As discussed in the introductory chapter, EpCAM is the primary molecule used to affinity-purify first

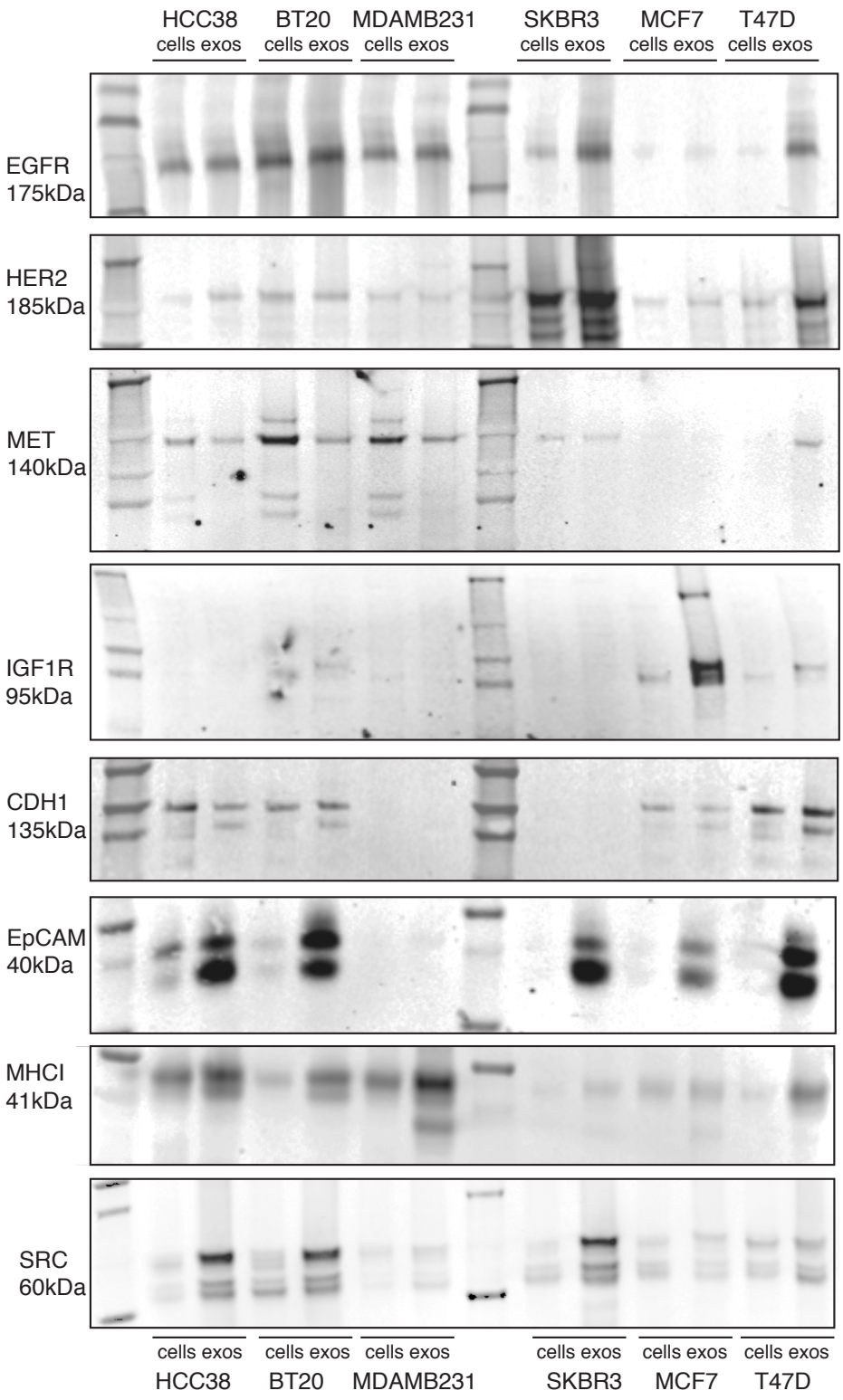

Figure 3.8: Comparative western blots for whole cells and their corresponding exosome lysates.

circulating tumor cells and more recently exosomes from blood samples. Its over-representation in these extracellular vesicles ensures that the exosomes will not go undetected in the patient's circulation. One shortcoming of these diagnostic technologies is that breast cancer cell lines further along the epithelial-mesenchymal transition down-regulate or switch off EpCAM expression. These tumors are represented in our *in vitro* model by the EpCAM-negative MDAMB231 cells. One possible remedy to this limitations would be to affinity-purify circulating exosomes based on two receptors: EpCAM and EGFR.

In addition to developing informed purification strategies for blood biopsies, this cursory screen of exosome membrane proteins reveals that while only two receptors are sufficient to purify exosomes, three receptors is the minimum amount necessary to define the molecular subtype of a particular breast cancer from the circulating exosomes. These receptors are EGFR, HER2 and EpCAM. Indeed EGFR high/EpCAM high exosomes indicate Basal cells. EGFR high/ EpCAM low exosomes indicates the special category of invasive Basal B breast cancer with epithelial marker downregulation. The EGFR low/EpCAM high phenotype indicates luminal cells. And finally EGFR high/EpCAM high/HER2 high reflects the special category of HER2 overexpressing tumors.

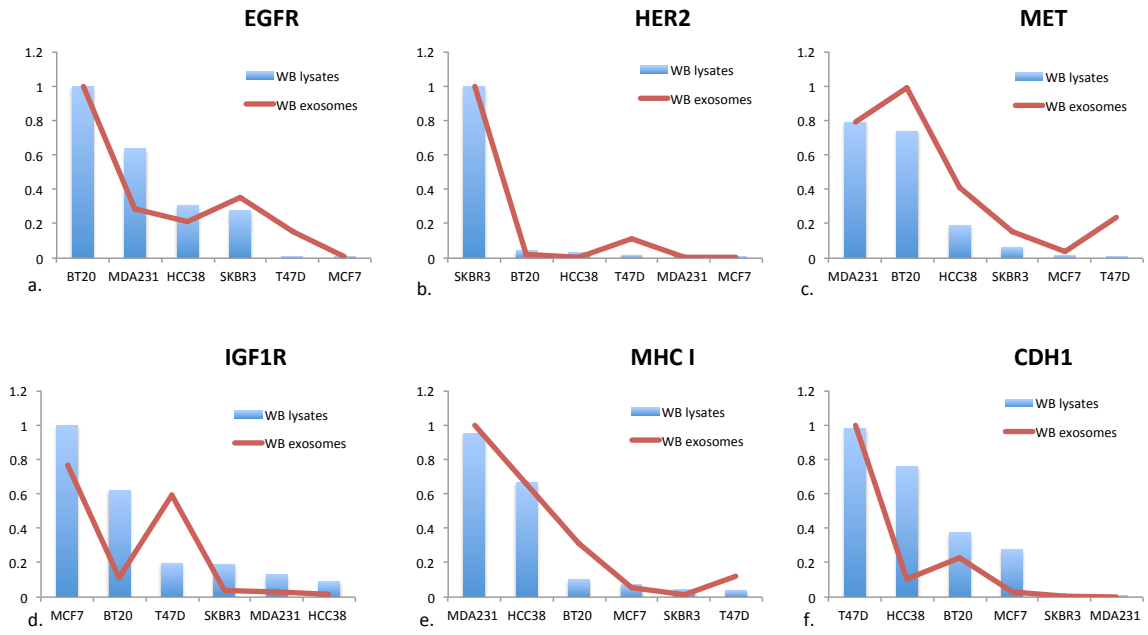

Figure 3.9: Quantitative comparison via western blot across six breast cancer cell lines for the following protein markers: a)EGFR, b)HER2, c)MET, d)IGF1R, e)MHC1 and f)CDH1 illustrating that the cell expression pattern of aforementioned proteins in the cells is accurately reflected in the corresponding exosomes.

In our subsequent experiment (figure 3.10) we blot for downstream cytoplasmic kinases: p38 MAPK, AKT, mTOR, PI3K 110alpha and PI3K. In addition we blot for beta-actin, a common cytoplasmic and cytoskeletal protein marker. The findings in this dataset are less expected and more intriguing. We see that actin and p38 MAPK and PI3K 110beta are detectable in all exosomes. In addition, AKT and PI3Kalpha are detectable in almost all exosomes tested, with the exeption of MDAMB231 exosomes. Lastly, mTOR is absent from both MDAMB231 cells and exosomes and displays a more erratic pattern of being enriched in some exosome types while depleted in others. These results suggest that in comparison to membrane proteins presence of intracellular kinases is more unpredictable in breast cancer-derived exosomes. Seeing that exosomes are membranous vesicles, this was to be expected.

Nevertheless, some kinases such as AKT and p38 MAPK appear to be more consistently expressed across all types of breast cancer exosomes. The mechanism by which some cytoplasmic proteins are represented in the exosomes while others are not is unknown at this point. Therefore intracellular protein presence will have to be determined in a case-by-case basis in a clinical setting

On figure 3.11 we plot the ratio of quantified protein level of the exosomes over the cell lysates in order to examine enrichment and depletion patterns. Figure 3.11a features the protein levels of basal exosomes (MDAMB231, HCC38 and BT20) while figure 3.11b features the protein levels of luminal exosomes (SKBR3, MCF7 and T47D). One salient feature of this analysis is that luminal cells have higher enrichment patterns across most proteins. Specifically in the intracellular proteins, basal exosomes display depletion of beta-actin and AKT while luminal exosomes are mostly enriched in these proteins. Even though all exosomes have detectable amounts of p38 MAPK, the protein is depleted in exosomes when compared to cell levels. Overall the most depletion is observed in intracellular proteins, while most membrane proteins, with the exception of the MET receptor, are enriched in the vesicles. This once again highlights these vesicles as robust extracellular reporters of membrane proteins. We specifically observe that exosomes are enriched in EpCAM, SRC and MHCI membrane receptors, from 10-fold to 400-fold in the extreme case of EpCAM. One possible interpretation for this is that while some proteins might be passively transferred in the exosomes during their biogenesis,

others might be selectively inserted based on an active mechanism of enrichment or depletion.

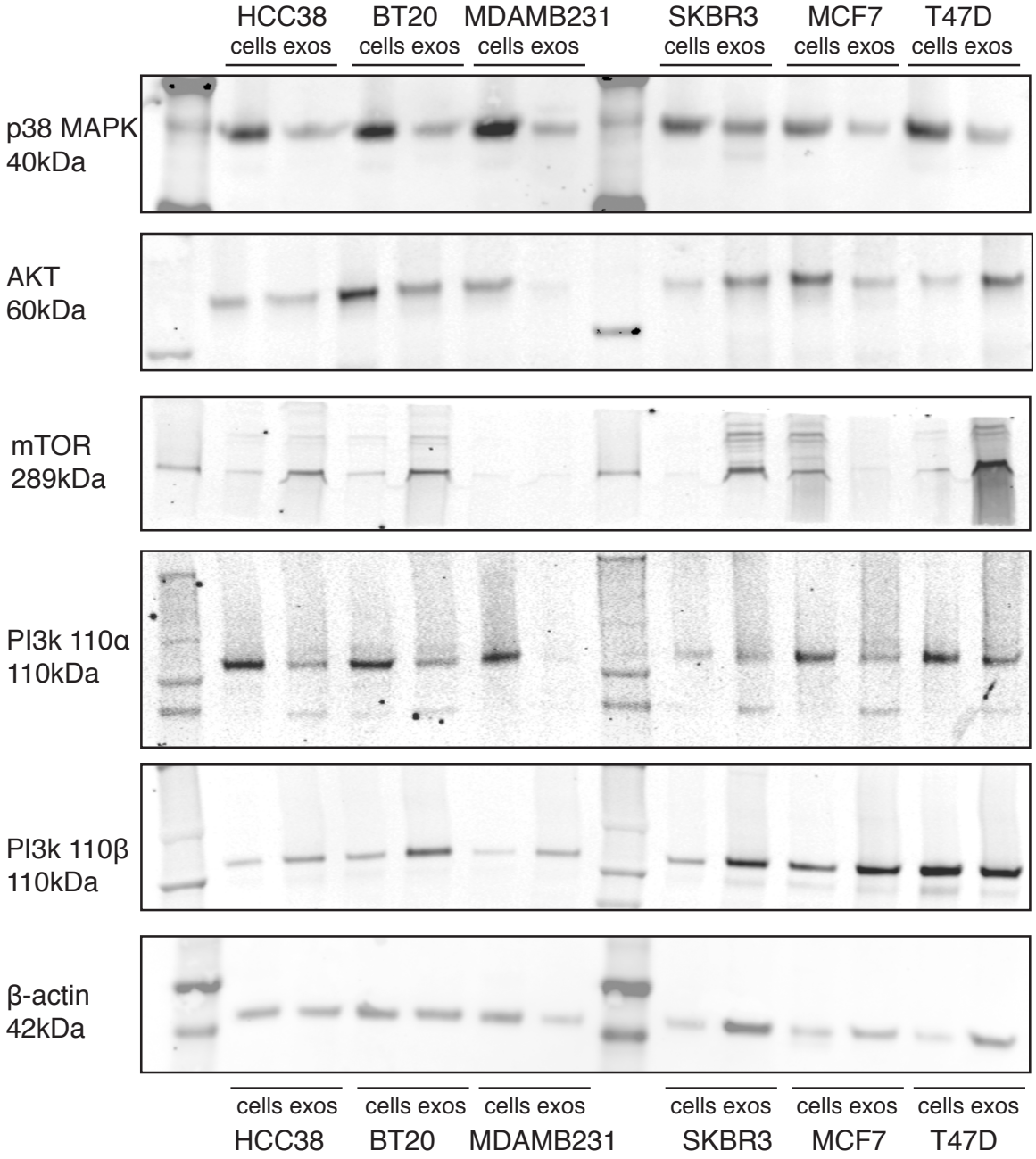

Figure 3.10: Comparative western blots for whole cells and their corresponding exosome lysates.

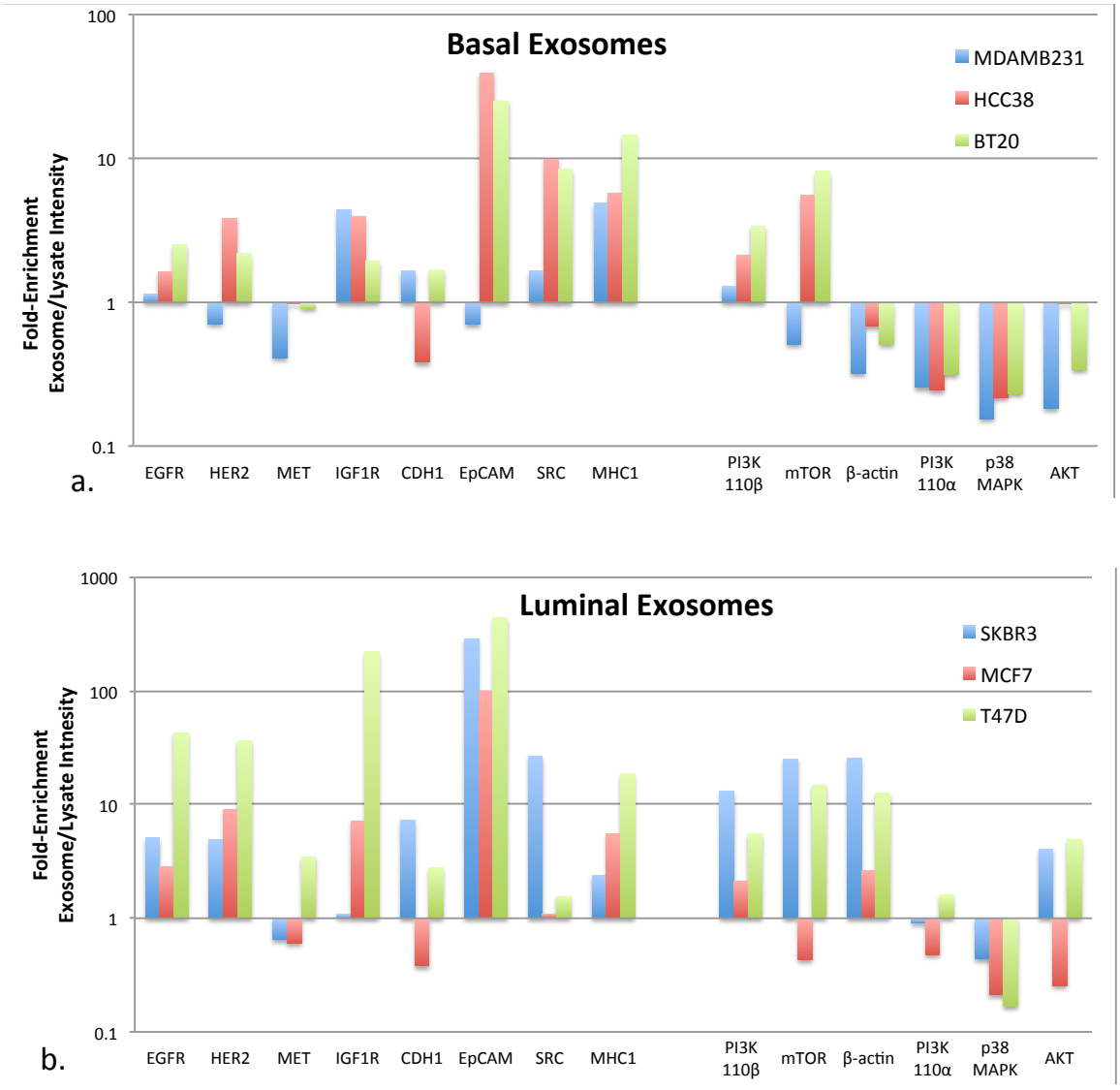

Figure 3.11: Fold-enrichment pattern of cell membrane and intracellular proteins in exosomes, comparatively to whole cell lysates. a) Basal cell line profiles of protein enrichment in the exosomes for cell types MDAMB231, HCC38 and BT20. b) Luminal cell line profiles of protein enrichment in the exosomes for cell types SKBR3, MCF7 and T47D.

Assessing Functionality of Receptor Tyrosine Kinase EGFR in Exosomes

In the previous section we established the presence EGFR and upstream kinases on breast cancer derived exosomes, while earlier in this chapter we reported mass spectrometry findings that revealed an abundance of glycolytic enzymes present in

the exosomes of BT20 and HCC38 cancer cell lines. An ensuing question is whether exosomes can convert extravesicular glucose to ATP and if so, are exosomes able to use ATP in order to phosphorylate the EGFR receptor. In this section we therefore examine exosomal EGFR more closely to determine whether the receptor remains functional on the extracellular vesicles. For this study we employ exosomes from two cell lines: HCC38, an EGFR expresser and BT20, an EGFR over-expresser.

The results are summarized in figures 3.12 for BT20-derived exosomes and figure 3.13 for HCC38-derived exosomes. In panels 3.12a and 3.13a we incubate exosomes in the presence of glucose with EGF and/or Lapatinib treatment. One striking feature is that both types of exosomes have detectable baseline amounts of phosphorylated EGFR. However, the phosphorylation does not statistically increase due to EGF treatment, nor does it decrease in the presence of EGFR/HER2 dual inhibitor Lapatinib. We conclude that in both cases, the exosomal EGFR is not functional in that it is not able to phosphorylate or de-phosphorylate in response to extravesicular stimulants. We want to note however that this was an activity study rather than a binding study. It is still entirely possible that the exosomes can bind EGF and/or Lapatinib. This was a phenomenon we did not specifically look at but there are reports in the literature that document binding ability of exosomes to various receptor TRK ligands. Instead our objective was to determine functional response of exosomes to these ligands and in that respect we conclude that the EGFR receptor is not functional on the exosomes.

In panels 3.12b and 3.13b we take a step back and incubate exosomes in the presence and absence of glucose in the extravesicular medium. In addition, instead of the EGF biological ligand we attempt to non-specifically increase the baseline EGFR phosphorylation by treating exosomes with orthovanadate phosphatase inhibitor. Lapatinib inhibitor is added in the presence or absence of glucose and phosphatase inhibitors. Finally, in addition to monitoring the phosphorylation of EGFR we also document the phosphorylation of the upstream kinase AKT. Even though we observe mild fluctuations in pEGFR and pAKT neither type of exosome displays statistically significant change in response to the various treatments. Once again we conclude that exosomal EGFR is present but not functional. Specifically the failure of exosomes to 'sense' a difference in glucose-free versus glucose-rich extravesicular buffer implicates a lack of intact glycolytic mechanism as the etiology behind EGFR functional failure.

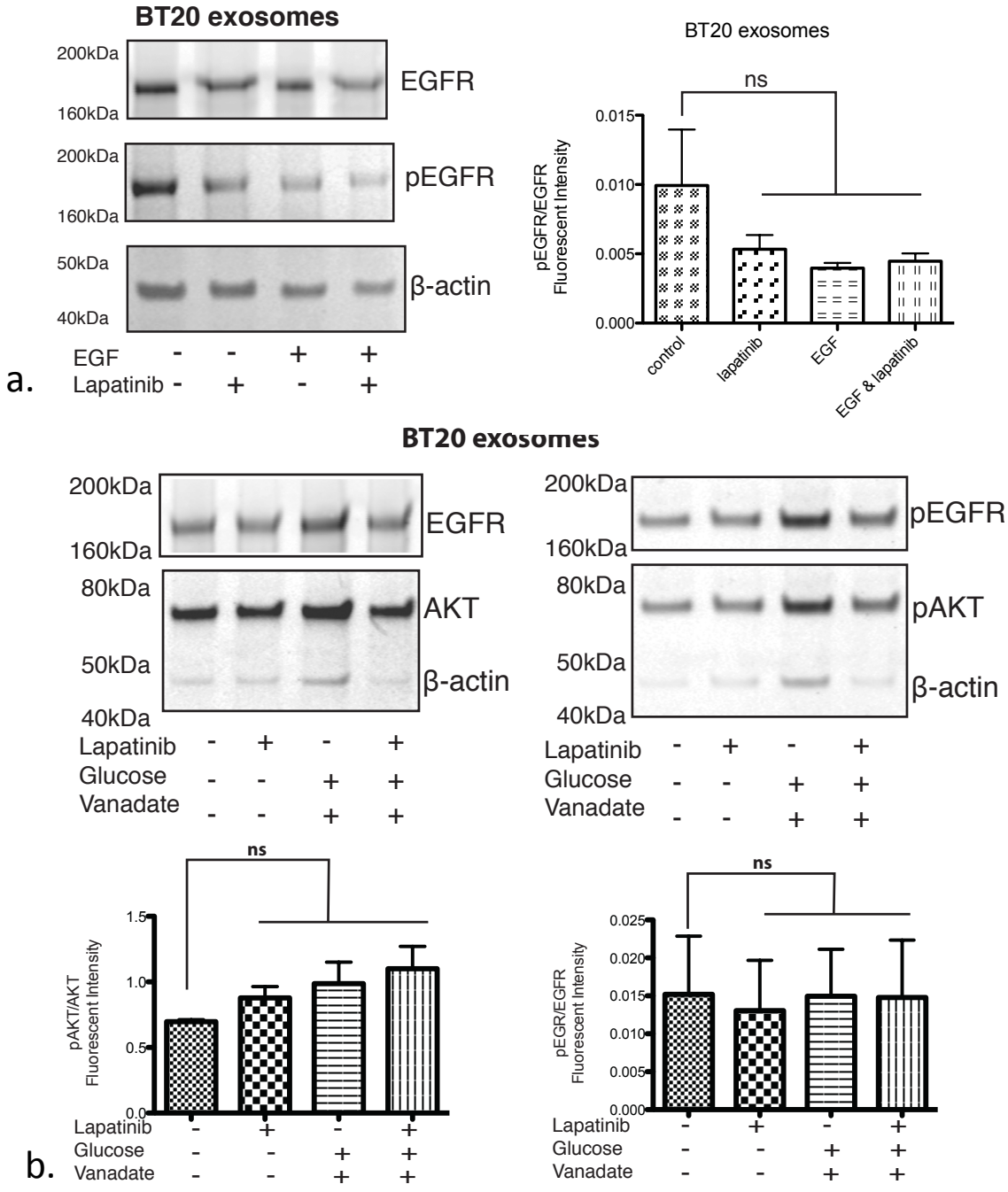

Figure 3.12: Determining the functionality of BT20 exosomes.
a) BT20 exosomes do not phosphorylate EGFR in response to glucose and biological ligand EGF.
b) BT20 exosomes do not phosphorylate EGFR in response to presence of glucose and non-specific phosphatase inhibitor the extravesicular medium. Lapatinib treatment of exosomes does not result in an observable decrease of baseline phosphorylation levels of EGFR in exosomes derived from BT20 cells.

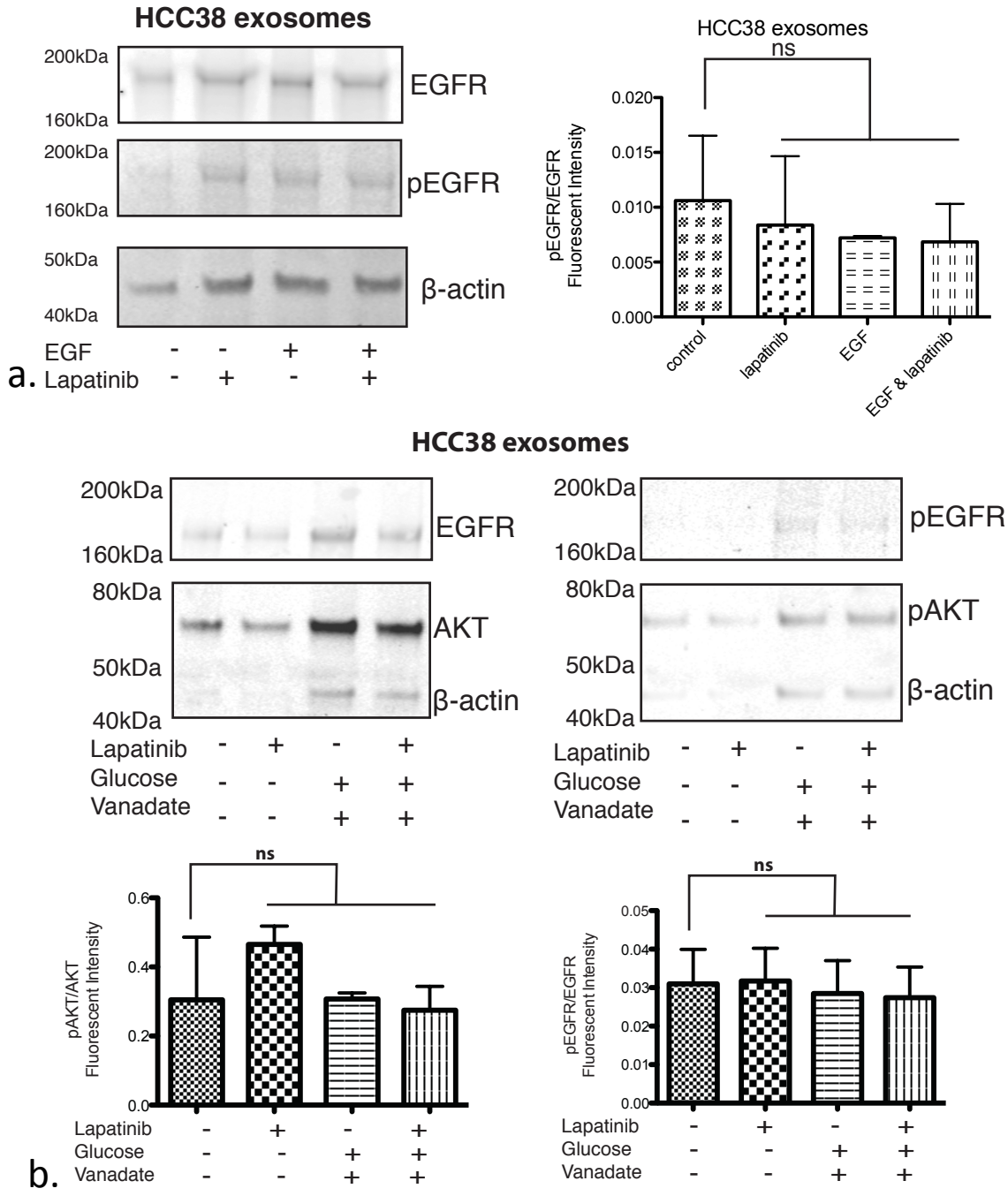

Figure 3.13: Determining the functionality of HCC38 exosomes.
a) HCC38 exosomes do not phosphorylate EGFR in response to glucose and biological ligand EGF.
b) HCC38 exosomes do not phosphorylate EGFR in response to presence of glucose and non-specific phosphatase inhibitor the extravesicular medium. Lapatinib treatment of exosomes does not result in an observable decrease of baseline phosphorylation levels of EGFR in exosomes derived from HCC38 cells.

Collection of Exosomes from EGF and/or Lapatinib Treated Cells

Having established that exosomal EGFR does not retain phosphorylation function, we now re-formulate our original hypothesis and query whether the phosphorylation level of EGFR and upstream AKT kinase on the exosomes can carry information regarding the phosphorylation state of the exosome-producing cells. In order to answer this question we treat serum-starved cell monolayers with EGF and Lapatinib separately as well as simultaneously. We allow 24hrs to pass before we collect and purify exosomes from the culture supernatants. In parallel to this experiment we also perform the corresponding in-cell control by treating cells with EGF and/or Lapatinib and collecting the cell lysates. Once again we perform these experiements with two types of cells and resulting exosomes: HCC38 and BT20.

Figure 3.14 displays results for BT20 cells, while figure 3.15 summarizes HCC38 cell results. Panels 3.14a and 3.15a show the extent of cellular EGFR and AKT phosphorylation in response to EGF and Lapatinib treatment. We observe a 10-fold rise of pEGFR in response to EGF stimulation. This response is completely mitigated my Lapatinib treatment in both cell types. We also observe a more moderate pattern when it comes to upstream AKT phosphorylation in response to EGF treatment. In BT20 cells pAKT approximately doubles during EGF treatment, while in HCC38 cells it retains baseline levels. Lapatinib has a more pronounced effect on pAKT, since it decreases it below baseline levels in both cases.

Panels 3.14b and 3.15b display the experiments where we are attempting to readout phosphorylation of AKT and EGFR on exosomes isolated from EGF and/or Lapatinib treated cells. Phospho-EGFR in both types of exosomes behaves similarly to the in-cell controls. The phosphorylation rises in response to EGF treatment, while Lapatinib returns pEGFR to baseline levels. However, in contrast to in cell-controls, pEGFR in BT20 exosomes only rises up two-fold more than the baseline control when in the cell the phosphorylation response to the same treatment goes up more than 10-fold. The potency of the information is somewhat mitigated in these exosomes. On the contrary, HCC38 exosomes display a 7-fold rise in phosphorylation in response to EGF treatment, which is close to the in-cell control amount. In both types of exosomes pAKT displays a similar rise-and-fall pattern as in the cells, yet once again the fold-induction is weaker than in the cells.

Further replicates are currently underway that will establish the statistical reproducibility of these results. However, this early finding suggests that breast cancer exosomes can mirror not only receptors from their cell lines of origin but furthermore the phosphorylation status of those receptors. Clinically, this feature of exosomes can be exploited as a real-time dynamic read out of tumor response to TRK inhibitor drug treatments.

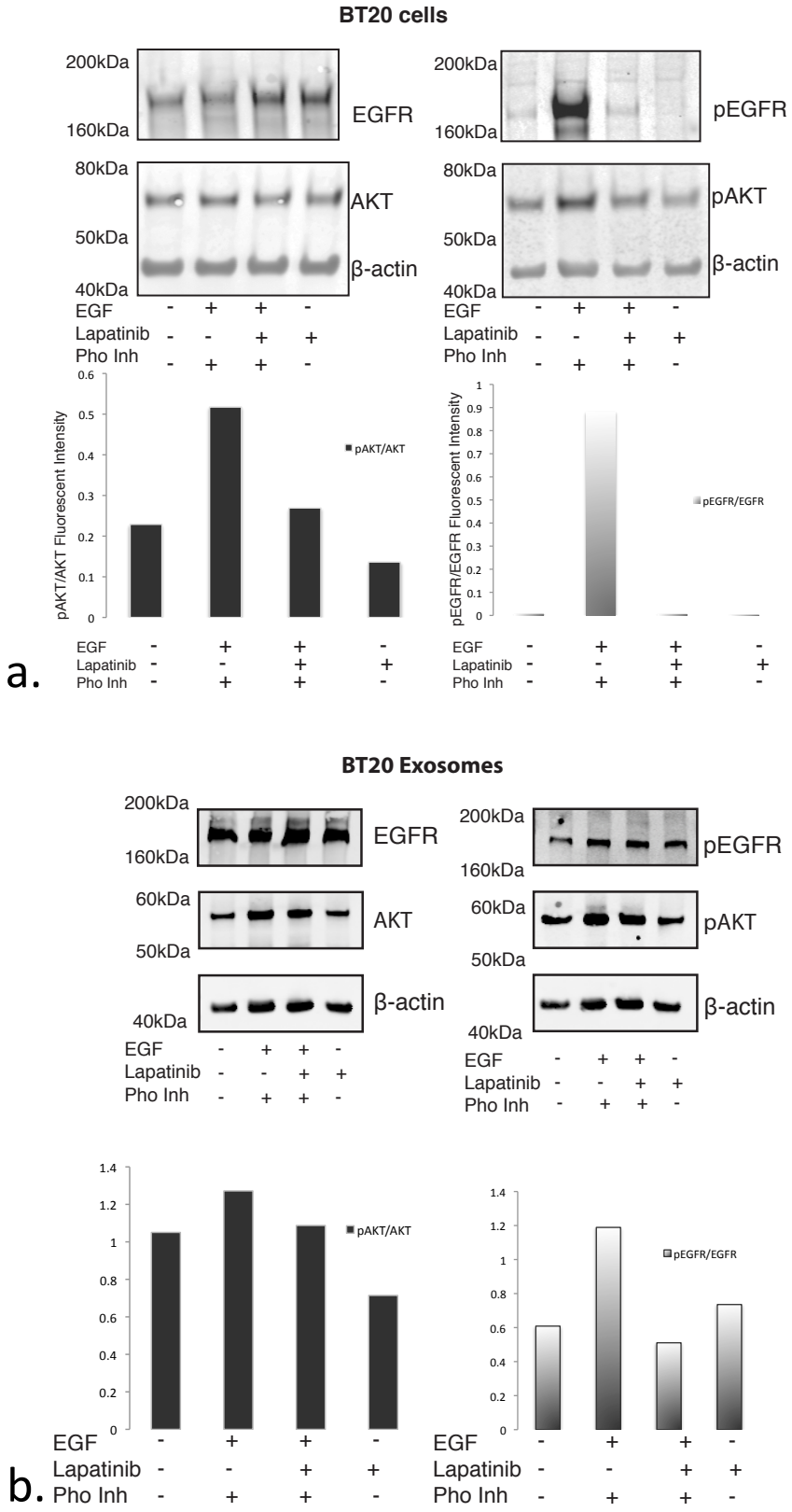

Figure 3.12: BT20 exosomes reflect the EGFR phosphorylation status of the cell line of origin.

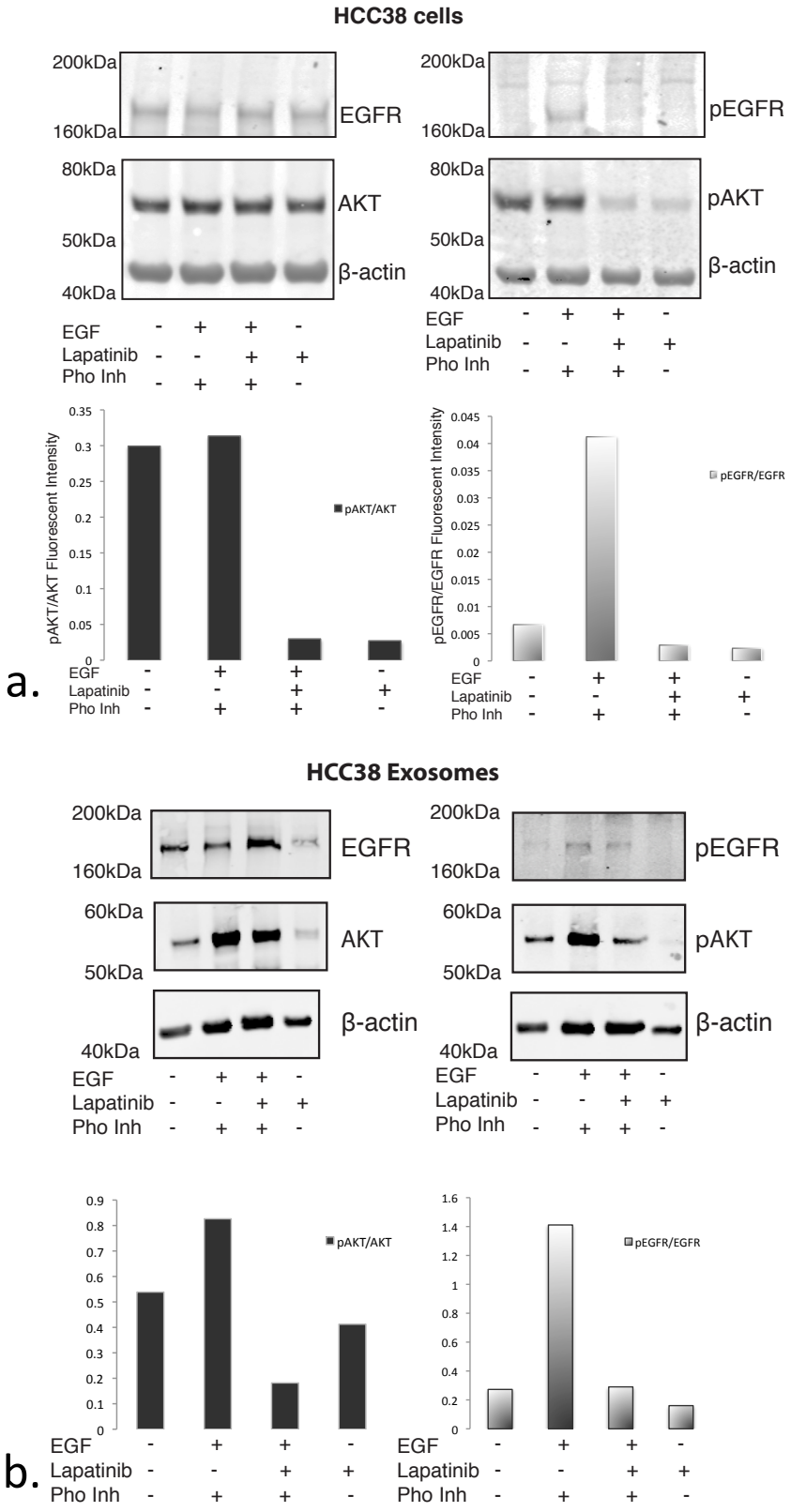

Figure 3.13: HCC38 exosomes reflect the EGFR phosphorylation status of the cell line of origin.

Receptor Transference from Receptor-Positive Exosomes to Receptor-Negative Cell Lines

In chapter 2 we presented time lapse imaging data showing the endocytosis of fluorescently-labeled exosomes by a heterologous cancer cell line. This data raised the question of whether exosomes are able to transfer biological material, in the form of microRNAs or proteins, into the recipient cell lines. In this section we devise a simple experimental assay in order to answer this question, as far as protein transfer goes. We realized that we had to make a strategic choice when it came to which protein to use as a reporter of exosome-mediated transfer. We needed to select a protein that is abundant in the exosomes, yet not expressed in the recipient cell lines so that a small amount of exosome-transplanted protein will be readily detectable in the recipient cell lysates. For this purpose we refer back to figure 3.8 and select CDH1 and EpCAM-positive exosomes derived from MCF7 and T47D cells. For the recipient cell lines we select MDAMB231 cells since they are both CDH1 and EpCAM-negative, as well as SKBR3 cells which as CDH1-negative and EpCAM positive.

Figure 3.16 summarizes the results of this experiment. We see that MCF7-derived exosomes are not significantly efficient at transferring CDH1 or EpCAM in either cell line. On the contrary, T47D exosomes induce a 5-fold increase in the amount of EpCAM present in SKBR3 cells and a two-fold increase in MDAMB231 EpCAM. Furthermore, T47D exosomes are successful at transferring a detectable 6-fold band of CDH1 in SKBR3 cells, and a corresponding 4-fold CDH1 band in MDAMB231 cells.

Perhaps the efficiency of T47D exosomes in protein transfer stems from the fact that these exosomes show higher levels of protein enrichment, in comparison to MCF7 exosomes (figure 3.11).

Further experimental replicates are needed to validate this result, yet this finding sheds some light into the biological role of exosomes. Future studies should center around the characterization of this transfer phenomenon by immunohistochemistry in order to unveil the localization of the transferred adhesion molecules. Are they transferred within the cytoplasm of the recipient cells or do they assume a functional role on the cell membrane and initiate changes in the cellular phenotype. Another issue that remains to be qualified is the precise timescale of the transfer phenomenon. When does transfer begin, when does it peak and is the presence of the transferred proteins transient or permanent in the recipient cells. Future studies geared toward biological activity of breast cancer exosomes will center around these critical questions.

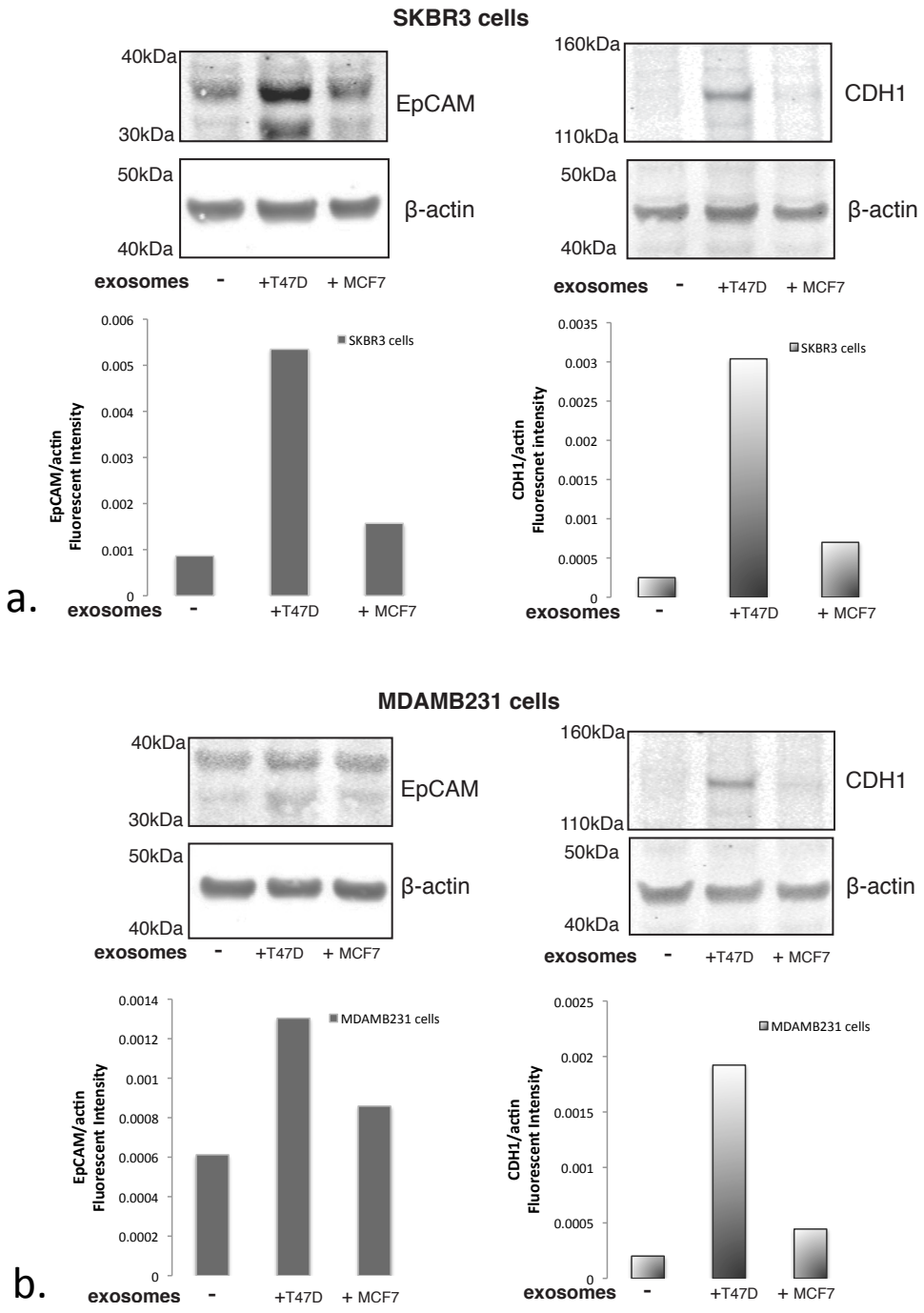

Figure 3.16: Treatment of CDH1-negative a) SKBR3 and CDH1 and EpCAM negative b) MDAMB231 cells with both EpCAM and CDH1 positive T47D and MCF7 exosomes, results in treansfer of the CDH1 and EpCAM receptor in the recipient cell lines.

References

1. Shao, H. *et al.* Protein typing of circulating microvesicles allows real-time monitoring of glioblastoma therapy. *Nat. Med.* **18,** 1835–40 (2012).

2. Biosciences, S. ExoQuick Exosome Precipitation Solution. (2013).

3. Isolation and Characterization of Exosomes from Cell Culture Supernatants. 1–29 (2006).

4. Mignot, G., Roux, S., Thery, C., Ségura, E. & Zitvogel, L. Prospects for exosomes in immunotherapy of cancer. *J. Cell. Mol. Med.* **10,** 376–88 (2006).

5. Mittelbrunn, M. *et al.* Unidirectional transfer of microRNA-loaded exosomes from T cells to antigen-presenting cells. *Nat. Commun.* **2,** 282 (2011).

6. Lässer, C. *et al.* Human saliva, plasma and breast milk exosomes contain RNA: uptake by macrophages. *J. Transl. Med.* **9,** 9 (2011).

7. Medina, A. & Ghahary, A. Transdifferentiated circulating monocytes release exosomes containing 14-3-3 proteins with matrix metalloproteinase-1 stimulating effect for dermal fibroblasts. *Wound Repair Regen.* **18,** 245–53 (2010).

8. Pegtel, D. M. *et al.* Functional delivery of viral miRNAs via exosomes. *Proc. Natl. Acad. Sci. U. S. A.* **107,** 6328–33 (2010).

9. Pierce. Micro BCA ™™ Protein Assay Reagent Kit. 1–7

10. Clayton, A., Al-Taei, S., Webber, J., Mason, M. D. & Tabi, Z. Cancer exosomes express CD39 and CD73, which suppress T cells through adenosine production. *J. Immunol.* **187,** 676–83 (2011).

11. Mathivanan, S., Ji, H. & Simpson, R. J. Exosomes: extracellular organelles important in intercellular communication. *J. Proteomics* **73,** 1907–20 (2010).

12. Peng, P., Yan, Y. & Keng, S. Exosomes in the ascites of ovarian cancer patients: origin and effects on anti-tumor immunity. *Oncol. Rep.* **25,** 749–62 (2011).

13. Mathivanan, S. *et al.* Proteomics analysis of A33 immunoaffinity-purified exosomes released from the human colon tumor cell line LIM1215 reveals a tissue-specific protein signature. *Mol. Cell. Proteomics* **9,** 197–208 (2010).

14. Heiser, L. M. *et al.* Subtype and pathway speci fi c responses to anticancer compounds in breast cancer. (2011). doi:10.1073/pnas.1018854108/-/DCSupplemental.www.pnas.org/cgi/doi/10.1073/pnas.1018854108

15. Ciravolo, V. *et al.* Potential role of HER2-overexpressing exosomes in countering trastuzumab-based therapy. *J. Cell. Physiol.* **227,** 658–67 (2012).

16. Shao, H. *et al.* Protein typing of circulating microvesicles allows real-time monitoring of glioblastoma therapy. *Nat. Med.* **18,** 1835–40 (2012).

Chapter 5

Conclusions

5.1 Indentifying pro-apoptotic factors in breast cancer conditioned media

In chapter 2 we showed that the conditioned media (CM) of triple negative breast cancer cell lines was toxic to breast cancer cells. Among the triple negative cell lines, HCC38 and BT20-derived CMs that were particularly pro-apoptotic and resulted in high apoptotic cell count on the majority of responder cell lines tested. We consequently embarked in further biochemical characterization of those two CMs. We showed that the apoptotic effect can be concentrated, heated to 95°C and frozen in liquid nitrogen. In contrast, a dilution series of CM HCC38 showed that the apoptotic effect cannot be diluted. Furthermore, we established that the apoptotic effect is retained in the soluble supernatant of the ultracentrifugation spin that pellets membranous particles present in the CMs.

Although interesting, this line of investigation presented significant challenges. There was batch-to-batch variability in the apoptotic potency of conditioned media that complicated the process of obtaining multiple biological replicates of the same experiment. In addition, as demonstrated by live cell timelapse movies presented in chapter 1, the apoptotic effect derived from incubation of target cell lines with the cytotoxic CMs set in at about 30hrs of culture. This made experiments of further characterization of the apoptotic effect significantly time consuming. For these

reasons we eventually changed course and turned to different approaches in order to elucidate the protein content of the CMs and generate leads, that is candidate proteins responsible for the apoptotic effect.

In chapter 3 we used transcriptomic as well as proteomic approaches in order to mine the secretome of HCC38 and BT20 cells for pro-apoptotic factors. Each of these approaches had some advantages as well as caveats associated with it. The transcriptional profiles of all 18 out of the 20 breast cancer cell lines were publicly available for this cancer cell library. Therefore we were able to correlate the transcriptome of 18 cell lines to the phenotypic data matrix presented in chapter 1. The obvious disadvantage of using transcriptional data to predict secreted protein profiles is that numerous biological events can alter the expression of a final protein product after transcription. For this reason we followed up this effort with proteomic analysis of BT20 and HCC38-derived conditioned media. We looked for pro-apoptotic hits in the protein pool that is common to both CMs, as well as among the proteins that where found to be unique for each media. As mentioned earlier, fractionation of the CM and re-testing of fractions for apoptotic activity had revealed that CM-induced apoptosis is retained in the particulate-free fraction of the media. In order to compress the list of proteomically-identified apoptotic hits, we also compared the proteome of CM-derived exosomes to that of the full CMs and examined the pool of CM-unique proteins for molecules with known apoptotic activity. We took this analysis one step further and looked for hit overlap between the two lists, CM HCC38 unique proteins and CM BT20 unique proteins. As

predicted, this approach resulted in a significantly shorter list of hits awaiting validation.

Symbol	Entrez Gene Name	Present in CM	Present in exosomes	Function
CTSD	Cathepsin D	Yes	No	1. Clinical marker for poor prognosis in breast cancer 2. Activates under acidic conditions 3. Evidence for both pro-apoptotic and pro-proliferative activity
CTSB	Cathepsin B	Yes	No	1. Activates under acidic conditions 2. Evidence for both pro-apoptotic and pro-proliferative activity
KLK6	Kallikrein-related peptidase 6	Yes	No	1. Downregulated in breast cancer relative to healthy tissue 2. Inhibited by serpins 3. Evidence for both pro-apoptotic and pro-proliferative activity
VASN	Vasorin	Yes	No	TGF-β inhibitor, regulates epithelial-to-mesenchymal transition
PTX3	Pentraxin 3	Yes	No	FGF-2 inhibitor, anti-angiogenic activity
LGMN	Legumain	Yes	No	1. Prognostic marker in breast cancer 2. Expression correlates to invasiveness
SPINT1	Serine peptidase inhibitor, Kunitz type 1	Yes	No	HDGF inhibitor, anti-proliferative activity
GGH	Gamma-glutamyl hydrolase	Yes	No	1. Degrades folates 2. Implicated in resistance to anti-folate therapy
IGFBP5	Insulin-like growth factor binding protein 5	Yes	Yes	1. IGF-1 inhibitor, pro-apoptotic activity 2. Cleaved and inactivated by kallikreins and cathepsins
S100A11	S100 calcium binding protein A11	Yes	Yes	1. Prognostic marker in breast cancer, overexpression indicates metastasis 2. Implicated in apoptosis
S100A6	S100 calcium binding protein A6	Yes	Yes	1. Prognostic marker in breast cancer, overexpression indicates metastasis 2. Implicated in apoptosis
QSOX1	Quiescin Q6 sulfydryl oxidase 1	Yes	Yes	Overexpression correlates with lower proliferation and anchorage dependent-growth

Table 5.19: Summary of pro-apoptotic protein hits obtained from proteomic analysis. For bibliographic references of functional annotations refer to chapter 2.

In addition to candidate apoptotic molecules present in HCC38 and BT20 secretions, this analysis also revealed that cancer exosomes contain the majority of

extracellular proteins while only a small minority of extracellular proteins is found free-floating in the soluble CM fractions. Another finding was that the soluble CM fraction features cytokines and growth-promoting factors (such as attractin ATRN and hepatocyte growth factor HDGF) in addition to pro-apoptotic molecules. A question that arises is whether these pro-growth cell stimulants act competitively against the pro-apoptotic factors or whether they actually act as co-factors amplifying the apoptotic activity of pro-death molecules. Validation of these hits is the next rational step that would answer remaining questions and unveil specific molecular mechanisms responsible for apoptotic activity.

In the future, fractionation of the active conditioned media by high-performance liquid chromatography could further condense the list of candidate apoptotic molecules. Some caveats associated with this approach are that we risk diluting the apoptotic activity beyond our assay's detection limit. Furthermore, in the case a co-factor is required in order to achieve the apoptotic effect, chromatographic separation of the CMs risks yielding no active fractions. Nevertheless, liquid chromatography constitutes the golden standard for biochemical purification and is therefore worth pursuing in the context of this study.

A less labor-intensive approach that also holds the potential of condensing the list of apoptotic hits is to extend the proteomic analysis to encompass conditioned media from cell lines that scored negative for apoptosis in our original 20x20 screen. We

expect that the comparison of these proteomes to the toxic CM proteomes will eliminate the vast majority of our current apoptotic hits.

In order to further validate apoptotic hits for activity in cells, a variety of methods can be employed. Neutralizing antibodies can be purchased to silence a pro-apoptotic protein in the CMs, or to block a particular receptor on the target cell lines. Alternatively, if the protein is commercially available in recombinant form, it can be tested directly in solution for apoptotic activity. RNA interference is also commonly used in order to transiently knock out target genes in either the producer or receiver cell line. The choice of method will be dependent on the specific protein hit and the amount of reagents commercially available for that particular protein.

5.2 Evaluating the effectiveness and functionality of breast cancer exosomes as diagnostic material

In chapters 2 and 3 we repeatedly collected breast cancer culture medium and attempted to tease out its protein contents in search of pro-apoptotic factors. One unexpected finding was that in addition to soluble proteins, conditioned media also featured a considerable amount of nuclear, cytoplasmic and plasma membrane proteins neatly compiled and exported in the extracellular space in the form of extracellular microvesicles known as exosomes. In chapter 4 we turned our attention to these vesicles and embarked in a series of studies aimed to characterize them.

Proteomic studies showed an abundance of cytoskeletal proteins, RAB GTP-ases, and glycolytic enzymes present in the exosomes of HCC38 and BT20 cells. More predictably, we also found numerous exosome markers, integrins and cell-adhesion molecules present in the vesicles. A series of western blots targeted towards receptor tyrosine kinases as well as upstream intracellular kinases revealed that exosomes quite accurately reflect the receptors of the cell line they originated from. Intracellular kinase enrichment patterns are more varied and unpredictable among exosomes derived from different cell lines, but in our screen encompassing six breast cancer cell lines spanning the spectrum from luminal to basal A and basal B, we found p38 MAPK to be consistently detectable among all exosomes and AKT kinase to be detectable in five out of the six exosome types.

Next we asked whether the exosome version of the TRK receptor EGFR retains functionality, i.e. the ability to add or subtract a phosphate group when exposed to EGF or Lapatinib respectively. We found the answer to this question to be negative. Specifically we were unable to readout changes in phosphorylation pattern of exosomal EGFR when treating exosomes with biological ligand, non-specific phosphatase inhibitor or Lapatinib inhibitor either in the presence or absence of extravesicular glucose. We conclude that despite the wealth of glycolytic enzymes present in the exosomes, these anuclear vesicles do not retain an intact glycolytic pathway and are unable to convert extravesicular glucose to ATP in order to complete the phosphorylation process.

We were however able to detect baseline phosphorylation levels of EGFR and upstream AKT kinase in cancer-derived exosomes and curiosity as to what is the origin of this phosphorylation pattern led us to formulate an alternate hypothesis. We hypothesized that if exosomes are unable to phosphorylate EGFR once secreted by the producer cell line, they must then incorporate phospho-EGFR during their biogenesis process within the producer cells. If this was indeed the case, we should be able to regulate phosho-EGFR and phosphor-AKT levels by challenging the producer cells with biological ligand EGF and/or Lapatinib and consequently observe the rise and fall of pEGFR and pAKT on the resulting exosomes. Experiments confirmed this alternate hypothesis as valid.

A final study on exosome biology examined the transfer of membrane cell adhesion molecules from EpCAM and CDH1-positive exosomes to cell types that are EpCAM and CDH1-negative. We found that T47D-derived exosomes were successful at transferring both adhesion molecules to recipient cell lines MDAMB231 and SKBR3. This was a pilot functional study and more experiments are needed in order to characterize the time-scale of the transfer event as well as the localization of the transferred molecules on the recipient cell lines.

In terms of clinical relevance, the implications of these findings are far-reaching. We showed that breast-cancer derived exosomes reflect not only the receptors from their originating cell lines, but also the phosphorylation status of these receptors. As such, breast cancer exosomes hold the promise of becoming real-time dynamic diagnostic material that can convey information regarding TRK inhibitor response of a tumor, right at the time of drug treatment.

In terms of affinity-capture methods aimed at purifying breast cancer exosomes from complex biological fluids such as blood or malignant ascites, we showed that the majority of breast-cancer derived exosome are highly enriched in the epithelial cell adhesion molecule EpCAM. Therefore EpCAM constitutes a good first-past capture molecule that will select specifically for epithelial tumor-derived vesicles in a clinical setting. We showed however that a minority of breast cancer cells will downregulate or cease expression of epithelial markers. In these cases EGFR is a

preferable molecule for affinity-capture methods since it is expressed at varying levels by all breast cancer exosomes we tested.

In terms of molecular typing of tumors using breast-cancer derived exosomes, this liquid biopsy method has an obvious hurdle to overcome: exosomes are anuclear units that lack the hormone receptors (estrogen and progesterone) typically used to classify luminal hormone receptor positive tumors. However we showed that three membrane markers are sufficient to classify all molecular types of breast cancer cells tested. Luminal tumor classification in exosomes can be interpreted as an EpCAM high/EGFR low phenotype. HER2 positive tumor classification in exosomes can be interpreted as a HER2 high/EGFR high phenotype, while triple negative classification will correspond to an EGFR high/EpCAM low/HER2 low phenotype.

Finally our study showing adhesion molecule transfer from exosomes to heterologous cells hints at roles exosomes potentially play during primary tumor development, the metastatic cascade and the homing of tumor cells in the metastatic niche. EpCAM and CDH1 are molecules conducive to an epithelial, less aggressive phenotype. Therefore, the successful transfer of functional adhesion proteins within aggressive EpCAM and CDH1-negative breast cancer cell lines opens novel therapeutic avenues. Studies in the field of biomedical engineering of cancer therapeutic vectors are presently exploring the delivery of cell adhesion molecules as a means of 're-programming' a tumor to assume a less metastatic, more epithelial-like phenotype. Exploring the efficiency and mechanistic underpinnings

by which exosomes achieve transfer of these molecules within triple negative breast cancer cells can inform engineering strategies for these therapeutic vectors.

Appendix

Measuring apoptosis in tissue culture cells

During the course of this research project I experimented with a variety of assays for measuring cellular apoptosis. In contrast to other cell-based measurements such as proliferation, measuring apoptosis presents some challenges. Apoptotic cells round up and eventually forgo attachment to the tissue culture plate, which makes it likely to loose these cells during plate washes and by consequence underestimate the apoptotic cell count. Another confounding factor that I ran into is that the specific phenotype associated with conditioned-media induced apoptosis held some similarity to the phenotype of dividing cells. CM-induced apoptotic cells round up much like cells about to undergo cell division. However, rather than dividing the apoptotic cells will eventually bleb and die. This prevented me from being able to read out apoptosis simply by glancing at cell plates under the microscope and required me to employ an assay that specifically probes for molecular apoptotic events in order to measure apoptotic cells. Below I summarize the assays used for this purpose throughout this study.

Method	Advantages	Disadvantages
Cleaved PARP Immunohistochemistry	✓ Single cell resolution ✓ Nuclear cell marker ✓ Can be multiplexed ✓ Low cost ✓ Straightforward protocol ✓ Plates can be stored and re-imaged in future	✧ Cell losses during fixation ✧ Readout requires time consuming microscope imaging and image segmentation algorithm
Cleaved PARP western blot	✓ Low cost ✓ Can be multiplexed	✧ Population ensemble measurement ✧ Low assay sensitivity ✧ Time consuming protocol ✧ Semi-quantitative readout
Caspase Glo Luminescence	✓ Fast protocol ✓ Quantitative readout	✧ Population ensemble measurement ✧ Low assay sensitivity ✧ High cost
M30 Cytodeath ELISA	✓ Early marker of apoptosis ✓ High assay sensitivity ✓ Quantitative readout	✧ Population ensemble measurement ✧ High cost ✧ Applicable exclusively to cells of epithelial phenotype ✧ Long protocol ✧ Cannot be multiplexed
NucView live cell apoptotic reporter	✓ Single cell resolution ✓ Fast protocol ✓ Nuclear marker ✓ Informative on the apoptotic phenotype ✓ High sensitivity	✧ Readout requires time consuming microscope imaging ✧ Qualitative readout ✧ High background in cells, prior to apoptosis

Table A.20: Summary of assays used to document and measure apoptosis in tissue culture cells.

Cleaved PARP Immunofluorescence

Full-length poly(ADP-ribose) polymerase PARP is a 116kDa nuclear protein involved in the repair of DNA, in differentiation and in chromatin structure formation. During apoptosis this protein is cleaved by caspase-3, and possibly other caspases, into an 89kDa fragment. Staining of cell monolayers with a p89 cleaved-PARP antibody after fixation and permeabilization reveals apoptotic cells. The obvious drawback of this method is that the fixation process eliminates all floating apoptotic cells that are the result of early events of apoptosis. Therefore the method captures only the late apoptotic events, i.e. the cells that are still adhered to the culture plate at the time of fixation. The reason I used this particular assay to acquire the 20x20 conditioned media screen data presented in the second chapter, is that it allows multiplexing with other readouts. In our case I was able to use a proliferative reporter in addition to the cleaved-PARP apoptotic reporter.

Cleaved PARP western blot

A variation of the previous assay is the cleaved PARP western blot. This is a rather time-consuming way of measuring cellular apoptosis. Yet the advantage of a western blot is that it can be multiplexed with a plethora of antibodies in order to readout a wealth of molecular information pertinent to the apoptotic phenotype. In order to minimize cell losses in this method, the cell culture supernatant is collected and centrifuged to pellet any floating apoptotic cells. These cells are then lysed along with the tissue culture monolayers and the cell lysate is used to run a standard western blot protocol. Nitrocellulose membranes are eventually blotted with the

116kDa full-length PAPR antibody, in order to visualize the amount of intact PARP as well as that of the cleaved 89kDa fragment.

Caspase Glo Luminescence[1]

The Caspase-Glo luminescent assay measures caspase-3 and -7 activities. The assay provides a luminogenic caspase-3/7 substrate, which contains the tetrapeptide sequence DEVD, in a reagent optimized for caspase activity, luciferase activity and cell lysis. Adding a single Caspase-Glo reagent in an "add-mix-measure" format results in cell lysis, followed by caspase cleavage of the substrate and generation of a "glow-type" luminescent signal, produced by luciferase. The assay readout is quantitative as luminescence is proportional to the amount of caspase activity present. The great advantage of this method is the speed and ease of use of the reagent. On the other hand, this assay is a population ensemble measurement that sacrifices sensitivity.

M30 Cytodeath ELISA[2]

This assay measures a fragment of the intermediate filament protein keratin 18 (K18) that gets cleaved by caspases during the apoptotic process. The advantage of the method is that it captures both the extracellular ccK18 that becomes released in the culture medium during secondary necrosis of the apoptotic cell bodies as well as the intracellular ccK18, which is an early event of apoptosis. Due to this advantage, the assay constitutes an extremely sensitive reporter of apoptosis. One limitation of the assay however is that it is only applicable to cells of epithelial phenotype that

express keratin 18. Even in cancer cell lines derived from epithelial tissues, that is not always the case as cell lines further along the epithelial-to-mesenchymal transition are prone to ceasing expression of epithelial protein markers.

Nucview Live Cell Apoptotic Reporter[3]

NucView 488 Caspase-3 substrate consists of a fluorogenic DNA dye and a DEVD substrate moiety specific for caspase-3. The substrate, which is initially not fluorescent and nonfunctional as a DNA dye, crosses the cell membrane to enter the cytoplasm, where it is cleaved by caspase-3 to form a high-affinity DNA dye. The released DNA dye migrates to the cell nucleus to stain the nucleus with bright green fluorescence. The obvious advantage of this reagent is that, when combined with timelapse imaging of live cells, it informs the viewer on the timescale of apoptotic onset.

References

1. Promega. Caspase-Glo 3/7 Assay Technical Bulletin, TB323.

2. Peviva. M30 CytoDeath™ ELISA.

3. Biotium. Apoptosis , Necrosis and Cell Viability Assays. 2–3